# OPTIMAL ENERGY MANAGEMENT OF CRUSHING PROCESSES IN THE MINING INDUSTRY

by

**Bubele Papy Numbi**

Submitted in partial fulfillment of the requirements for the degree

Philosophiae Doctor (Electrical Engineering)

in the

Department of Electrical, Electronic and Computer Engineering
Faculty of Engineering, Built Environment and Information Technology
UNIVERSITY OF PRETORIA

July 2015

# SUMMARY

## OPTIMAL ENERGY MANAGEMENT OF CRUSHING PROCESSES IN THE MINING INDUSTRY

by

**Bubele Papy Numbi**

| | |
|---|---|
| Promoter: | Prof. Xiaohua Xia |
| Department: | Electrical, Electronic and Computer Engineering |
| University: | University of Pretoria |
| Degree: | Philosophiae Doctor (Electrical Engineering) |
| Keywords: | Energy management, energy modeling, optimal control, operation efficiency, crushing process, jaw crusher, vertical shaft impact crusher, parallel high-pressure grinding rolls, time-of-use tariff |

It has been shown that mining processes, especially the comminution processes (grinding and crushing) are some of the biggest consumers of electricity in the world where energy management application would have a significant impact on the sustainability of both the energy supply and demand sides. However, very little research has been done in this area. Energy efficiency management in the mining industry can be done at four levels, namely the technology level, equipment level, operational level and performance level. In this work, operation energy management is considered for crushing circuits with the aim of minimizing the total energy cost by accounting for the time-of-use (TOU) electricity tariff. The work is limited to three types of crushing machines, namely the jaw crusher, vertical shaft impact (VSI) crusher and high-pressure grinding rolls (HPGR) crusher. Firstly, the energy model of each crusher is developed and expressed in terms of its control variables. Secondly, an optimal energy control model is formulated, where both physical and technical/operational constraints of the crushing process are taken into account. Thirdly, a case study is done in order to evaluate the effectiveness of the developed models. Lastly, experimental results of the performance model of the jaw crusher are presented.

Simulation results show that when TOU electricity tariff is applied there is potential for

achieving energy cost saving in all types of crushing processes, depending on the size of storage systems and plant production requirement. However, achieving energy saving is not always evident. When the throughput rate and product size distribution of the crusher are both controlled by a unique variable, as in the case of the jaw crusher, it is shown that no significant energy saving can be achieved. This is due to the trade-off between the throughput rate, product size distribution and specific energy consumption of the jaw crushing machine. Increasing the closed-side setting (unique control variable) of the jaw crusher with the aim to decrease the specific energy consumption will result in coarse particles in the product. However, there is a great opportunity for energy saving through optimal switching control due to the high no-load power consumption of the jaw crusher. On the other hand, when the throughput rate and product size distribution are controlled by more than one variable, as in the case of the VSI and HPGR crushers, more energy saving can be achieved in presence of varying feed size. In the VSI crushing process, for instance, the product size distribution is controlled by the rotor speed while the throughput rate is controlled by the rotor feed throttle. Hence, energy consumption reduction is achieved through any small decrease of the crusher rotor speed whenever the feed size decreases. The same applies to the HPGR crushing processes where the rolls operating pressure is used to control the product size distribution and the throughput rate is controlled by the rotor speed.

The analysis of the performance model of the jaw crusher reveals that although the Bond energy model presents larger prediction error compared to the throughput and product quality index, this can still be used as performance indicator in jaw crushing energy optimization, as it shows a strong linear correlation with experimental results. However, for actual energy consumption and energy saving calculation, a field test should be conducted.

# OPSOMMING

## OPTIMALE ENERGIEBESTUUR VAN VERGRUISINGPROSESSE IN DIE MYNBOU-INDUSTRIE

deur

**Bubele Papy Numbi**

| | |
|---|---|
| Promotor(s): | Prof. Xiaohua Xia |
| Departement: | Elektriese, Elektroniese en Rekenaar-Ingenieurswese |
| Universiteit: | Universiteit van Pretoria |
| Graad: | Philosophiae Doctor (Elektriese Ingenieurswese) |
| Sleutelwoorde: | Energiebestuur, energiemodellering, optimale kontrole, operasionele doeltreffendheid, vergruisingproses, bekvergruiser, vertikaleskag-impakvergruiser, parallele hoëdruk- breekrollers, tyd-van-gebruiktarief |

Daar is aangetoon dat mynbouprosesse, veral die vergruisingproses (maal en breek) een van die grootste verbruikers van energie in die wêreld is, waar die toepassing van energiebestuur' n beduidende impak sal hê op die volhoubaarheid van sowel die engergievoorsiening- as aanvraagkant. Daar is egter nog min navorsing op hierdie gebied gedoen. Die bestuur van energie-effektiwiteit in die mynbou-industrie kan op vier vlakke plaasvind, naamlik die vlakke van tegniek, toerusting, werkverrigting en prestasie. In hierdie werk word werkverrigtingbestuur oorweeg vir vergruisingkringlope, met die doel om die totale energiekoste te minimeer deur die tyd-van-gebruik-elektrisiteitstarief in berekening te bring. Die werk word beperk tot drie tipes vergruisingsmasjiene, naamlik die bekvergruiser, vertikaleskag-impakvergruiser (VSI) en parallele hoëdruk- breekrollervergruiser (HDBR). Eerstens word die energiemodel van elke vergruiser ontwikkel en uitgedruk volgens die kontrole-veranderlikes daarvan. Tweedens word 'n optimale energiekontrolemodel geformuleer, waarin sowel die fisiese as tegniese/operasionele beperkings van die proses in ag geneem word. Derdens word 'n gevallestudie gedoen om die effektiwiteit van die modelle wat ontwikkel is, te evalueer.

Laastens word die eksperimentele resultate van die werkverrigtingmodel van die bekvergruiser aangebied.

Simulasies toon aan dat wannneer die tyd-van-gebruik-elektrisiteitstarief toegepas word, energiekostebesparings potensieel in alle tipes vergruisingsprosesse bereik kan word, afhangend van die grootte van die bergingstelsels en aanlegproduksievereiste. Die bereiking van energiebesparing is nogtans nie altyd duidelik nie. Wanneer die toevoertempo en produkgrootteverspreiding van die vergruiser albei deur een veranderlike beheer word, soos in die geval van die bekvergruiser, word aangetoon dat geen beduidende energiebesparing bereik kan word nie. Dit is die gevolg van die ruil tusen die toevoertempo, produkgrootteverspreiding en spesifieke energieverbruik van die bekvergruisermasjien. Om die sluitsystelling (kontrole-veranderlike) van die bekvergruiser te verhoog met die doel om die spesifieke engergieverbruik te verminder, sal lei tot growwe deeltjies in die produk. Daar is nogtans goeie geleentheid vir energiebesparing deur optimale skakelkontrole omrede die hoë geenlading-kragverbruik van die bekvergruiser. Aan die ander kant, as die toevoertempo en produkgrootteverspreiding deur meer as een veranderlike beheer word, soos by die VSI- en HDBR-vergruiser, kan groter energiebesparing bereik word saam met veranderlike toevoergrootte. In die VSI-vergruisingproses word die produkgrootteverspreiding byvoorbeeld deur die rotorspoed beheer, terwyl die toevoertempo deur die rotortoevoerversneller beheer word. 'n Afname in energieverbruik word gevolglik verkry deur enige klein afname in die vergruiserrotorspoed wanneer die toevoergrootte afneem. Dieselfde geld in die HDBR-vergruisingprosesse, waar die operasionele druk van die rollers gebruik word om die produkgrootteverspreiding te beheer en die toevoertempo deur die rotorspoed beheer word.

Analise van die werkverrigtingmodel van die bekvergruiser toon dat alhoewel die Bond-energiemodel 'n groot voorspelfout lewer, dit steeds gebruik kan word as 'n aanduiding van werkverrigting in energie-optimering vir die bekvergruiser, aangesien dit sterk lineêre korrelasie toon met eksperimentele resultate. Nietemin sal veldwerktoetse uitgevoer moet word om die werklike energieverbruik en energiebesparing te bepaal.

# DEDICATION

To

The Almighty God;

For giving me the breath, strength and for all the blessings upon my life;

and

my dear father Jacques BUBELE;

for his love, encouragement, prayers, positive wishes and support.

# ACKNOWLEDGEMENT

This research work has been conducted with the National Hub for Energy Efficiency and Demand Side Management (EEDSM), Department of Electrical, Electronic and Computer Engineering, University of Pretoria. The financial support released by the University of Pretoria and National Hub for EEDSM is gratefully acknowledged.

I am also very grateful to the National Research Foundation of South Africa for financial support under grant unique number 88744.

I would like to express my sincere gratitude and appreciation to my supervisor, Prof. X. Xia, for his valuable guidance, encouragement, inspiration and help; many thanks, Prof.

To my former supervisor, Prof. J. Zhang, now at the University of Strathclyde, Glasgow, United Kingdom, I would like to say thank you for initiating this work.

Thanks to all my colleagues in the National Hub for EEDSM, Department of Electrical, Electronic and Computer Engineering, who assisted me while completing this work.

I am indebted to my parents who, with a lot of love, supported me during the entire period of my studies. Today, this highest degree is dedicated to you. Thank you very much for the great job you have done for me to be who I am. I am proud of you.

# PUBLICATIONS

The work presented in this thesis has resulted in the following publications:

1) B.P. Numbi, J. Zhang, X. Xia, "Optimal energy management for a jaw crushing process in deep mines,"*Energy*, Vol. 68, 2014, pp. 337-348.

2) B.P. Numbi, X. Xia, "Optimal energy control of a crushing process based on vertical shaft impactor," *Applied Energy*, 2014 (Article in Press), http://dx.doi.org/10.1016/j.apenergy.2014.12.017.

3) B.P. Numbi, X. Xia, "Systems optimization model for energy management of a parallel HPGR crushing process," *Applied Energy*, Vol. 149, 2015, pp. 133-147.

4) B.P. Numbi, X. Xia, J. Zhang, "Optimal energy control modelling of a vertical shaft impact crushing process," *Energy Procedia*, Vol. 61, 2014, pp. 560-563.

5) B.P. Numbi, X. Xia, "A model predictive control for operation efficiency in a vertical shaft impact crushing process," *The* $9^{th}$ *International Green Energy Conference-IGEC-IX*, 25-28 May, 2014, Tianjin, China.

6) B.P. Numbi, X. Xia, J. Zhang, "Optimal energy control modelling of a vertical shaft impact crushing process," *The* $6^{th}$ *International Conference on Applied Energy-ICAE2014*, 30 May-02 June, 2014, Taipei, Taiwan.

# ABBREVIATIONS

| | |
|---|---|
| AG | Autogenous grinding |
| CSS | Closed-side setting |
| DR | Demand response |
| DSM | Demand-side management |
| EE | Energy efficiency |
| EEDSM | Energy efficiency and demand-side management |
| HPGR | High-pressure grinding rolls |
| ISO | International organization for standardization |
| LHD | Load-haul-dump |
| LM | Load management |
| LSQ | Least squares |
| MPC | Model predictive control |
| NER | National electricity regulator |
| POET | Performance, operation, equipment and technology |
| RMS | Root mean square |
| ROM | Run-of-mine |
| SAG | semi-autogenous grinding |
| TBC | Total bin capacity |
| TOU | Time-of-use |
| UK | United Kingdom |
| VL | Variable load |
| VSD | Variable speed drive |
| VSI | Vertical shaft impact |

# TABLE OF CONTENTS

# LIST OF FIGURES

# LIST OF TABLES

# CHAPTER 1

# GENERAL INTRODUCTION

## 1.1 RESEARCH BACKGROUND AND MOTIVATION

The difficulty of the power utilities to meet the steadily growing energy demand has led to the implementation of energy management programmes at both the supply and demand sides. However, power utilities, energy regulators, policy-makers or grid operators have been more interested in energy management at the demand side, referred to as demand-side management (DSM), because of its cost-effectiveness compared to supply-side management. In the past, DSM aimed to plan the power grid at the customers' side in such a way as to influence their energy consumption behavior in order to meet the utility's desired load shape [1]. In the new definition, however, DSM includes both load shaping (also called load management (LM)) and energy efficiency (EE) (also called energy conservation) activities [2].

In South Africa, for instance, Eskom, the main electricity supplier, introduced time-of-use (TOU) tariff-based DSM in the 1990s owing to the electricity crisis, in an attempt to motivate big electricity consumers, such as mining industries, to shift their loads out of the peak period [3].

Mining sectors account for about 15 % of the total electrical energy consumption in South Africa, of which gold mining leads with 47 %, followed by platinum mining, taking 33 %, whilst 20 % is consumed by the remaining mines.[1] It is further indicated that processing occupies the second place in mining energy consumption in the country, with 19 % of the total

[1]Eskom, The Energy Efficiency series: Towards an energy efficient mining sector, <http://www.eskomidm.co.za>.

energy, slightly less than materials handling, which consumes 23 %. This shows that mining sectors, especially gold mines have an important role to play in reducing South Africa's energy consumption, which will also reduce the associated cost.

Worldwide, mineral processing is one of the biggest electricity consumers. About 5 % of the total electrical energy produced in the world is consumed by mineral processing circuits, of which 80 % goes to the comminution process (crushing and grinding) [4]. Comminution is the first operation in mineral processing whereby the coarse ore coming from mines, usually referred to as run-of-mine (ROM) ore, is fragmented into particles of reduced or smaller size in order to extract the valuable minerals. Different types of crushers are used for mineral processing, depending on the ore characteristics and plant throughput capacity to be achieved. In a primary crushing station, for instance, jaw and gyratory crushers are generally employed to reduce large amounts of coarse and hard ROM ore of a larger size, say $0-1000\ mm$ down to $0-250\ mm$. The primary crushing operation is done either in underground mines or surface mines. This is followed by a secondary crushing station usually at surface mines, where crushing machines such as cone crushers are used to further reduce the hard ore from $0-250\ mm$ down to less than $70\ mm$. From this stage, the fragmented ore is further reduced in tertiary crushing station, from $0-70\ mm$ down to $0-12\ mm$. The tertiary crushing station is usually based on cone crushers or vertical shaft impact (VSI) crushers. The fragmented ore product from the crushing plant is thereafter reduced to very smaller particles say, from $0-12\ mm$ down to the range of $50-100\ \mu$m, in milling/grinding circuits by grinding machines to allow mineral recovery process [5].

While comminution accounts for 80 % of the overall energy consumption of the processing plant, this is known to be an inefficient process. In grinding circuits, for instance, the efficiency of tumbling mills such as balls mills, autogenous gringing (AG) mills and semi-autogenous grinding (SAG) mills is as low as 1 %, or less [6]. In order to increase the efficiency of mineral processing plants in terms of both energy consumption and throughput capacity, high-pressure grinding Rolls (HPGR) machine, which is a type of roll crusher, has recently been designed and introduced in mineral comminution circuits as replacement for tertiary and quaternary crushers, SAG mills, ball mills and rod mills [7, 8, 9, 10]. Replacing the above-mentioned machines with an HPGR machine in comminution circuits is part of equipment efficiency improvement [11]. While efforts have been made to improve the comminution efficiency at equipment level in order to decrease the energy cost associated with

the comminution process, more energy cost saving can be achieved at the operational level, especially when the TOU electricity tariff is applied, as in many mining industries.

For materials handling in mining sectors, some research has been carried out to investigate the potential of reducing the energy cost based on the TOU tariff. In [12] for instance, the DSM technique is studied for optimal hoist scheduling of a deep level mine twin rock winder system. Optimal energy control strategies for coal mining belt conveyors are investigated in [13, 14, 15]. All of these studies demonstrate great potential in reducing the energy cost associated with the operation of mining materials handling based on TOU tariff.

However, relatively less research has been dedicated to the energy cost management of crushing and grinding circuits, which are the first two stages of mineral processing in mining industries. A recent research paper was published in the area of energy cost optimization of a ROM ore grinding/milling circuit [16]. It is indicated that a cost reduction of \$9.90 per $kg$ of unrefined product can be achieved when the optimal energy cost management is applied to a ROM ore grinding circuit processing platinum. Very little research to date has been undertaken on reducing the crushing electricity bill. Other papers, such as those of [17, 18, 19, 20, 21], use the TOU tariff-based DSM for the optimal operation of a water pumping station. An optimal LM for air conditioning loads is studied in [22], where a case study shows a reduction of 38 % in peak demand with an annual cost saving of 5.9 %, under the TOU tariff. The benefit of the optimal load shifting based on the TOU tariff with application to manufacturing systems is also shown in [23]. In [24, 25], a dynamic or more flexible TOU tariff-based DSM, referred to as real-time pricing-based DSM, is applied to the optimal scheduling of electrical energy supply systems.

In the past, the common objectives in the mining comminution process consisted of achieving a large production capacity (throughput maximization) and amount of fines [16]. Minimizing the energy consumption was the last objective because of the relatively lower electricity price in the past. However, in response to the electricity crisis encountered by many countries nowadays, the electricity price is seen to increase annually at a fast rate. An annual price increase of 8 % is applied from 1$^{st}$ April 2013 to 31$^{st}$ March 2018 in South Africa, for instance.[2] Hence, for crushing processes, the control objectives can be adapted as follows (adapted

[2]Eskom, Revenue Application - Multi Year Price Determination 2013/14 to 2017/18 (MYPD3), <http://www.eskom.co.za>

from [16]):

1. achieve a product size less than a specified value;

2. achieve a specified average production capacity (throughput);

3. minimize the costs associated with the power consumption.

With this in mind, the effort of this work is put on developing optimal control models for the energy management of crushing processes in mining industries. Three different types of crushing machines are chosen in order to cover a wide range of crushing circuit types. The first is the jaw crusher, which is based on reciprocating compressive action and usually found in a primary crushing circuit and sometimes in a secondary crushing circuit if on the surface. The second is the VSI crusher, which is based on impact action to reduce the rock size. This is usually found in tertiary and sometimes in secondary crushing circuits. The third crusher used in this work is the HPGR crusher. This is based on rotating compressive action and found in last crushing circuits, such as tertiary and quaternary crushing.

For all crushing processes, the performance index is defined as the energy cost to be minimized by taking into account the TOU electricity tariff. Both physical and operational/technical constraints are taken into account in the optimization models. On the one hand, physical constraints are limitations on control variables (for instance, closed-side setting (CSS) for jaw crushers, rotational speed for VSI crushers and rotational speed and rolls operating pressure for HPGR crushers) and limitations on state/dependent variables such as rock/ore levels in the storage systems (bins, hoppers, stockpiles, ore pass). On the other hand, operational or technical constraints are limitations or requirements linked to the crushing process in order to meet the desired production as well as the desired product quality.

## 1.2 CONTRIBUTIONS OF THE THESIS

In this work, the contributions are as follows:

1) Two optimal control models for energy management of jaw crushing processes in deep mines are developed. The first model is referred to as variable load (VL)-based optimal energy control and the second is optimal switching control. The two optimal control

models are compared to the current control technique used in the mining industry, where the control objective is the minimization of the deviation around the daily production target.

2) An optimal control model for energy management of the VSI crushing processes is developed and compared to the current control technique. An energy model, appropriate for optimal energy control purposes, is developed based on an existing model and this is validated through manufacturer's data. The existing energy model of the VSI crusher is appropriate for process design and not operation. The effect of variation in the feed size is analyzed for energy saving.

3) An optimal control model for energy management of the HPGR crushing processes with a parallel configuration is developed and compared to the existing control technique in the mining industry. An energy model, appropriate for optimal energy control purposes, is also developed based on the existing model. The effect of unequal overall efficiencies of the two HPGR crushing machines, and slight decrease in the rolls operating pressure, are analyzed for energy saving.

4) Laboratory experiments for the analysis of the jaw crusher performance model, which can be used for optimal control purposes, are carried out. The effect of variation of the closed-side setting (CSS) of the jaw crusher on throughput rate, specific energy consumption and the coal particle size distribution is analyzed.

## 1.3 LAYOUT OF THE THESIS

This thesis is laid out as follows:

### 1.3.1 Chapter One

This forms the introductory chapter of this thesis. Background and motivation of the topic, and research contribution are given here.

### 1.3.2 Chapter Two

In this chapter, a literature review of energy management, systems efficiency optimization in industries and energy management standards is given. More specifically, the industrial EE based on the POET (performance, operation, equipment and technology) concept is discussed.

### 1.3.3 Chapter Three

Two optimal energy control models of a jaw crushing process with applications in deep mines are developed and discussed in this chapter.

### 1.3.4 Chapter Four

In contrast to Chapter 3, in this chapter, an optimal energy control model of the VSI crushing process is developed and discussed.

### 1.3.5 Chapter Five

Optimal energy control of the HPGR crushing process with a parallel configuration is modelled and discussed in this chapter.

### 1.3.6 Chapter Six

In order to assess the applicability of the performance prediction model (throughput rate, specific energy consumption and product distribution size) of the jaw crusher used in Chapter 3, results from laboratory experiments are presented and discussed in this chapter.

### 1.3.7 Chapter Seven

All work done in previous chapters is concluded in this chapter. Recommendations for further research are also given.

# CHAPTER 2

# ENERGY MANAGEMENT: LITERATURE REVIEW

## 2.1 INTRODUCTION

Although energy management is a concept applied to both the supply and demand sides [26] while different objectives are to be achieved, in this work, the word "energy management" is defined with reference to the demand side, under which the topic of this work falls. This chapter is mainly intended to give a literature review of energy management in an industrial framework.

## 2.2 OVERVIEW OF INDUSTRIAL ENERGY MANAGEMENT

Energy management in industries can be defined as a strategy of efficiently using energy by optimizing certain performance objectives such as energy consumption cost and greenhouse gas emissions without lowering the service (production and quality) levels. The first objective can be achieved either through minimization of energy waste, referred to as EE improvement activities and through LM also called load shaping activities. On the other hand, the second objective is achievable through EE improvement or through use of renewable energy systems.

Energy management in the form of LM activities, was first conceptualised and published by Clark W. Gellings in 1985 [1] and is referred to as DSM. According to Gellings, DSM activities are only those that modify the load at a certain time (e.g. during peak time), referred to as load-shape modifying activities, to allow the utility to meet the demand constantly. It is

further pointed out that activities such as EE, that reduce the overall energy consumption (demand) are not classified under DSM. Some energy policies such as those of the national electricity regulator (NER) in South Africa and references such as [27, 28] share the above DSM definition. In South Africa, DSM is limited to LM activities such as reducing the energy consumption during peak time, while EE refers to the reduction of the total (overall) energy consumption during all time periods.[1] However, other energy policies, such as the one in UK, refer to DSM as activities that include both LM and EE programs [2]. Reference [2] gives a good review of past research on DSM concepts and proposes a new and broad DSM definition. The DSM definition given in [2] is found to meet most countries' energy policy objectives, such as greenhouse gas emissions reduction, energy security and affordability, EE, etc. This justifies consideration of the last-named definition of DSM throughout this thesis and therefore means the same thing as industrial energy management.

### 2.2.1 Application of demand-side management in industries

Demand-side management is nowadays seen as an effective way of maximising profit in manufacturing and mining industries through reduction of the cost associated with energy consumption. As mentioned above, DSM is generally classified into LM, referred to as demand response (DR), EE but also on-site back-up activities as shown in Fig 2.1 (adapted from [2]).

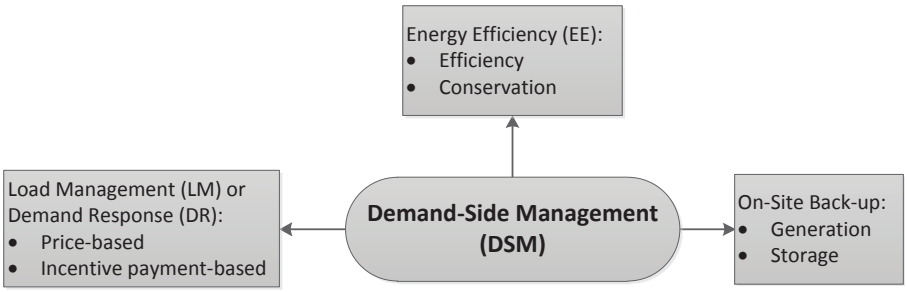


**Figure 2.1:** Classifying demand-side management (DSM)

[1] NER, Regulatory policy on energy efficiency and demand-side management for South African electricity industry, <http://www.cityenergy.org.za>

#### 2.2.1.1 Energy efficiency

The aim of EE is to reduce overall energy consumption of the industry, which can be achieved at four levels: performance (P), operation (O), equipment (E) and technology (T) (POET) [29, 30, 11]. With reference to [29, 11], the POET efficiency concept is defined as follows:

**Performance efficiency** of an industrial energy system is any measurable index/indicator that is considered to evaluate its energy performance. For materiel handling equipment such as belt conveyors, for instance, the specific or unit energy consumption expressed in $kWh/t/km$ is considered the most suitable energy performance indicator [31]. This expresses the energy consumed ($kWh$) per tonne ($t$) in order to transport the material over a given conveying distance ($km$). Although in reference [13], the performance efficiency of the belt conveyor systems is expressed in $kWh/t$, this would not be appropriate if, for instance, the performance efficiencies of two belt conveyors of the same capacity but different conveying lengths were compared. In this case, although the two belt conveyors have equal $kWh/t$, the one with the longer conveying length will normally be said to be of higher efficiency, since transporting material over a long distance is also one the conveyor's performance objectives. Taking $kWh/t/km$ as energy performance indicator of any transport system is more meaningful compared to $kWh/t$, since higher transport efficiency in reality means less energy consumption ($kWh$), higher production ($t$) and a longer transportation distance ($km$). This is due to the conflict between economic performance objectives (energy consumption, energy cost to be minimized) and technical performance objectives (production and transportation distance to be maximized). Similarly, $kWh/m^3/km$ can be considered for a pumping system, which expresses the energy required ($kWh$) to pump a certain volume of fluid ($m^3$) to a certain heigh (pumping head) ($km$). For comminution machines (crushers and grinders) and screens in mining and aggregate industries, the energy performance indicator can be simply expressed in $kWh/t$, denoting the energy required to crush/grind/screen a tonne of rock or ore material.

**Operation efficiency** of an energy system can be achieved by proper (optimal) coordination (control) of different components of the system or process [11] while the given energy performance index is optimized during the operation. This can be achieved either automatically using control systems or manually through human intervention. An example of this is optimal control of a belt conveyor where the belt speed is matched with the material feed

rate whenever the latter changes [14]. A variable speed drive (VSD) is usually used to achieve this. The same scheme referred to as load matching is also used in pumping, compressor and fan systems where through VSDs, the load speed is matched with the fluid flow rate whenever the latter changes [32, 33].

**Equipment efficiency** of an industrial energy system or process can be obtained by improving the efficiency level of each isolated equipment/component taken individually within the system with respect to technology design specifications [11]. A belt conveyor can be considered to illustrate this definition. In this system, the equipment efficiency can be improved through high-level maintenance of the existing equipment/components such as transmission drive (gearbox lubrication), idler sets (solve misalignment problem), etc. This can also be improved by replacing old or existing components with new and high-efficiency components. For instance, standard idlers can be replaced with energy-saving idlers [34], standard-efficiency motors-IE1 can be replaced with high-efficiency motors-IE2, premium-efficiency motors-IE3 or super-premium efficiency motors-IE4 [35], standard belts (steel cord-based belt) can be replaced with low-loss belts (aramid material-based belts) [36].

**Technology efficiency** is achievable through new and improved energy conversion method (e.g. way of conventing electrical energy to mechanical energy and vice versa), processing method (eg. way of reducing rock/ore size), transportation/transmission method (eg. way of transporting bulk material or transmitting electrical signal), etc [11]. For instance, the study on improving the electric motor, pump, compressor, fan or ventilator technology to consume less energy is part of technology efficiency. Technology efficiency improvement can also be achieved by introducing new/advanced technologies to the existing energy systems, for instance, the introduction of new control system technologies such as VSDs for the coordination of mechanical loads such as pumps, fans, compressors and conveyors.

#### 2.2.1.2 Load management/demand response

While EE concentrates on reducing the overall energy consumption all the time, LM or DR aims at reducing the energy consumption only during specific time periods, called peak times, when the utility has difficulty in meeting the increased demand because of the energy capacity shortage. The consumers are therefore encouraged to reduce the peak time demand by shifting their loads to off-peak times when the utility has a larger energy capacity. By

doing so, customers benefit from a lower electricity price by consuming energy during off-peak times, or incentives, thus leading to a reduction in their electricity bill. DR is fully explained in [37]-[38] to which the reader can refer to for more in-depth information. The two main types of DR programs are shown in Fig. 2.2 (adapted from [37]-[38]).

On the one hand, when customers enrol for the incentive-based DR programs, the incentives offered by utilities, policy-makers or grid operators may be in the form of explicit bill reduction or payment for the measured or pre-contracted load reduction [37]. On the other hand, for those who enrol for price-based DR, their bill reduction will depend on their response in reducing or completely shifting their loads from peak times charged at a high price to off-peak times charged at a lower price.

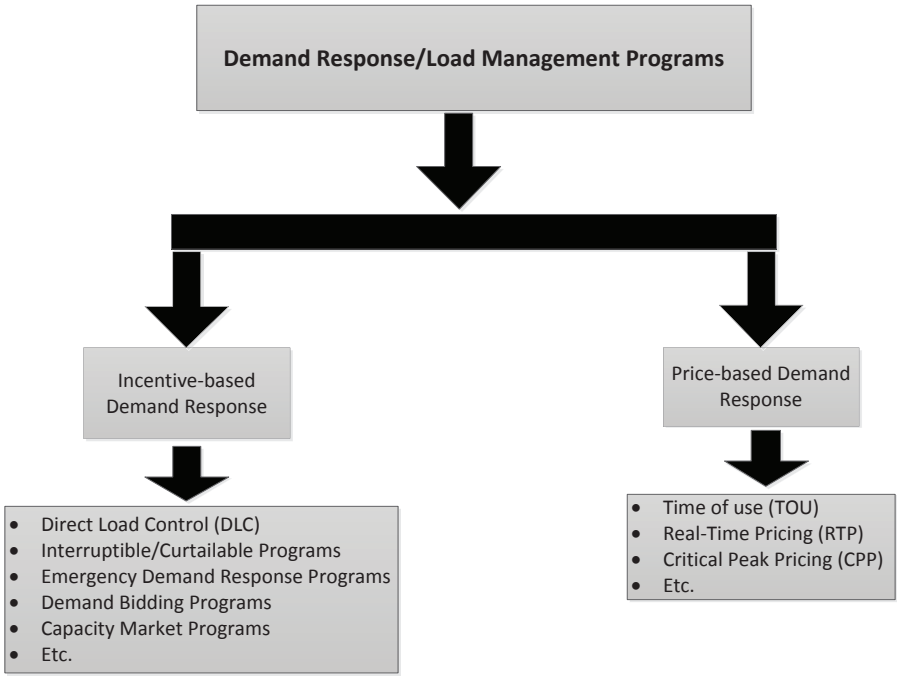


**Figure 2.2:** Classifying demand response (DR)

#### 2.2.1.3 On-site back-up

The third and last category of DSM programs is the on-site back-up program. This scheme consists of installing at the customer side (usually big consumers, such as industries) power generation systems, such as diesel generators or renewable energy systems, or energy storage systems, such as thermal energy storage. The aim of this in the past was to smooth/balance

the load by reducing the peak energy consumption from the grid [2]. However, as far as industries are concerned, the electricity bill can be reduced when water heated up during off-peak times is used during peak times to avoid high energy cost. Also, by selling the energy produced from generation systems to the grid at a high price, during peak times, customers can maximize their profits.

## 2.3 SYSTEMS EFFICIENCY OPTIMIZATION IN INDUSTRIES

Systems optimization is widely employed in several industrial processes as a supervisory control system at the upper control layer, in order to improve the operation efficiency of the energy system. It aims at optimally adjusting in real-time, the set points of the regulatory control system at the lower control layer by minimizing or maximizing a given performance index of the process.

Depending on the control objective to be achieved in a process, several performance indices can be optimized. These are, for instance, the maximization of the EE, minimization of the energy cost, maximization of the total plant throughput, minimization of the downtime, maximization of the product quality, minimization of emissions, etc. Various algorithms can be embedded in the supervisory control system to achieve systems optimization of processes.

In general, systems optimization can be classified into two main categories, depending on the level of automation. The first is referred to as open loop systems optimization where for a given control horizon, the optimization model is solved once (usually offline) and the optimal set points obtained are manually entered into the regulatory control system. The other is closed-loop systems optimization, where the optimization model is solved online and the optimal set points are automatically entered into the regulatory control system.

Traditionally, in mining industries, systems optimization has been successfully applied to grinding circuits while maximizing either the milling circuit throughput or the grinding process profit. Reference [39], for instance, the milling circuit throughput is maximized using the “IF-THEN” rule-based algorithm. The results obtained show an improvement of the milling throughput by approximately 5 %. In [40], linear programming supervisory control is employed to maximize the grinding circuit throughput, while in [41], the grinding circuit

throughput is maximized using an expert system based on fuzzy logic where an increase of 10 % in feed tonnage is achieved. On the other hand, in [42, 16], the cost function to be maximized is taken as the grinding circuit profit instead of the grinding circuit throughput as in [39, 40, 41]. The Hooke and Jeeves search routine algorithm is used in [42], while in [16], model predictive control (MPC) is implemented.

However, because of the continual increase in energy cost, the importance of using systems optimization in minimizing the energy cost of material handling equipment in mining industries is shown in research works such as [15, 13, 14, 12].

In chemical industries, systems optimization is studied in [43] for throughput maximization in a gas processing plant and in [44] for fuel cost minimization of a sugar and ethanol heat and power system. An MPC strategy is adopted in [43] while in [44], a model adaptation and gradient correction strategy is applied.

Systems optimization is also used for energy cost minimization of water pumping processes in [19, 17, 18, 20].

References [13, 14, 18] are those where open loop systems optimization is applied, while in [39, 40, 41, 42, 16, 15, 12, 43, 44, 19, 17, 20], closed-loop systems optimization is applied.

## 2.4 ENERGY MANAGEMENT STANDARDS

For better energy management implementation and continual improvement of energy performance in industries, a certain engineering standard has to be followed. Nowadays, several international and national standards exist that have been designed to meet this objective. Most of these standards are based on the "plan-do-check-act" cycle [45]. Other energy management practices, simpler and easier than standards, referred to as energy management maturity models, are being developed to cope with even those organizations with lack of professional and financial resources for energy management implementation [45, 46]. On international level, the two most widely recognized standards are the International Organization for Standardization (ISO) Standard-ISO 50001:2008 and the European Union Standard-EN 16001:2009 [46, 47]. National standards for energy management systems such as ANSI/MSE 2000:2008 in United States, VDI 4602/1 in Germany, UNE-216301:2007 in Spain, DS2403 in

Denmark, SS627750 in Sweden, IS 393 in Ireland also exist [46, 47].

## 2.5 SUMMARY

In this chapter, literature on energy management programs, systems efficiency optimization and energy management standards on industrial level was reviewed. The energy management scheme is discussed under the old and new concept, while the industrial EE is discussed under the POET concept.

# CHAPTER 3

# OPTIMAL ENERGY MANAGEMENT OF A JAW CRUSHING PROCESS IN DEEP MINES

## 3.1 INTRODUCTION

Compressive crushers such as jaw crushers form the core heavy-duty machines used for decades for crushing of coarse and hard ROM ores such as gold, copper, cobalt and Zinc ores, in primary stations of mining industries, usually found underground [48, 49, 50]. These are also used for the same purpose for run-of-quarry rocks in aggregate industries. However, jaw crushers are known to be inefficient crushing machines owing to their high no-load power ranging between 40 and 50 % of their rated power [51, 52].

In this chapter, two optimal control models for energy management of a underground jaw crushing process are developed. The performance index for both models is defined as the energy cost to be minimized under TOU tariff. The first model is referred to as the VL-based optimal control, while the second is optimal switching control. The former takes account of the jaw crushing energy model and optimally coordinates the feeder speed, closed-side setting (CSS) and the working time of the jaw crusher for energy cost minimization. Optimal switching control optimally coordinates the on/off status and working time of the jaw crushing station to achieve the energy cost reduction. Solutions of the two techniques are compared to the current strategy used as a baseline solution in order to validate the effectiveness of the results. The content of this chapter has been published in [53].

## 3.2 MODEL DEVELOPMENT

### 3.2.1 System description

A typical configuration of a deep underground mine is shown in Fig. 3.1 (adapted from [54]). The coarse ROM/blasted ore is loaded from different production stops (muckpiles) by load-haul-dump (LHD) vehicles, and hauled to the tipping points [55] of the ore pass, from where the ore material is transferred by gravity to the lower level of the mine. On the collection

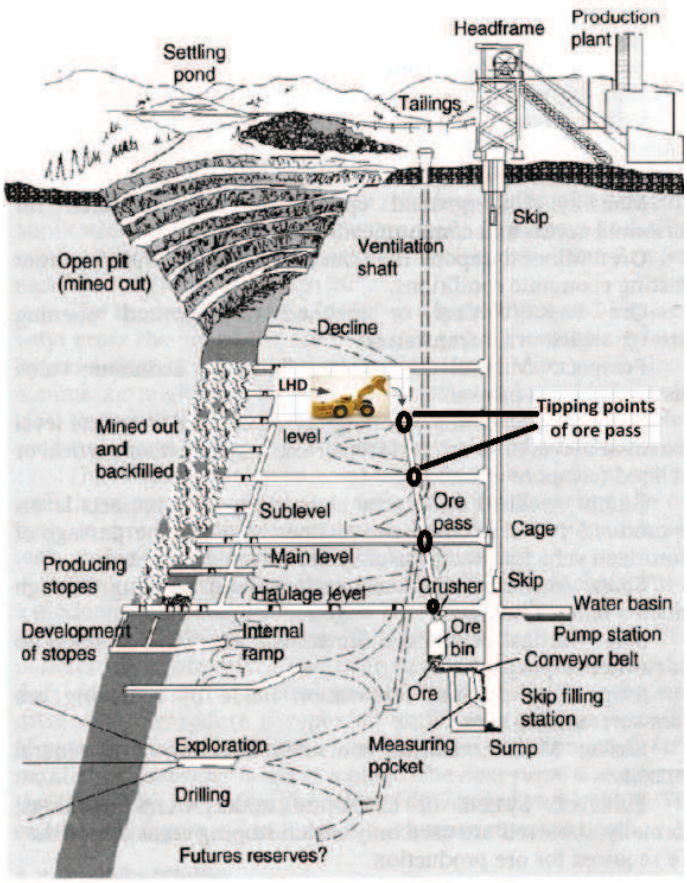


**Figure 3.1:** Typical configuration of a deep underground mine

level, the ore is reduced to smaller size by primary crushers and stored in a storage buffer such as an ore bin or silo. The crushed ore is then transported to the bottom of the shaft station by conveyor belts, dump trucks or trains (in this figure, a conveyor belt is considered), loaded into skips/buckets and hoisted to the surface bins, silos or stockpiles by the rock winder. From here, the ore is transported to the production plant for further processes such as secondary and tertiary crushing, grinding/milling, concentration, etc., for extraction of the valuable

mineral.

The primary jaw crushing station is usually installed underground in mines and operates in open circuit, as shown in Fig. 3.2. The ROM ore is fed to the crushing station through the discharging zone, also called gate of the ore pass, at a controlled mass flow rate. This flow

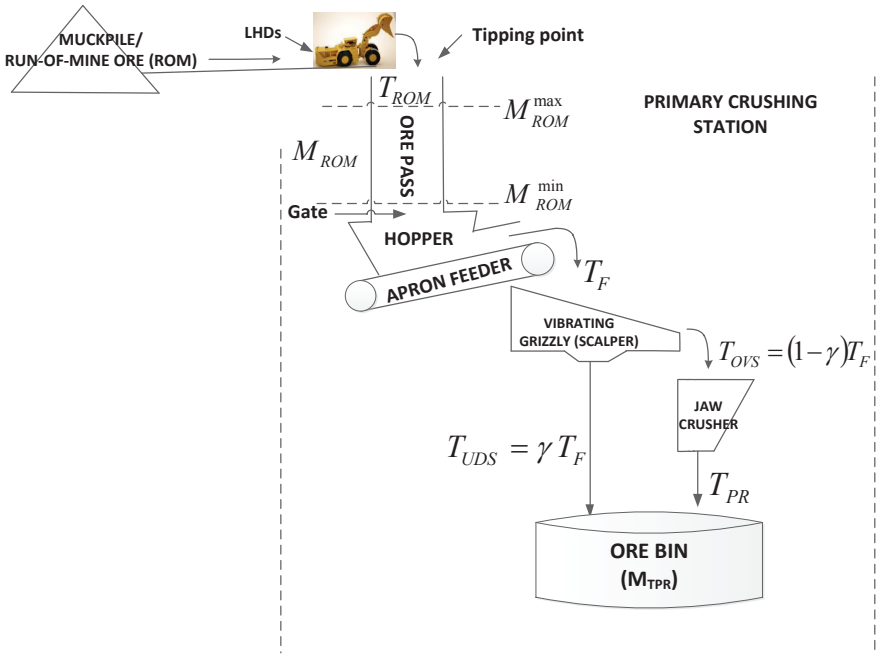


**Figure 3.2:** Primary jaw crushing station in a deep mine

rate is usually controlled through a control gate at the ore pass exit zone by using control chains, a chute with control chains [55, 56, 57, 58] or an ore feeder [58]. An apron feeder and a vibrating feeder are the main machines used to feed the ROM ore to primary crushers. In this work, an apron feeder is used for flow rate control. Notations in Fig. 3.2 are defined as follows: $T_{ROM}$ is the mass flow rate of ROM ore into the ore pass storage system; $M_{ROM}$ represents the ore mass available in the storage system and $M^{min}_{ROM}$ and $M^{max}_{ROM}$ are respectively, the minimum and maximum of $M_{ROM}$. $T_F$ is the mass flow rate of ROM ore from the feeder to the scalper; $T_{OVS}$ and $T_{UDS}$ are, respectively, the mass flow rate of oversize and undersize ore from the scalper while $\gamma$ is the undersize fraction of ore material, and $M_{TPR}$ is the total mass production of crushed ore during a given period.

The different components in this primary crushing station are:

- ore pass and feed hopper system: a storage buffer that receives the ore dumped from

LHD vehicles;

- apron feeder: machine used to control the ore flow rate from the ore pass and feed hopper system;
- vibrating grizzly: a scalping equipment that receives the controlled ore flow rate from the apron feeder and feeds the jaw crusher by scalping (removing) fines (ROM ore size less than the CSS of the jaw crusher);
- primary jaw crusher: a compressive crusher machine used for crushing of coarse and hard ROM ore, and
- ore bin: a storage equipment to receive the crushed ore material that will later be conveyed to the shaft station.

### 3.2.2 Operating principle of a jaw crusher

The operating principle of a jaw crusher is shown in Fig 3.3 [49]. The ore/rock is fed to the crusher from the top opening, called gape. Once the ore in the crushing chamber, formed by the fixed and moving jaws, this is crushed into smaller sizes when the moving jaw comes towards the fixed jaw. The crushed particles are thereafter squeezed down when the moving

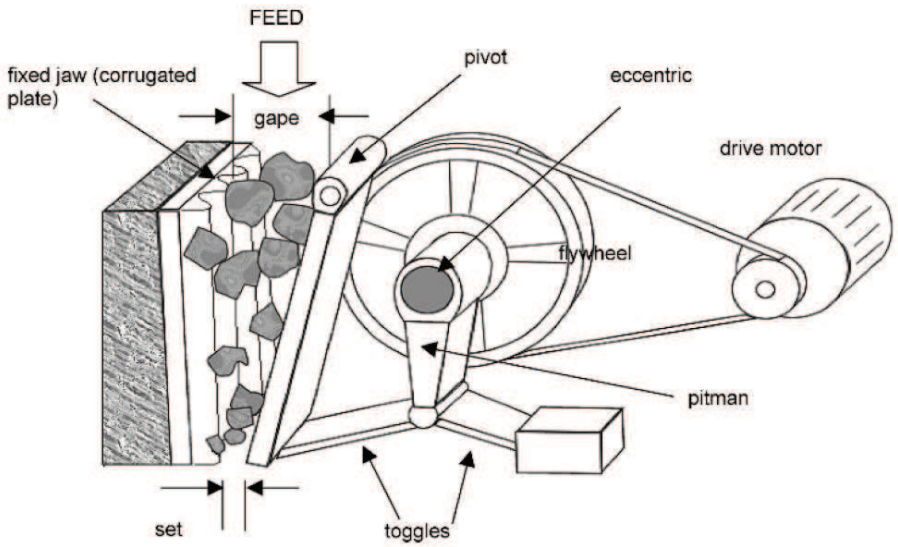


**Figure 3.3:** Schematic of a jaw crusher

jaw moves away from the fixed jaw, through toggle mechanism. The process is repeated until particle sizes are less than the bottom opening (discharge aperture), called set. The reciprocating motion of the moving/swing jaw is obtained through the eccentric shaft which converts the rotation motion of the drive motor to a linear motion. During the displacement of the swing jaw, the set between jaws varies from its minimum to maximum openings, called closed-side setting (CSS) and open-side setting (OSS), respectively.

### 3.2.3 General assumptions for the system

- The time delay associated with the crushing process, from the ore pass tipping points to the ore bin is ignored.
- The start-up and shut-down energy consumption rates of the jaw crusher are neglected.
- The storage capacity of the ore bin is sufficient to store the total mass production of the ore material crushed for the given control horizon.

### 3.2.4 Model for VL-based optimal control of a primary jaw crushing process

The model involves the energy model of the jaw crushing process and achieves the system energy cost minimization through the coordination of the feeder speed, the CSS of the jaw crusher and the working time of the crushing process based on the TOU tariff.

The objective in this work is to minimize the total energy cost, $J_C$, of a jaw crushing process, subject to physical and operational constraints, and mostly, the power utility constraint such as the TOU electricity tariff, $p(t)$, during the control interval defined by the initial time, $t_0$, and final time, $t_f$. This optimal energy control problem can be formulated as:

$$min\, J_C = \int_{t_0}^{t_f} f_P\left(V_F\left(t\right), CSS\left(t\right)\right) p\left(t\right) dt, \tag{3.1}$$

subject to different constraints that will be later defined. In Eq.(3.1), $f_P$ denotes the power function of the jaw crusher; $V_F$ and CSS are, respectively, the apron feeder speed and CSS of the jaw crusher representing the control variables. In practice, the apron feeder speed is adjusted by using a variable speed drive (VSD), while the CSS of the jaw crusher is infinitely adjustable, with setting limits, through the actuation of hydraulically controlled wedges and

tension rod spring.[1]

The aim is therefore to find an optimal control law that will transfer the ROM ore from the ore pass and hopper storage system to the ore bin through a crushing process, with minimum energy cost, during the given operation period from $t_0$ to $t_f$. Continuous-time optimal control problems are traditionally solved by Pontryagin's maximum principle [59]. However, the applicability of this principle assumes that the objective function and the associated constraint functions are continuously differentiable, which is referred to as the smooth condition. As can be seen, the discrete nature of the TOU electricity price function may lead to the energy cost function, expressed by Eq.(3.1), being continuous but not differentiable and hence non-smooth. Moreover, it is noted that for complex problems such as the one addressed in this work, a numerical approach may be a preferred alternative.

#### 3.2.4.1 Objective function

To date, the generally accepted and explicit expression to predict the specific net energy consumption of comminution machines during material size reduction has been given by Bond's law as follows (in kWh/short-ton) [60, 5]:

$$W = 10W_i \left( \frac{10^{-3}}{\sqrt{P_{80}}} - \frac{10^{-3}}{\sqrt{F_{80}}} \right), \tag{3.2}$$

where $W_i$ is the Bond's work index (in kWh/short-ton). $P_{80}$ is the particle size that is larger than 80 % by mass, of all particles in a product material sample (in m), and $F_{80}$ is the particle size that is larger than 80 % by mass, of all particles in a feed material sample (in m) [5]. Eq.(3.2) can be expressed in kWh/metric-ton by a multiplication of 1.1. Hence, the net crushing power consumption will be a simple product of the specific net energy consumption (in kWh/metric-ton) and the feed mass flow rate to the crusher, $T_{OVS}$, as given below:

$$P_{Net} = 11W_i \left( \frac{10^{-3}}{\sqrt{P_{80}}} - \frac{10^{-3}}{\sqrt{F_{80}}} \right) T_{OVS}. \tag{3.3}$$

For jaw crusher application, the specific energy term in Eq.(3.3) can be controlled by the CSS of the jaw crusher [49, 61], while the feed mass flow rate, $T_{OVS}$, can be controlled through the apron feeder speed, $V_F$ [62]. Hence, as previously discussed, two control variables are

[1] Terex, JW Series jaw crushers, <http://www.armstrongequipment.com>

used for the optimal control of energy cost in this work; these are CSS and $V_F$, which are adjustable in real-time. In [49, 61] and [62], the relationships between the terms in Eq.(3.3) and the two control variables are given, respectively, by Eqs.(3.4) and (3.5), as follows (in $m$):

$$\begin{cases} P_{80} = 0.85\,(CSS + \mathcal{T})\,, \\ F_{80} = 0.8 S_F F_{max} + 0.2 S_C, \end{cases} \tag{3.4}$$

and

$$Q_F = k V_F, \tag{3.5}$$

where

$$k = 3600 \rho B D \eta_V. \tag{3.6}$$

In Eqs.(3.5-3.6), $\mathcal{T}$ denotes the throw or stroke of the jaw crusher (in m); $S_F$ is the ore shape factor, defined as the ratio of the intermediate to minimum particle dimension (ranges from about 1.7 for cubic shapes to about 3.3 for slabby rock) [49]; $F_{max}$ is the maximum size of feed ore material (in $m$); $S_C$ is the opening of the scalping screen, which equals the distance between the grizzly bars; $\rho$ is the material bulk density ($t/m^3$); $B$ is the skirt width of the apron feeder; $D$ is the bed depth of material and $\eta_V$ is the volumetric efficiency. Note that all apron feeder parameters are referred to its discharging zone. $k$ is assumed to be constant. However, this may vary with the apron feeder speed during the operation. As can be seen from Fig. 3.2, the feed mass flow rate $T_{OVS}$ going to the jaw crusher is related to the feed mass flow rate $T_F$ from the apron feeder through the ore undersize fraction, as follows [49]:

$$T_{OVS} = (1 - \gamma)\, T_F, \tag{3.7}$$

where

$$\gamma = \frac{P_{80}}{F_{80\,USC}} = \frac{0.85\,(CSS + \mathcal{T})}{0.8 S_F F_{max}}, \tag{3.8}$$

with $F_{80\,USC} = 0.8 S_F F_{max}$.

In contrast to Eq.(3.4), $F_{80\,USC}$ in Eq.(3.8) denotes the $F_{80}$ for unscalped feed ore material (in $m$). Substituting Eqs.(3.5) and (3.8) in Eq.(3.7) yields:

$$T_{OVS} = \left(1 - \frac{1.0625\,(CSS + \mathcal{T})}{S_F F_{max}}\right) k V_F. \tag{3.9}$$

Hence, the mass flow rate from the vibrating grizzly (scalper), referred to as undersize mass flow rate $T_{UDS}$ can be expressed as:

$$T_{UDS} = \left(\frac{1.0625\left(CSS + \mathcal{T}\right)}{S_F F_{max}}\right) kV_F. \tag{3.10}$$

In this work, it is assumed that the scalping screen $S_C$ of the vibrating grizzly used is controllable in real-time. Hence, by setting $S_C$ to CSS so that the fines or feed material with size lower than CSS can always be removed by the vibrating grizzly, Eq.(3.4) becomes:

$$\begin{cases} P_{80} = 0.85\left(CSS + \mathcal{T}\right), \\ F_{80} = 0.8 S_F F_{max} + 0.2 CSS. \end{cases} \tag{3.11}$$

The total power consumption of the jaw crusher can be now expressed in terms of the two control variables, $V_F$ and CSS, by the following function:

$$f_P\left(V_F, CSS\right) = \frac{11 W_i}{\eta_D} \left[\left(\frac{1.0846.10^{-3}}{\sqrt{(CSS+\mathcal{T})}} - \frac{10^{-3}}{\sqrt{(0.8 S_F F_{max} + 0.2 CSS)}}\right) \times \left(1 - \frac{1.0625(CSS+\mathcal{T})}{S_F F_{max}}\right) kV_F + P_0\right], \tag{3.12}$$

with $\eta_D$, the overall drive efficiency (electric motor and transmission system) and $P_0$, the no-load mechanical power consumption of the jaw crusher [63], assumed to be constant for a given jaw crusher speed. Hence, the objective function given by Eq.(3.1) can be discretized as follows:

$$min\, J_C = \frac{11 W_i}{\eta_D} t_S \sum_{j=1}^{N_S} p_j \left[\left(\frac{1.0846.10^{-3}}{\sqrt{(CSS_j+\mathcal{T})}} - \frac{10^{-3}}{\sqrt{(0.8 S_F F_{max} + 0.2 CSS_j)}}\right) \times \left(1 - \frac{1.0625(CSS_j+\mathcal{T})}{S_F F_{max}}\right) kV_{F_j} + P_0\right], \tag{3.13}$$

where $N_S$ is the total number of sampling intervals; $j$ is the $j^{th}$ sampling interval; $p_j$ is the electricity price at $j^{th}$ sampling interval; and $t_S = \frac{t_f - t_0}{N_S}$ is the sampling time within the control horizon $[t_0, t_f]$.

#### 3.2.4.2 Constraints

**A. Control variable limits**

$$CSS^{min} \leq CSS_j \leq CSS^{max}, \ \ (1 \leq j \leq N_S), \tag{3.14}$$

$$V_F^{min} \leq V_{F_j} \leq V_F^{max}, \ \ (1 \leq j \leq N_S)\,, \tag{3.15}$$

where the supercripts "$min$" and "$max$" denote, respectively, the minimum and maximum of the variable. This notation applies to the rest of this chapter.

**B. Limits on maximum size of ore product, $P_{max}$**

Based on various data provided by manufacturers of jaw crushers, the product maximum size of the ore product, noted $P_{max}$, has been shown to be directly proportional to CSS with a proportional constant of 1.5, that is, $P_{max} = 1.5CSS$.[2] This constraint can therefore be written as:

$$1.5CSS_j \leq P_{max}^{up}, \ \ (1 \leq j \leq N_S)\,, \tag{3.16}$$

where $P_{max}^{up}$ is the upper bound of the maximum size of the ore product.

**C. Limits on mass storage capacity**

The dynamics of the mass stored in the ore pass and hopper system can be expressed in the discrete-time domain by a first order difference equation as follows:

$$M_{ROM(j)} = M_{ROM(j-1)} + t_S \left(T_{ROM(j-1)} - kV_{F_{j-1}}\right), \ \ (1 \leq j \leq N_S)\,. \tag{3.17}$$

By recurrence manipulation, the mass stored in the storage system at $j^{th}$ sampling interval can be expressed in terms of the initial mass, $M_{ROM(0)}$ as follows:

$$M_{ROM(j)} = M_{ROM(0)} + t_S \sum_{i=1}^{j} \left(T_{ROM(i)} - kV_{F_i}\right), \ \ (1 \leq j \leq N_S)\,. \tag{3.18}$$

Hence, the mass storage constraints are given as:

$$M_{ROM}^{min} \leq M_{ROM(0)} + t_S \sum_{i=1}^{j} \left(T_{ROM(i)} - kV_{F_i}\right) \leq M_{ROM}^{max}, \ \ (1 \leq j \leq N_S)\,. \tag{3.19}$$

**D. Limits on mass flow rate from the apron feeder**

$$T_F^{min} \leq kV_{F_j} \leq T_F^{max}, \ \ (1 \leq j \leq N_S)\,. \tag{3.20}$$

[2]Metso, C Series jaw crushers, <http://www.metso.com>

**E. Mass balance in the jaw crusher**

This equality constraint protects the machine's crushing chamber from obstruction [48]. The equation is given as follows:

$$T_{OVS(j)} = T_{PR(j)}, \ \ (1 \leq j \leq N_S)\,. \tag{3.21}$$

The analytical model of the product mass flow rate from the jaw crusher in terms of $CSS$ is expressed as [61]:

$$T_{PR} = 60Nw\,(CSS + 0.5\mathcal{T})\left(\frac{D_V\mathcal{T}}{G-(CSS+\mathcal{T})}\right)K_1K_2K_3\rho, \tag{3.22}$$

where $K_1 = 0.85 - \left(\frac{F_{av}}{G}\right)^{2.5}$, $K_2 = 1.92.10^{\frac{6.5\mathcal{T}}{G}}$ and $K_3$ is assumed to be 0.6 for softer materials such as coal and 1 for harder materials. In Eq.(3.22), $N$ is the speed of the jaw crusher, $D_V$ is the vertical depth between jaws, $G$ is the gap of the jaw crusher, $w$ is the width of the jaw crusher and $F_{av}$ is the average feed size (in $m$). Other parameters are the same as previously defined.

For simplicity, Eq.(3.22) can be approximated to a linear function of CSS, taking advantage of the fact that the sum $(CSS + \mathcal{T})$ is generally too small compared to $G$. This therefore leads to a simpler equation:

$$T_{PR} = 60K_4NwCSS + 30K_4Nw\mathcal{T}, \tag{3.23}$$

where $K_4 = \frac{D_V\mathcal{T}K_1K_2K_3\rho}{G}$.

For a given operational speed and material characteristics such as gradation, bulk density, crushability, moisture and clay content, jaw crusher manufacturers usually provide practical data expressing the relationship between $T_{PR}$ and CSS. Based on an ore density of 2.7 $t/m^3$ with a scalped feed, the curve fitting of the data for C-series jaw crushers[3] as shown by Fig. 3.4 proves a linear relationship of the form:

$$T_{PR} = aCSS + b. \tag{3.24}$$

In Fig. 3.4, the markers indicate the real data and the solid lines represent their corresponding curve fitting. It can be seen that Eq.(3.24) validates the assumption of neglecting the sum

[3]Metso, C Series jaw crushers, <http://www.metso.com>

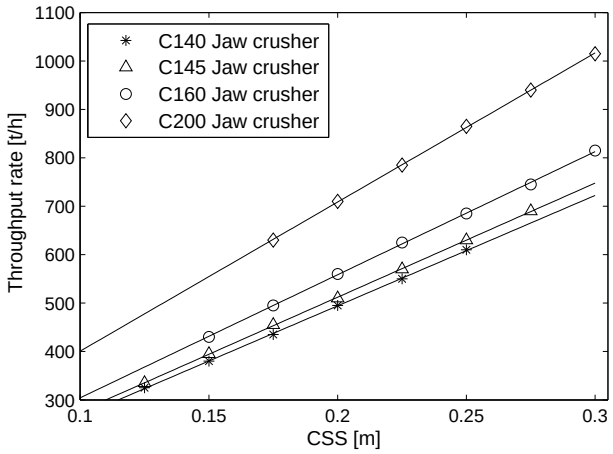


**Figure 3.4:** Fit of throughput rate (in metric-ton/h) of C-series jaw crushers

$(CSS + \mathcal{T})$ before $G$ since Eqs.(3.23) and (3.24) are the same by identification of $a = 60K_4Nw$ and $b = 30K_4Nw\mathcal{T}$. The coefficients $a$ and $b$ can therefore be found either based on analytical model or manufacturer's data. The equality constraint given by Eq.(3.21) is finally expressed as:

$$\left(1 - \frac{1.0625\,(CSS_j + \mathcal{T})}{S_F F_{max}}\right) kV_{F_j} = aCSS_j + b, \;\; (1 \leq j \leq N_S)\,. \tag{3.25}$$

**F. Limits on mass flow rate from the jaw crusher**

$$T_{PR}^{min} \leq aCSS_j + b \leq T_{PR}^{max}, \;\; (1 \leq j \leq N_S)\,. \tag{3.26}$$

**G. Total production requirement**

$$\sum_{j=1}^{N_S} \left(T_{UDS(j)} + T_{PR(j)}\right) t_S \geq M_{TPR}. \tag{3.27}$$

This can be rewritten as:

$$\sum_{j=1}^{N_S} \left(\frac{1.0625\,(CSS_j + \mathcal{T})}{S_F F_{max}} kV_{F_j} + aCSS_j + b\right) t_S \geq M_{TPR}. \tag{3.28}$$

#### 3.2.4.3 Reduction of the problem dimension

The equality constraint given by Eq.(3.25) indicates the interdependency between the two control variables namely, the CSS of the jaw crusher and the apron speed $V_F$. In order to

reduce the dimension of the problem and consequently, the computational time, $CSS$ can be expressed from Eq.(3.25) in terms of $V_F$ as follows:

$$CSS = \frac{kV_F\left(S_F F_{max} - 1.0625\mathcal{T}\right) - bS_F F_{max}}{1.0625kV_F + aS_F F_{max}}. \tag{3.29}$$

Hence, Eq.(3.29) is substituted in the objective function as well as in all constraints to eliminate CSS in such a way that the apron feeder speed $V_F$ is the only control variable. This therefore reduces the problem dimension by half, from $2N_S$ to $N_S$. Furthermore, after some mathematical simplification, the optimization model can finally be expressed as:

$$\begin{aligned} min\, J_C\left(V_{F_j}\right) = \tfrac{11W_i}{\eta_D} t_S \textstyle\sum_{j=1}^{N_S} p_j \quad & \left[\left(\frac{1.0846.10^{-3}}{\sqrt{\left(\frac{kV_{F_j}C - bS_F F_{max}}{1.0625kV_{F_j} + aS_F F_{max}} + \mathcal{T}\right)}}\right.\right. \\ & \left.\left. - \frac{10^{-3}}{\sqrt{\left(0.8S_F F_{max} + 0.2\frac{kV_{F_j}C - bS_F F_{max}}{1.0625kV_{F_j} + aS_F F_{max}}\right)}}\right)\right. \\ & \left. \times \left(a\frac{kV_{F_j}C - bS_F F_{max}}{1.0625kV_{F_j} + aS_F F_{max}} + b\right) + P_0\right], \end{aligned} \tag{3.30}$$

where $C = S_F F_{max} - 1.0625\mathcal{T}$, subject to

$$M_{ROM}^{min} \leq M_{ROM(0)} + t_S \sum_{i=1}^{j}\left(T_{ROM(i)} - kV_{F_i}\right) \leq M_{ROM}^{max},\ (1 \leq j \leq N_S), \tag{3.31}$$

$$kt_S \sum_{j=1}^{N_S} V_{F_j} \geq M_{TPR}, \tag{3.32}$$

$$\begin{aligned} & max\left(V_{F_1}^{min}, V_F^{min}, \tfrac{T_F^{min}}{k}, V_{F_3}^{min}\right) \leq V_{F_j} \\ & \leq min\left(V_{F_1}^{max}, V_F^{max}, \tfrac{T_F^{max}}{k}, V_{F_2}^{max}, V_{F_3}^{max}\right),\ (1 \leq j \leq N_S), \end{aligned} \tag{3.33}$$

where

$V_{F_1}^{min} = \frac{bS_F F_{max} + aS_F F_{max} CSS^{min}}{k(S_F F_{max} - 1.0625\mathcal{T}) - 1.0625kCSS^{min}}$,

$V_{F_1}^{max} = \frac{bS_F F_{max} + aS_F F_{max} CSS^{max}}{k(S_F F_{max} - 1.0625\mathcal{T}) - 1.0625kCSS^{max}}$,

$V_{F_2}^{max} = \frac{bS_F F_{max} + aS_F F_{max} P_{max}^{up}}{1.5k(S_F F_{max} - 1.0625\mathcal{T}) - 1.0625kP_{max}^{up}}$,

$V_{F_3}^{min} = \frac{aS_F F_{max} T_{PR}^{min}}{ak(S_F F_{max} - 1.0625\mathcal{T}) + 1.0625kb - 1.0625kT_{PR}^{min}}$ and

$V_{F_3}^{max} = \frac{aS_F F_{max} T_{PR}^{max}}{ak(S_F F_{max} - 1.0625\overline{T}) + 1.0625kb - 1.0625kT_{PR}^{max}}$.

### 3.2.5 Model for optimal switching control of a primary jaw crushing process

Unlike in the previous case, this model does not involve the energy model of the jaw crusher. The controller optimally coordinates the on/off status and working time (based on TOU tariff) of the jaw crushing process in order to minimize the associated energy cost. Hence, for this case, the energy cost is reduced through load shifting based on the TOU electricity tariff.

Because of the high no-load power of the jaw crusher, ranging from 40 to 50 % of its rated power [51, 52], the switching frequency of this machine has to be minimized as much as possible in order to reduce the impact of mechanical stresses and high starting currents on the electric motor. The time delay is another concern when switching off the jaw crusher. The feeding equipment has to be stopped a few minutes before switching off the jaw crusher. This precaution allows the crusher sufficient time to process all the ore material present in the crushing chamber, to avoid overload condition for its next starting up.

To reduce the negative effect of the on/off switching frequency on the crusher drive system (electrical motor and drive transmission), as well as on the power supply systems, a soft starter is assumed to be available to the jaw crusher. In contrast to the VL-based optimal control model, here, the sampling time will be chosen to be large enough in such a way as to further minimize the drawback of the multiple switching associated with the switching controller. The consideration of a larger sampling time will also allow one to neglect the time delay between switching off the feeder and jaw crusher, that can range from 1 to 3 minutes, depending on the size of the machine and working conditions. For these reasons, in the process system defined in Fig. 3.2, the feeding equipment and jaw crusher can share the same switching function. This means that they are considered to be synchronously switched on or off when the relevant time delay is ignored.

#### 3.2.5.1 Objective function

Here, the problem consists of optimally coordinating the on/off status of the jaw crusher in a synchronous way with that of the feeding equipment, in such a way as to minimize the crushing energy cost based on the TOU tariff. This is formulated as follows:

$$min\, J_C = \frac{1}{\eta_D}\sum_{j=1}^{N_S}\left(P_{Net-P_{max}^{up}} + P_0\right) u_j p_j t_S = \frac{1}{\eta_D} P_t t_S \sum_{j=1}^{N_S} p_j u_j, \tag{3.34}$$

where $P_t = P_{Net-P_{max}^{up}} + P_0$ is the total crushing power consumption of the jaw crusher. In Eq.(3.34), $P_{Net-P_{max}^{up}}$ denotes the net crushing power consumption of the jaw crusher which corresponds to the upper bound of the maximum product size $P_{max}^{up}$. The $CSS$ is therefore set in such away as to satisfy the required $P_{max}^{up}$. The throughput flow rate of the jaw crusher is accordingly obtained. In Eq.(3.34), $u_j$ is a discrete-switching function that takes the value of either 0 or 1. $u_j = 1$ means the machines are switched on during the $j^{th}$ sampling interval, while $u_j = 0$ means the machines are switched off. The other notations are the same as in the previous problem.

#### 3.2.5.2 Constraints

These are the limits on the mass storage capacity and also the requirement on the total mass production of ore.

**A. Mass storage capacity**

$$M_{ROM}^{min} \leq M_{ROM(0)} + t_S \sum_{i=1}^{j}\left(T_{ROM(i)} - T_F u_i\right) \leq M_{ROM}^{max},\ (1 \leq j \leq N_S)\,. \tag{3.35}$$

**B. Requirement on total production**

$$t_S \sum_{j=1}^{N_S} T_F u_j \geq M_{TPR}. \tag{3.36}$$

Note that the mass balance $T_F = T_{OVS} + T_{UDS}$ is supposed to be verified within the control interval.

### 3.2.6 Model for current control of a primary jaw crushing process

In practice, jaw crushers operate continuously in mining and aggregate industries. The feed rate is usually controlled in such a way as to prevent the jaw crusher from being overloaded while achieving the plant production target. Hence, the current control model is formulated in the same way as the VL-based optimal model defined in Section 3.2.4, the only difference being that the total production target is considered as the control objective to be achieved. This is formulated as minimizing the quadratic deviation function, $J_{PR}$, between the actual plant production and the total plant production target $M_{TPR}$, expressed as follows:

$$min\, J_{PR} = \left( kt_S \sum_{j=1}^{N_S} V_{F_j} - M_{TPR} \right)^2, \tag{3.37}$$

subject to constraints (3.31)-(3.33).

## 3.3 SIMULATION RESULTS

### 3.3.1 Algorithms

Several optimization algorithms can be used to solve the problems defined in this work.

Since the VL-based optimal control problem has a nonlinear objective function, based on convexity assumption, the *fmincon* function of MATLAB R2013 Optimization Toolbox is used. Its canonical form is given as follows:

$$min\, f\,(X) \tag{3.38}$$

subject to

$$\begin{cases} AX \leq b\ (linear\, inequality\, constraint)\,, \\ A_{eq}X = b_{eq}\ (linear\, equality\, constraint)\,, \\ C\,(X) \leq 0\ (nonlinear\, inequality\, constraint)\,, \\ C_{eq}\,(X) = 0\ (nonlinear\, equality\, constraint)\,, \\ L_b \leq X \leq U_b\ (lower\, and\, upper\, bounds)\,. \end{cases} \tag{3.39}$$

For VL-based optimal control, the vector $X$ contains the feeder speed for all sampling intervals. Three linear inequality constraints of which two of (3.31) and one of (3.32) are integrated

into $A$ and $b$. The lower and upper boundary constraints (3.33) are incorporated into $L_b$ and $U_b$. After solving the problem, recall that the corresponding CSS control variables at each sampling interval are obtained using Eq.(3.29).

The optimal switching control is solved using the *ga* function of MATLAB Optimization Toolbox that can easily handle mixed-inter, integer or binary optimization problems with lower computational time.[4] The canonical form of *ga* is the same as for the $fmincon$ function, except that for this problem, the control variable is the on/off status of the jaw crushing station, denoted by $u_j$ which is set to be an integer number bounded within [0, 1].

The objective function of the current control model is a nonlinear function. Hence, the $fmincon$ function of MATLAB Optimization Toolbox is also used for the current control model.

### 3.3.2 Data presentation

#### 3.3.2.1 Time-of-use electricity tariff

One of the important parameters in the optimal energy control problem formulated in this work is the TOU electricity tariff. The recent Eskom Megaflex Active Energy-TOU tariff (non-local authority rates) with VAT included is used for a high-demand season weekday in this case study. The high-demand season (from June to August) is chosen since the peak period is charged at a very high cost compared to the lower demand season. The energy cost management for the high-demand season is therefore crucial for electricity bill reduction. However, a slight modification is made to this TOU tariff in order to appreciate the effectiveness of the model better. The time interval of the standard period, [20, 22] is considered to be a peak period. This is given as:[5]

$$p(t) = \begin{cases} p_o = 0.3656R/KWh \; if \; t\epsilon\,[0,6] \cup [22,24]\,, \\ p_s = 0.6733R/KWh \; if \; t\epsilon\,[6,7] \cup [10,18]\,, \\ p_p = 2.2225R/KWh \; if \; t\epsilon\,[7,10] \cup [18,22]\,, \end{cases} \tag{3.40}$$

where $p_o$, $p_s$ and $p_p$ are, respectively, the off-peak, standard and peak TOU active energy tariffs for the higher demand season (June-August); $R$ is the South African currency rand

[4] Matlab, Mixed Integer Optimization, <http://www.mathworks.com>

[5] Eskom, Tariffs & Charges Booklet 2013/2014, <http://www.eskom.co.za>

and $t$ is the time of any weekday in hours (from 0 to 24).

The control horizon $[t_0, t_f]$ and sampling time $t_S$ of, respectively, 24 $h$ and 10 $min$ are used for VL-based optimal control and current control problems. As discussed in Section 3.2.5, a relatively large sampling time of 30 $min$, not greater than the shortest time period of the change in the TOU tariff function $p(t)$, is used for optimal switching control in order to reduce the machine switching frequency. This means that the time period between two consecutive start-ups of the jaw crusher cannot be less than 30 minutes.

#### 3.3.2.2 Ore pass storage system and ore characteristics

Note that the hopper capacity may be neglected compared to that of the ore pass. In this study, the ore pass capacity of one of South Africa's deep mines processing gold is considered [64]. For this ore pass, the diameter is 2.4 $m$ and the length or height is 170 $m$. To ensure free flow, it is reported that the ratio between the ore pass dimension diameter $D_{OP}$ and the largest ROM ore size $F_{max}$ lies between 3 and 10 [55]. Hence, with a minimum ratio of 3, the maximum ore size of ore gold is assumed to be 0.8 $m$for this case study. With the ore bulk density of gold ore being 2.7 $t/m^3$,[6] the maximum storage capacity of the ore pass is calculated as $170 \times 2.7 \times \pi (2.4)^2 /4 = 2075$ $t$. The minimum storage capacity is set to 10% of the maximum capacity. The ore is assumed to be of cubic shape, hence a shape factor $S_F$ of 1.7 is considered. The reader is referred to Section 3.2.4.1 for the definition of the rock/ore shape factor $S_F$. The Bond's work index $W_i$ of gold ore is 14.83 $KWh/short-ton$ [49].

#### 3.3.2.3 Jaw crusher, apron feeder and vibrating grizzly

For simulation purposes, a primary jaw crushing station is assumed to be installed under the ore pass described above.

In general, the largest feed size (lump size) is the major index for the choice of processing equipment such as crushers, feeders and scalpers; the flow rate capacity follows.

[6] Ari Jaakonmaki and Metso, Aspects of Underground Primary Crusher Plant Design,<http://www.miningcongress.com>

**A. Jaw crusher**

For a jaw crusher, the maximal feed size $F_{max}$ should be equal to or less than 85% of its gap $G$, that is, $F_{max} \leq 0.85G$ [49]. Hence, with $F_{max} = 800\ mm$, $G$ should be larger than 940mm. With this, the C160 jaw crusher is used. Technical data and other specifications of C160 are as follows:[7] $G = 1200\ mm$, the installed power is 250kW, $CSS^{max} = 300\ mm$, $CSS^{min} = 150\ mm$, extended to 100 $mm$ for simulation purposes (since smaller CSS is practically possible with a machine reduction ratio that can go up to 10/1 [51]). The throw $\mathcal{T}$ is obtained to be 0.06 $m$ (60 $mm$) based on the formula, $\mathcal{T} = 0.0502G^{0.85}$ [49]. The crusher speed $N$ is 220 $rpm$, the no-load power $P_0$ of the jaw crusher is assumed to be 40% of its rated power, that is, 100 $kW$ for C160 jaw crusher. The fitting coefficients of the C160 throughput capacity found from Fig. 3.4 are: $a = 2543$ and $b = 50$. Hence, the maximum and minimum flow rates of the C160 jaw crusher are found to be, respectively, 813 $t/h$ and 304 $t/h$. The overall drive efficiency $\eta_D$ is assumed to be 0.95.

**B. Apron feeder**

An apron feeder with a skirt width $B$ bigger than 1600 $mm$ is considered (since $B \geq 2F_{max}$). This corresponds to the apron feeder span width of 1829 $mm$.[8] With a clearance of 100 $mm$ between the pan width and skirt, $B$ is found to be 1729 $mm$ for this apron feeder. The bed depth $D$ is obtained as $0.75B = 1297\ mm$. The maximum speed of the feeder is 60 $fpm = 0.3048\ m/s$ which corresponds to $T_F^{max} = 5000\ t/h$ , with $\eta_V = 0.75$ when using Eq.(3.5).

#### 3.3.2.4 Vibrating grizzly or Scalper

The vibrating grizzly is used for scalping (removing) fines from the ROM ore without controlling the flow rate. This machine is therefore considered as a simple separation point with appropriate stroke length, speed, and inclination angle for scalping efficiency.

[7] Metso, C Series jaw crushers, <http://www.metso.com>
[8] Metso, World-Class Apron Feeders, <http://www.metso.com>

#### 3.3.2.5 Ore bin and ore production requirement

The capacity of the ore bin is assumed sufficient to store the total plant production target $M_{TPR}$ for 24 $h$. The maximum of ore production is to be achieved by meeting equipment constraints and product quality. The product quality is expressed in terms of the maximum size of product material $P_{max}$ given by Eq.(3.16), which should be equal or less than 400 $mm$ (0.4 $m$).

### 3.3.3 Results and discussion

Usually, an ore pass has several tipping points where a mass flow rate $T_{ROM}$ is dumped into it by LHD vehicles from different stops. The intermittent characteristic of LHD feeding devices makes $T_{ROM}$ uncontrollable but predictable. For all simulation cases, the forecast of the feed rate $T_{ROM}$ is assumed to vary around 700 $t/h$ as given bellow:

$$T_{ROM}(t) = \begin{cases} 680t/h \; if \; t\epsilon\,[0,6]\,, \\ 720t/h \; if \; t\epsilon\,[6,12]\,, \\ 700t/h \; if \; t\epsilon\,[12,18]\,, \\ 690t/h \; if \; t\epsilon\,[18,24]\,, \end{cases} \tag{3.41}$$

where $t$ is the time of any weekday in hours (from 0 to 24). For all simulation scenarios in this work, the initial ore mass in the ore pass storage system $M_{ROM(0)}$ is assumed to be 50% of the maximum ore pass capacity $M_{ROM}^{max}$, while the total plant production target $M_{TPR}$ is fixed to 15000 $t$ for 24 hours.

#### 3.3.3.1 Performance analysis of the optimal control techniques

***Case I: Ore pass with maximum storage capacity of 2017 t***

Figs. 3.5 and 3.6 show the simulation results for the current control and VL-based optimal control strategies. The legends of Fig. 3.5 also apply to Fig. 3.6. The result for optimal switching control is shown in Fig. 3.7. Tables 3.1-3.3 give the performance of the optimal control techniques used. For the optimal switching control technique, a CSS of 0.266 $m$ that limits the maximum product size from the C160 jaw crusher to 0.4m is used. The corresponding throughput rate and net crushing power consumption are found, respectively,

to be 726.4 $t/h$ and 114.67 $kW$. The undersize fraction is therefore found to be 0.2536, which based on mass balance, yields a mass flow rate from apron feeder $T_F$ of 973.2 $t/h$, feeder speed $V_F$ of 0.06 $m/s$, and undersize feed rate $T_{UDS}$ of 246.8 $t/h$. Note that the dotted lines in figures showing the simulation results, denote the maximum and minimum of the variable.

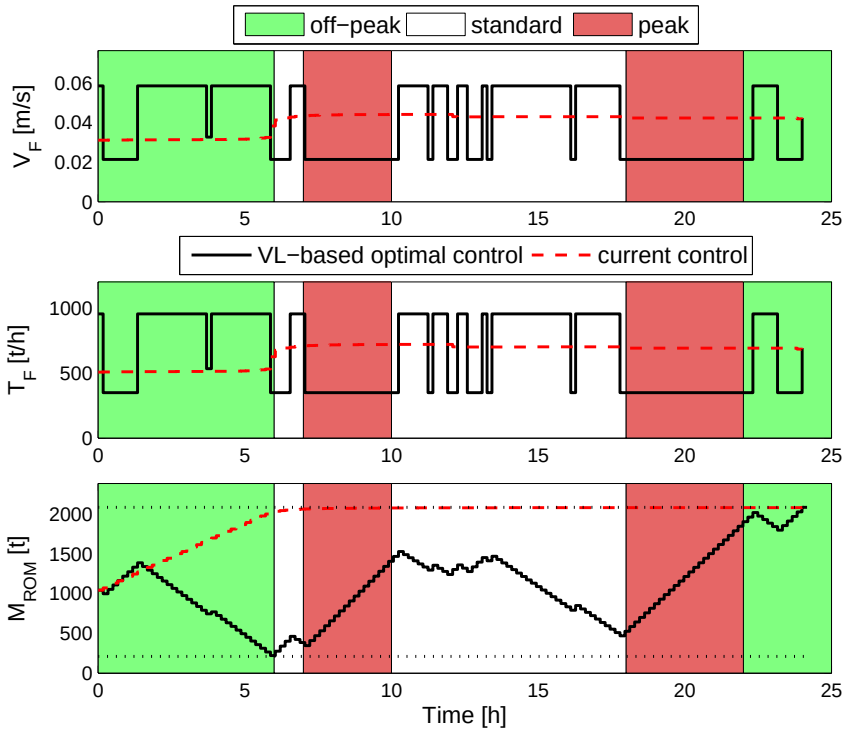


**Figure 3.5:** VL-based optimal control and current control techniques - case I

The feasibility of both optimal control approaches is shown through Figs. 3.5-3.7. As can be seen from Figs. 3.5 and 3.6, with the current control strategy, the crushing plant continuously runs without consideration of the TOU tariff. It is easy to notice that the feeder speed $V_F$, feeder flow rate $T_F$ and the crusher flow rate $T_{PR}$ are almost evenly distributed for a long period within the control interval. This will result in high energy cost, as the peak-load is not reduced or shifted, since the TOU tariff is not taken into account in the control scheme. However, the VL-based optimal controller shifts as much of the crusher load $T_{PR}$ as possible out of peak period by optimally decreasing the feeder speed $V_F$ and hence the feeder flow rate $T_F$ and the jaw crusher flow rate $T_{PR}$ during peak periods in order to minimize the crushing energy cost. The feeder speed is increased for a long period during off-peak and standard

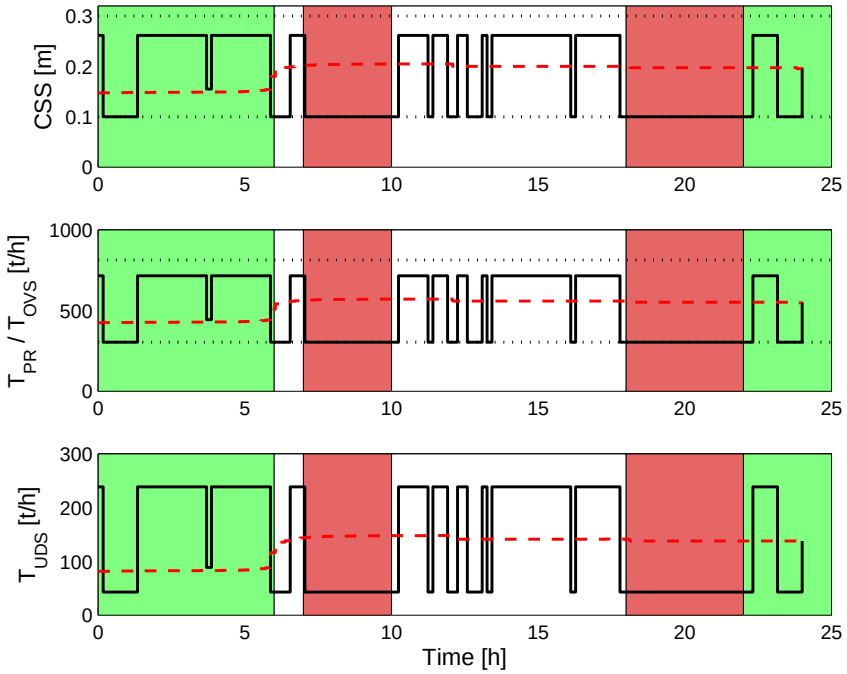


**Figure 3.6:** VL-based optimal control and current control techniques - case I (continued)

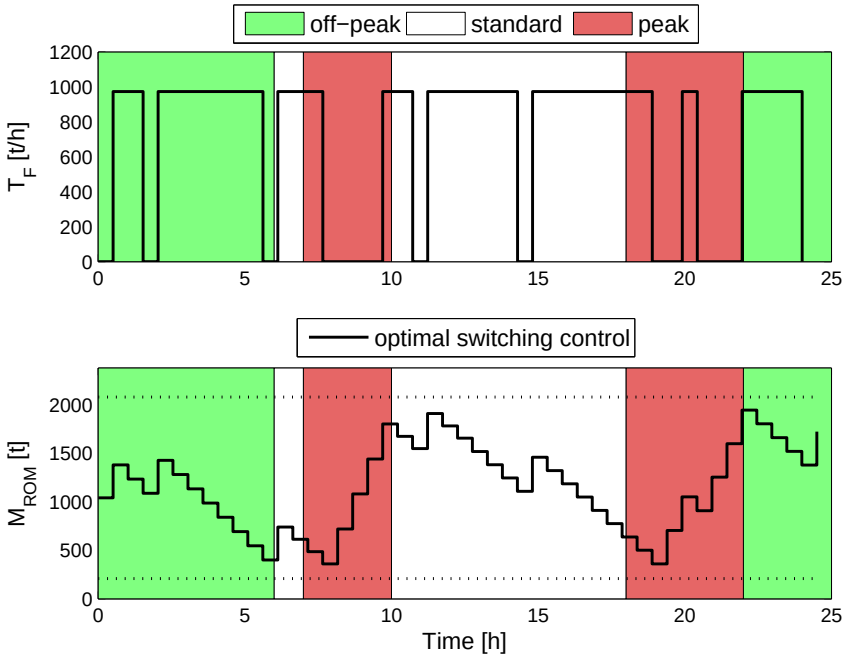


**Figure 3.7:** Optimal switching control technique - case I

periods in order to meet the total production target of the station, as given in Table 3.1, at a cheaper energy cost. During these periods, the CSS of the jaw crusher will continuously follow the pattern of $V_F$, as shown from the first graphs of Figure 3.5 and Fig. 3.6, in order to meet the mass balance constraint of the jaw crusher (input flow rate $T_{OVS}$ = output flow rate $T_{PR}$) constantly. This also demonstrates that the relationship between the CSS of the jaw crusher and the apron feeder speed $V_F$, given by Eq.(3.29), is almost linear, which will lead the mass flow rates $T_F$, $T_{PR}$, $T_{OVS}$, $T_{UDS}$ to have a linear relationship with either of the two control variables ($V_F$ and CSS) too, as can be seen from Figs. 3.5 and 3.6. For this reason, achieving a relatively high energy cost reduction with a VL-based optimal controller is less likely because the decrease of $V_F$ and hence $T_F$ and $T_{PR}$ will be restricted by the constraints imposed on the $CSS$ of jaw crusher. As given in Tables 3.2 and 3.3, 6.09 % of cost saving and 2.54 % of energy saving are achieved. It is therefore worth mentioning that more than half of the energy cost reduction is due to the optimal shifting of the crusher load based on the TOU tariff, whilst the rest comes from the 2.54 % of energy saving.

With respect to the mass storage dynamics given by the second graph of Fig. 3.5, the same conclusion as previously discussed can be drawn. It is shown that, unlike the current control strategy, during peak period the ore mass $M_{ROM}$ is stored instead of being fed to the crusher, while in off-peak and standard periods, a large amount of ore material is drawn from the ore pass storage system and fed to the crusher owing to the lower energy cost. The effectiveness of the algorithm is also demonstrated with regard to the constraints. Figs. 3.5 and 3.6 show that all control and dependent variable constraints lie within their limits. Although the predicted maximum product size from the jaw crusher is not plotted, the first graph of Fig. 3.6 indicates that the CSS of the jaw crusher will never go beyond 0.2661 $m$, which corresponds to a maximum ore product size of 0.399 $m$, less than 0.4 $m$ (fixed as requirement).

For the optimal switching control strategy, it is inferred from Fig. 3.7 that during the peak period, the jaw crushing station is on off-status for a longer period than when it is on on-status so that the ore mass $M_{ROM}$ is stored as much as possible. However, this is not the case for off-peak and standard periods, where the on-status period is rather longer than the off-status period because of the lower energy cost and also to meet the 24 $h$ production capacity. According to Tables 3.2 and 3.3, a cost saving of 45.92 % and energy saving of 30.12 % are achieved with the optimal switching control of the jaw crushing station.

In contrast to findings in reference [13] for optimal energy control of belt conveyors, it is shown in this work that the optimal switching control strategy yields more cost saving and energy saving than the VL-based optimal control strategy. However, this is achieved at the cost of switching the machines. Note that the VL-based optimal control in [13] is referred to as VSD-based optimal control. Two reasons could explain the higher savings achieved by the optimal switching control approach. The first and major reason is that compressive crushers such as jaw crushers are inefficient machines because of their no-load power consumption ranging between 40 and 50 % of the total power consumption. This means that running continuously, the jaw crusher will lead to almost 50 % of energy consumption that does not contribute to the work done and is therefore regarded as a waste of energy and money. Hence, by optimally switching the jaw crushing station, both net crushing and no-load power consumptions are shifted, while with the VL-based optimal control approach, only the net crushing power consumption can be controlled. The second reason is that the net crushing power of the jaw crusher is not controllable to zero with VL-based optimal control. This is due to the lower constraint imposed on CSS, preventing the crusher throughput rate $T_{PR}$ from being controlled to zero during the peak period (see Fig. 3.6), in order to achieve more energy cost reduction.

***Case II: Ore pass with maximum storage capacity doubled to 4150 t***

In order to analyse the influence of the size of the ore pass storage system on the performance achieved by the two optimal energy control strategies, the previous storage capacity considered in case I is doubled. Figs. 3.8-3.10 show the results for this case study.

As discussed in case I, it is also seen that the energy cost is reduced when using the VL-based optimal control strategy compared to the current control strategy. This is because the load is shifted as much as possible out of the peak period when using VL-based optimal control, while with the current control technique, the load is kept almost constant along the control interval. However, with the same initial condition (the initial mass stored in the ore pass is half of its maximum storage capacity) and production requirement (greater or equal to 15000 $t$), it is obvious that the increase in storage capacity leads to a higher initial amount of ore material compared to case I. This means that with case II, at the beginning of the control interval, a larger amount of ore material will be available and therefore processed during the off-peak period, leading to a smaller amount of ore material having to be processed during

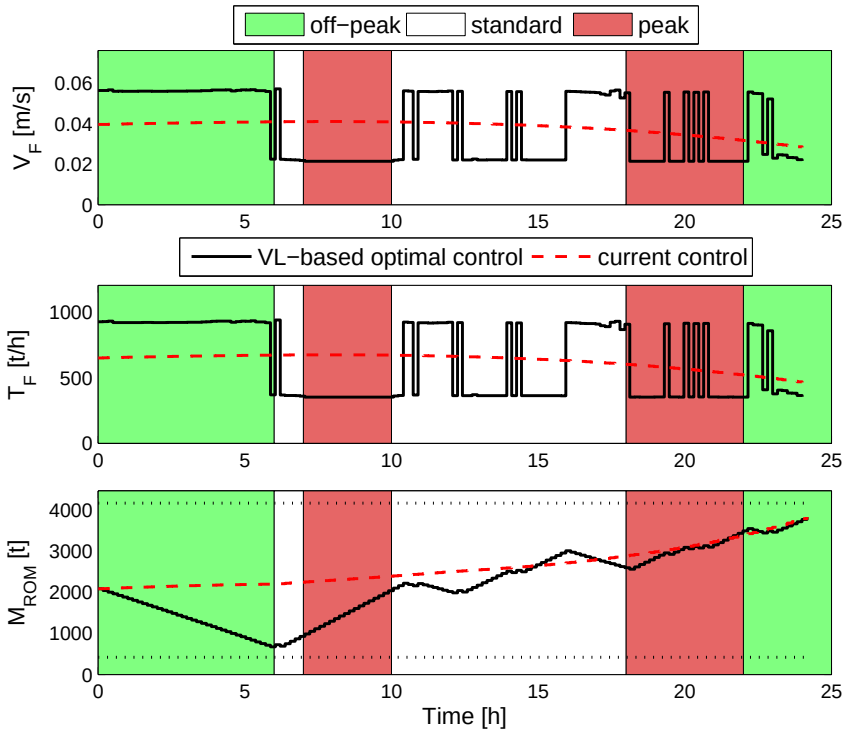


**Figure 3.8:** VL-based optimal control and current control techniques - case II

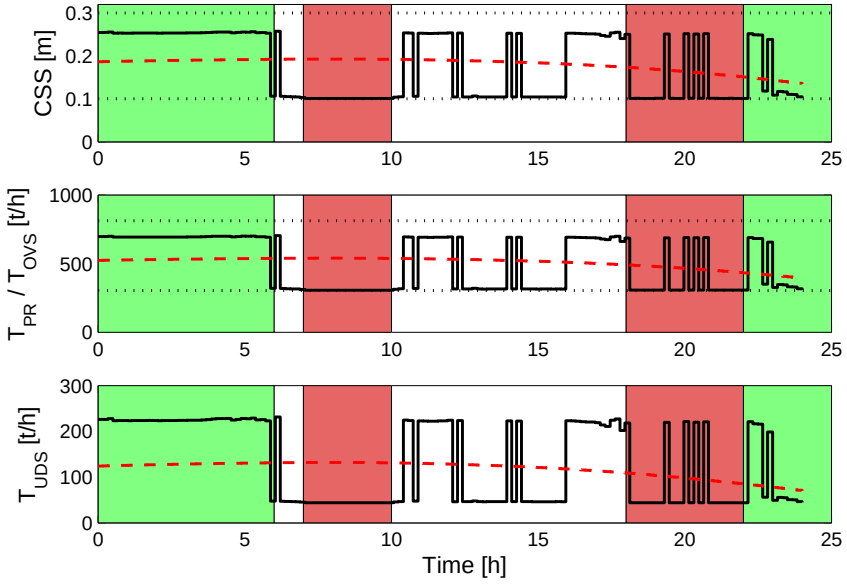


**Figure 3.9:** VL-based optimal control and current control techniques - case II (continued)

the standard period. This can be seen by comparing Figs. 3.5-3.6 of case I with Figs. 3.8-3.9 of case II, where it is shown that in case I, the apron feeder and jaw crusher operate

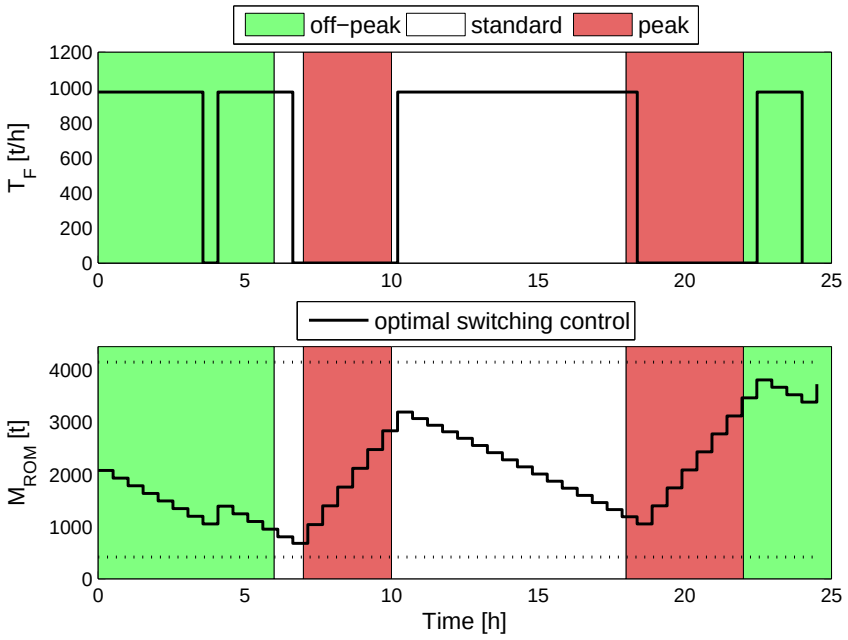


**Figure 3.10:** Optimal switching control technique - case II

for a shorter period at, respectively, higher speed $V_F$, feeder flow rate $T_F$, and crusher flow rate $T_{PR}$ during off-peak period (from 0 to 6 $h$) because of the lower initial stored material, compared to case II. Hence, in order to meet the production requirement, the same figures show that during standard period, in case I, the apron feeder and jaw crusher operate for a longer period at higher load ($T_F$ and $T_{PR}$), compared to case II.

**Table 3.1:** Total ore production and corresponding energy cost and consumption

| Techniques | Total ore production (t) | Energy cost (R) | Energy consumption (kWh) |
|---|---|---|---|
| **CASE I: $\mathbf{M_{ROM}^{max} = 2075}$ t** | | | |
| Current control | 15703 | 5368.1 | 5217.9 |
| VL-based optimal control | 15703 | 5041.2 | 5085.5 |
| Optimal switching control | 16058 | 2968.4 | 3728.5 |
| **CASE II: $\mathbf{M_{ROM}^{max} = 4150}$ t** | | | |
| Current control | 15000 | 5304.6 | 5194.0 |
| VL-based optimal control | 15004 | 5053.9 | 5072.2 |
| Optimal switching control | 15085 | 1871.5 | 3502.5 |

**Table 3.2:** Cost savings of the optimal control techniques

| Techniques | Unit energy cost (R/t) | Cost saving (%) |
|---|---|---|
| **CASE I: $M_{ROM}^{max} = 2075$ t** | | |
| Current control | 0.3419 | / |
| VL-based optimal control | 0.3210 | 6.0893 |
| Optimal switching control | 0.1849 | 45.927 |
| **CASE II: $M_{ROM}^{max} = 4150$ t** | | |
| Current control | 0.3536 | / |
| VL-based optimal control | 0.3368 | 4.7516 |
| Optimal switching control | 0.1241 | 64.916 |

**Table 3.3:** Energy savings of the optimal control techniques

| Techniques | Unit energy consumption (kWh/t) | Energy saving (%) |
|---|---|---|
| **CASE I: $M_{ROM}^{max} = 2075$ t** | | |
| Current control | 0.3323 | / |
| VL-based optimal control | 0.3239 | 2.5375 |
| Optimal switching control | 0.2322 | 30.125 |
| **CASE II: $M_{ROM}^{max} = 4150$ t** | | |
| Current control | 0.3463 | / |
| VL-based optimal control | 0.3381 | 2.3720 |
| Optimal switching control | 0.2322 | 32.945 |

Since in case II, a larger amount of ore material is shifted from standard and peak periods to off-peak period when compared to case I, one would expect more cost saving to be achieved in case II. However, Table 3.1 shows that the energy cost and energy consumption in case II are almost equal to those obtained in case I. This is because, with VL-based optimal control in case II, a slightly larger amount of load is processed during [18, 22 h] peak period, at a very high energy cost, in order to meet the production requirement. One of the reasons why the increase in storage capacity does not improve the energy and cost savings is that the optimization search space is severely restricted by the constraints imposed on CSS, as

previously explained.

From Tables 3.2 and 3.3, it is noticed that the increase in storage capacity leads to a slight decrease in cost saving, by 1.3377 % (from 6.0893 to 4.7516 %) and energy saving, by 0.1655 % (from 2.5375 to 2.3720 %) compared to case I. This is explained by the lower production capacity achieved in case II (15004 $t$) compared to case I (15703 $t$), while both energy cost and energy consumption for the two cases are almost the same as previously mentioned.

With the optimal switching control strategy, Fig. 3.10 shows that the increase of ore pass storage capacity will have a positive impact in reducing the switching number of the jaw crushing station. In case I, the jaw crushing station is switched on eight (8) times, while in case II, the station is switched on four (4) times only. Compared to Fig. 3.7 of case I, Fig. 3.10 of case II shows that almost all peak load is shifted out from the peak-time period, which therefore explains the increase of the energy cost saving from 45.92 % to 64.9 %, as shown in Table 3.2. However, it is shown in Table 3.3 that increasing the ore pass capacity does not yield a significant improvement in energy saving compared to case I.

#### 3.3.3.2 Corollary

The simulation results show that because of the high no-load power consumption of the jaw crusher, the optimal switching control of the jaw crushing process can achieve considerable energy saving and cost saving compared to VL-based optimal control.

However, switching the jaw crusher will result in a severe impact on practice. During the starting period, the high no-load power consumption of the jaw crusher will be responsible for high current transients or starting current and torque pulsations on the jaw crusher itself, the drive electrical motor, electrical power supply system and even the concrete foundation supporting the crusher.

On the one hand, a high starting current will lead to electrical stress on the electrical motor winding and power system components such as transformers, electrical cables, transmission lines, generators, breakers, etc. On the other hand, high starting torque pulsations will lead to mechanical stress on mechanical drive systems such as the drive belt, bearings and shafts of the motor and crusher. Moreover, the vibrations caused by the high amplitude of the pulse

of the starting motor torque will be transmitted to the concrete foundation of the crusher and lead to pavement vibration and noise. This will therefore have a negative impact on the practical working environment.

Nowadays, a soft starter is used to solve the aforesaid problem [65]. Another option is to use a VSD. The use of a soft starter or VSD device makes it possible to smooth the motor acceleration caused by the high transient accelerating torque, while reducing the starting current of the electrical motor at the same time. The reduction in the pulse magnitude of the motor torque will also decrease the vibration and noise level in the working environment. Hence, some of the benefits from reducing the mechanical stress will be the improvement of the lifetime and reliability of the mechanical drive components due to wear rate reduction [66].

Smoothing the accelerating torque will result in reduction of the starting current, which will lead to minimization of the electrical stress on both electrical motor winding and power system components. One of the benefits from this is the EE improvement, since less line current is drawn from the power supply systems. It will also allow several crusher motors to be started more frequently for their optimal energy management, therefore allowing overall LM within a cluster approach.

In practice, if the jaw crusher is not equipped with a soft starter or VSD device, extra capital cost needs to be considered. However, for a constant speed application such as the jaw crushing process, the soft starter can be regarded as competitive in terms of cost and efficiency compared to VSD. Furthermore, a very short payback period can be expected because of the larger energy and cost savings achieved by optimal load shifting, but also the cheaper initial capital cost of the soft starter.

## 3.4 SUMMARY

In this chapter, two optimal control techniques for the TOU-based optimal energy management of a jaw crushing station in deep mines under both physical and operating constraints are developed. The first technique is referred to as a VL-based optimal control, while the second is optimal switching control.

Two scenarios are carefully studied in order to analyse the influence of storage capacity on the developed models. With the initial storage capacity, it is shown that 6.09 % and 2.54 % of cost and energy savings are, respectively, obtained when the VL-based optimal control strategy is used. With the optimal switching control technique, 45.92 % cost saving and 30.12 % energy saving are achieved. When the initial storage capacity is doubled, the VL-based optimal control does not show any improvement on either energy consumption or cost, while with the optimal switching control strategy, an energy cost saving of 64.9 % is achieved compared to 45.92 % in the initial case (case I).

Hence, it is shown through simulation results that, unlike the VL-based optimal controller, the optimal switching controller has greater potential to achieve a high reduction in both the energy consumption and cost of a jaw crushing process. However, this is achieved at the cost of switching the machines. With the same ore production requirement, the influence of using a larger storage capacity is seen to be of considerable benefit in reducing the switching frequency of the process and further achieving more energy cost saving.

# CHAPTER 4

# OPTIMAL ENERGY MANAGEMENT OF A VSI CRUSHING PROCESS

## 4.1 INTRODUCTION

Contrary to Chapter 3, where optimal energy management models of a jaw crushing process are developed, this chapter deals with the energy management optimization of a VSI crushing process. The main difference between the two processes is that, while jaw crusher machines are based on compressive action in order to break the ore/rock material, VSI crushers break the rock by impact action. This makes the operating principle of the two machines different. Another major difference is that jaw crushers are mainly intended for primary crushing circuits while VSI crushers are secondary or tertiary crushing machines.

VSI crusher is one of the most frequently used crushing machines in the last stage (tertiary) of crushing processes in both mining and aggregate industries. This is due to its high technology efficiency, ability to yield a large amount of fines (valuable for mining industries) and product with a cubical shape (valuable for aggregate industries). However, the possibility of improving the efficiency operation of the VSI crushing process during its operation is not covered in the literature.

In this chapter, first, the energy model of a VSI crusher is derived from the Euler turbine equation. The model validation is done through the manufacturer's data. Secondly, the optimal control model is formulated with the control variables being the belt conveyor feed rate, the material feed rate into the VSI crusher, the bi-flow or cascade feed rate and the rotor tip speed of the crusher. Both physical operational/technical constraints are taken into

account in the model. Through a case study, the optimal solution is compared to the current control solution in order to evaluate the effectiveness of the optimal control model. The work presented in this chapter has been published in [67].

## 4.2 MODEL DEVELOPMENT

### 4.2.1 System description

The operating principle of the VSI crusher is given in [5, 68, 69, 70, 71]. Fig. 4.1 shows a 3-D

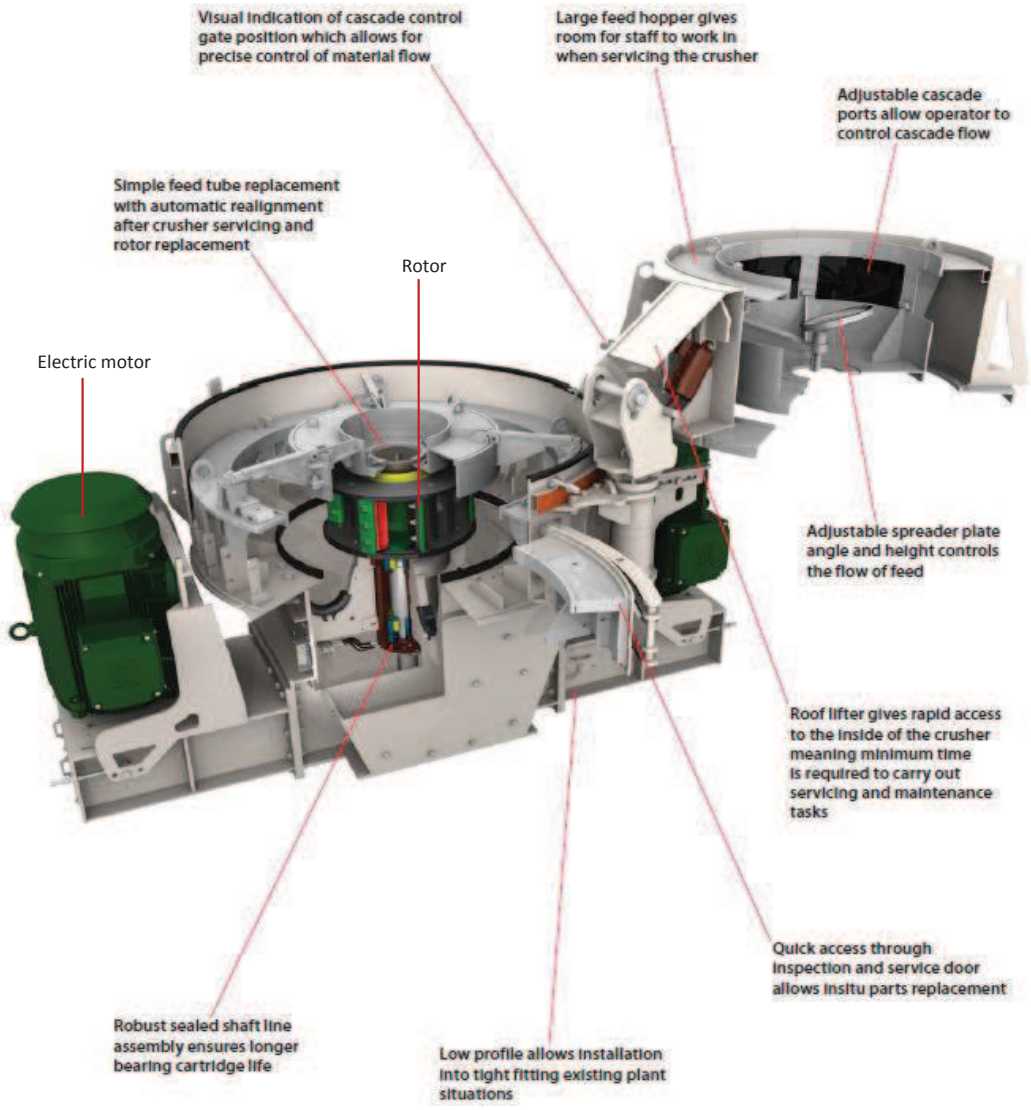


**Figure 4.1:** Schematic of a VSI crusher

schematic of a VSI crusher. [1] In this type of crushing machine, the ore/rock material falls vertically into the rotor through the feed hopper and then accelerated to an edge speed of the high-speed rotor of about $50 - 85\ m/s$, before being projected towards the surrounding rock bed formed during operation. However, during operation, a fraction of material does not pass through the rotor, and this is crushed through collision action with the projected rock particles from the rotor. This fraction is commonly referred to as cascade flow or bi-flow. Rock breaking in a VSI crusher is therefore achieved through rock-to-rock impact; hence the name impact crusher.

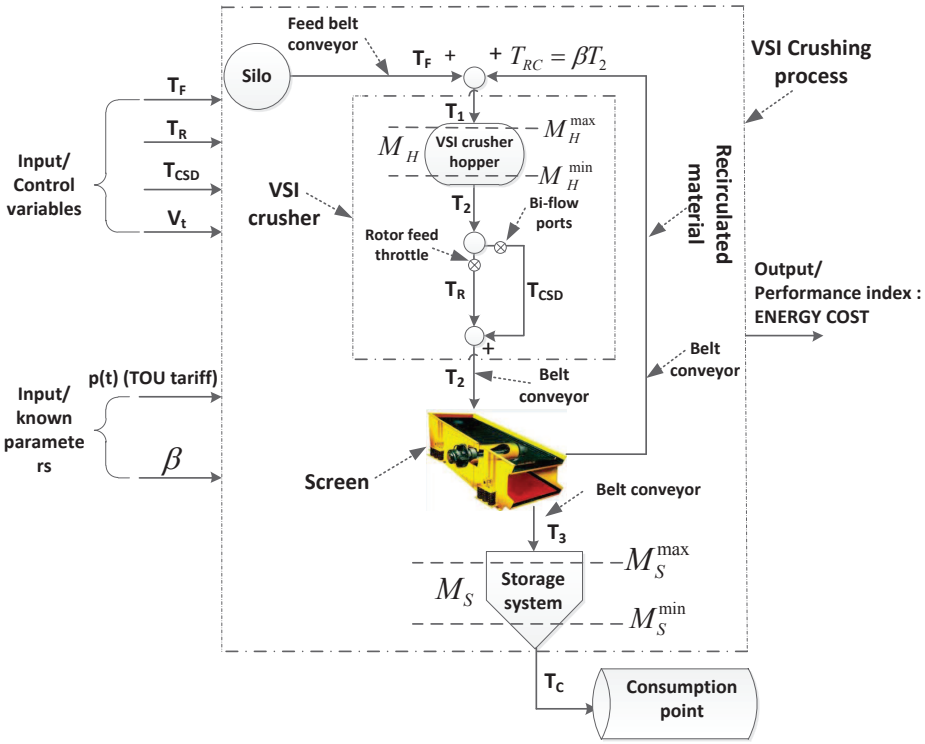


**Figure 4.2:** Schematic of a tertiary mining VSI crushing station

A typical VSI crushing station with closed circuit is shown in Fig. 4.2 where $T_R$ denotes the material feed rate into the crusher $(t/h)$; $T_F$ is the belt conveyor feed rate into the crusher $(t/h)$; $T_{CSD}$ is the cascade flow rate or bi-flow rate $(t/h)$; $T_1$ and $T_2$ are mass flow rates into and from the crusher hopper $(t/h)$, respectively; $T_3$ is the mass flow rate from the screen $(t/h)$; $T_{RC}$ is the recirculated material mass flow rate $(t/h)$; $T_C$ is the mass flow rate of the material consumption $(t/h)$; $V_t$ is the rotor tip speed of the crusher $(m/s)$; $\beta$ is the recirculated mass flow ratio $(-)$; $p(t)$ is the TOU electricity tariff $(currency/kWh)$; $M_H$ and $M_S$, respectively,

[1] Metso, Barmac VSI crushers, <http://www.metso.com>

represent the material mass available in the crusher hopper and storage system ($t$); "$min$" and "$max$" denote, respectively, the minimum and maximum of the corresponding variable, which applies to the rest of this chapter.

In practice, the four control variables considered in this work are plausable choices. The belt conveyor feed rate, $T_F$, and the crusher rotor speed, $V_t$, are adjusted through VSD systems. The material feed rate into the VSI crusher rotor, $T_R$, is adjustable through a throttle [68], also called a rotor feed throttle, which is controlled by a hydraulic motor. The cascade feed rate, $T_{CSD}$, is adjustable through a certain number of adjustable bi-flow (or cascade) ports in the hexagonal hopper [2] as shown in Fig. 4.1.

One should note that the rotor feed throttle and the bi-flow ports are normally located inside the VSI crusher hopper.[3] Hence, the fact that these two adjustment devices are put outside the VSI crusher hopper as shown in Fig. 4.2, is just to achieve a more clear representation.

In mining or aggregate industries, the tertiary crushing station is usually preceded by coarser crushing stations, namely the primary and secondary crushing stations. In a tertiary crushing station with closed circuit as shown in Fig. 4.2, the crushed material from the crusher is screened. The rock material with a size less than the screen aperture size goes to the storage system and larger material is recirculated to the crusher input.

### 4.2.2 General assumptions for the system

The following assumptions are made to build the optimal energy model strategy of the VSI crushing process in this work:

1. At any time, the silo feeding the VSI has enough material to supply the feed belt conveyor.

2. The time delay associated with the crushing process, from the silo to the consumption point, is not taken into account.

[2] Sandvik, Merlin-VSI:Setting the standard in VSI crushing, <http://www.miningandconstruction.sandvik.com>
[3] Metso, Barmac VSI crushers, <http://www.metso.com>

3. Any form of dynamic energy consumption of the crushing process is ignored.

### 4.2.3 Objective function

The optimal control model of a VSI crusher system in this work considers the total energy cost, $J_C$, as the objective function to be minimized by incorporating the TOU electricity tariff as an input to the model. A general function expressing this objective function can be written as:

$$J_C = \int_{t_0}^{t_f} P_{el}(t)p(t)dt, \tag{4.1}$$

where $P_{el}(t)$ is the electrical power $(W)$ of the crusher expressed as a function of time $t$ $(h)$; $t_0$ and $t_f$ are the initial and final time $(h)$ of the control horizon, respectively.

The net mechanical (shaft) power model of the VSI crusher based on the Euler turbine equation is expressed in [68] as a function of the tangential component of the particle velocity entering the rotor, $u_1$, tangential component of the particle velocity exiting the rotor, $u_2$, and the rotor angular speed, $\omega_R$, where the motion of the particle is shown in Fig. 4.3 [68].

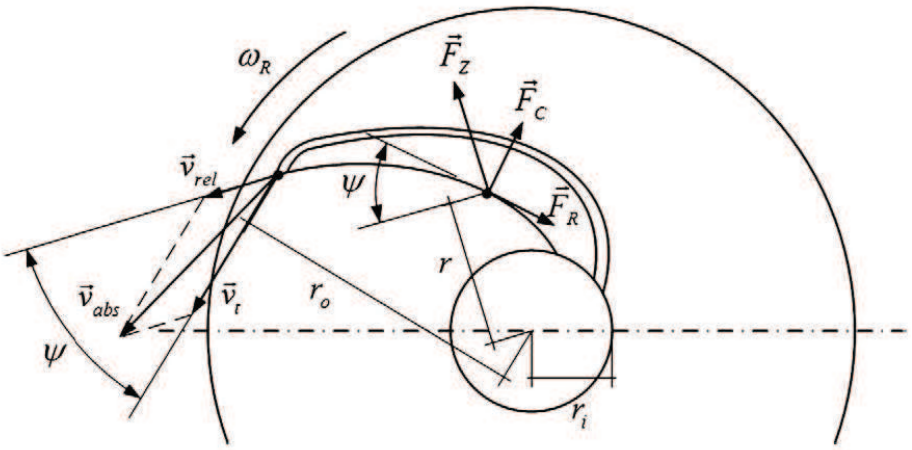


**Figure 4.3:** Schematic of the particle motion

This is given as follows:

$$P_{m_{net}} = T_R \left(\omega_R R_1 u_1 - \omega_R R_2 u_2\right), \tag{4.2}$$

with

$$u_1 = \frac{T_R}{\rho \frac{\pi D_{open}^2}{4}} cos\psi + \omega_R R_1, \tag{4.3}$$

$$u_2 = V_t cos\psi + \omega_R R_2, \tag{4.4}$$

$$V_t = \omega_R R_2, \tag{4.5}$$

where other notations such as $P_{m_{net}}$ denote the net mechanical power $(W)$ of the crusher; $R_1$ (equivalent to $r_i$ in Fig. 4.3)and $R_2$ (equivalent to $r_o$ in Fig. 4.3) , the inner radius and outer radius $(m)$ of the crusher rotor, respectively; $\psi$, the angle $(rad)$ between the tangential velocity and relative velocity of the particle; $D_{open}$ is the average diameter $(m)$ of the crusher inlet; $\rho$ is the bulk density $(kg/m^3)$ of the rock material.

Combining Eqs.(4.2)-(4.5) yields a new Euler turbine equation expressed as a function of the material feed rate into the crusher rotor $T_R$ and rotor tip speed $V_t$ as:

$$P_{m_{net}} = \frac{R_1 cos\psi}{3.24\pi R_2 \rho D_{open}^2} V_t T_R^2 + \frac{1}{3.6}\left(\frac{R_1^2}{R_2^2} - cos\psi - 1\right) T_R V_t^2. \tag{4.6}$$

Note that in Eq.(4.2), $T_R$ is expressed in $kg/s$ while in Eq.(4.6), this is expressed in $t/h$. Letting $k_1 = \frac{R_1 cos\psi}{3.24\pi R_2 \rho D_{open}^2}$ and $k_2 = \frac{1}{3.6}\left(\frac{R_1^2}{R_2^2} - cos\psi - 1\right)$, the analytical model to predict the net mechanical power of the VSI crusher is obtained as follows:

$$P_{m_{net}} = k_1 V_t T_R^2 + k_2 T_R V_t^2. \tag{4.7}$$

The total mechanical power $(W)$, $P_m$, is obtained by adding the no-load mechanical power consumption of the VSI crusher to Eq.(4.7). The no-load mechanical power is the power required to overcome the VSI crusher rotor inertia and the bearing friction. Both of these vary with the VSI crusher speed. However, the power required to overcome the bearing friction is relatively small, hence it can be neglected. A fair estimation is to assume that the no-load mechanical power is directly proportional to the rotor tip speed $V_t$ with a proportional constant $k_3$. In Chapter 3, the no-load mechanical power of the jaw crusher is assumed constant since the jaw crusher speed is considered as an input parameter (or fixed variable). Hence, the analytical model to predict the mechanical power consumption of the VSI crusher is expressed as:

$$P_m = k_1 V_t T_R^2 + k_2 T_R V_t^2 + k_3 V_t. \tag{4.8}$$

If the angle $\psi$ is assumed to be constant, the coefficients $k_1$, $k_2$ and $k_3$ are constant and mainly depend on the VSI crusher geometry and the characteristic of the material (material density) to be crushed. These three constants can be derived from design parameters or estimated through experiments. However, because of continuous wear of machine parts and variation in the feed characteristic over time, deriving $k_1$, $k_2$ and $k_3$ through experiments would yield accurate results. The least squares (LSQ) parameter estimation algorithm [72] can be used to estimate the coefficients $k_1$, $k_2$ and $k_3$ when experimental data are available.

To validate the power model given by Eq.(4.8), Figs. 4.4 and 4.5 show the comparison between the predicted crushing power and manufacturer's data for Bermac VI-series VSI crushers.[4] The coefficients in the power model have been estimated to be $k_1 = 7.1 \times 10^{-4}$, $k_2 = 2 \times 10^{-1}$ and $k_3 = 0.6256 \times 10^3$. In Fig. 4.4, the power requirement of the VSI crusher is plotted against the rotor throughput rate for three given rotor tip speeds of 50 $m/s$, 60 $m/s$ and 70 $m/s$, while in Fig. 4.5, the power requirement is plotted against the rotor tip speed for three given rotor throughput rates of 100 $t/h$, 300 $t/h$ and 500 $t/h$. The comparative results show good agreement between the predicted power consumption of the VSI crusher and the manufacturer's data. However, for higher accuracy, the parameters in model (4.8) need to be estimated based on field test data for a particular VSI crusher.

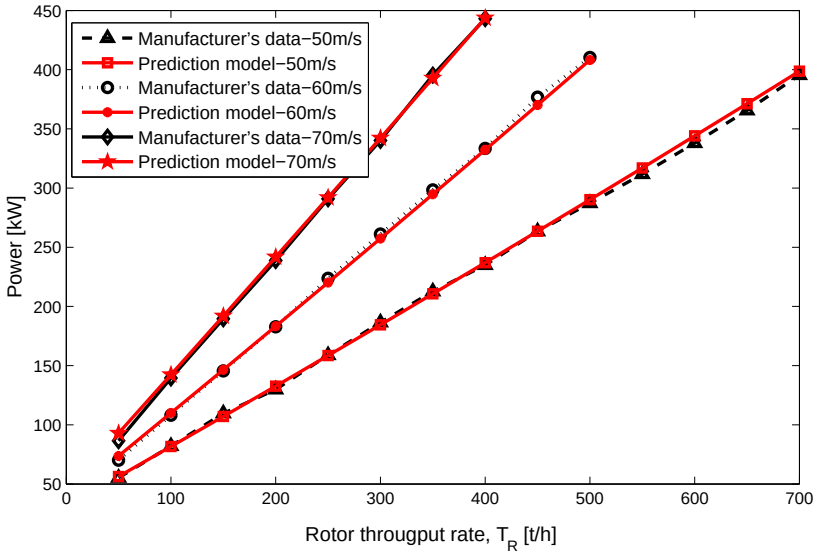


**Figure 4.4:** Power curves for given rotor tip speeds

[4]Metso, Nordberg Barmac VI-Series VSI Crusher, <http://www.metso-bulgaria.com>

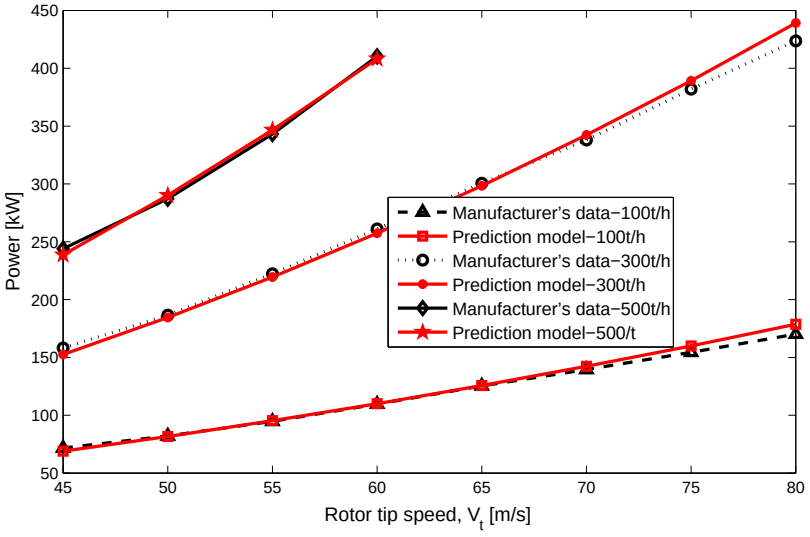


**Figure 4.5:** Power curves for given rotor throughput rates

Note that since the model (4.8) is derived from Euler turbomachinery equations, this can also be used to predict the power consumption of turbopumps and fans.

The electric power consumption function $P_{el}$ of the VSI crusher defined in Eq.(4.1) can be expressed as:

$$P_{el} = \frac{1}{\eta_D}\left(k_1 V_t T_R^2 + k_2 T_R V_t^2 + k_3 V_t\right), \tag{4.9}$$

where the drive efficiency, $\eta_D$, composed of the electric motor drive and transmission belt drive, is assumed to be constant in this work. However, in practice, the efficiency of the electric motor drive decreases as the load decreases and can be improved by adapting the flux level to the loading level of the motor, especially at very light load [73]. The substitution of Eq.(4.9) into Eq.(4.1) yields the explicit form of the objective function as follows:

$$J_C = \frac{1}{\eta_D}\int_{t_0}^{t_f}\left(k_1 V_t(t) T_R^2(t) + k_2 T_R(t) V_t^2(t) + k_3 V_t(t)\right) p(t) dt. \tag{4.10}$$

Because of the discrete nature of the TOU electricity tariff, the objective function given by Eq.(4.10) may be continuous but not differentiable. Hence, a numerical approach is suitable to solve this problem. The objective function expressed in continuous-time domain by Eq.(4.10) can therefore be discretized as follows:

$$J_C = t_s \frac{1}{\eta_D}\sum_{j=1}^{N_s}\left(k_1 V_{t_j} T_{R_j}^2 + k_2 T_{R_j} V_{t_j}^2 + k_3 V_{t_j}\right) p_j, \tag{4.11}$$

where $t_s$ is the sampling time; $N_s$, the number of sampling intervals and $p_j$, the electricity price, assumed constant at the $j^{th}$ sampling interval.

### 4.2.4 Constraints

#### 4.2.4.1 Limits on control variables

$$\begin{cases} T_F^{min} \leq T_{F_j} \leq T_F^{max}, & (1 \leq j \leq N_s), \\ T_R^{min} \leq T_{R_j} \leq T_R^{max}, & (1 \leq j \leq N_s), \\ T_{CSD}^{min} \leq T_{CSD_j} \leq T_{CSD}^{max}, & (1 \leq j \leq N_s), \\ V_t^{min} \leq V_{t_j} \leq V_t^{max}, & (1 \leq j \leq N_s). \end{cases} \tag{4.12}$$

#### 4.2.4.2 Mass balance in the crushing circuit

The mass balance equations at different nodes of the VSI crushing process as shown in Fig. 4.2 can be written as:

$$\begin{cases} T_1 = T_F + T_{RC}, \\ T_2 = T_R + T_{CSD}, \\ T_2 = T_3 + T_{RC}. \end{cases} \tag{4.13}$$

The recirculating mass flow rate $T_{RC}$ can be related to the total mass flow rate into the screen $T_2$ through a ratio, referred to as recirculating mass flow rate ratio $\beta$ as follows:

$$T_{RC} = \beta T_2. \tag{4.14}$$

The mass balance given by Eqs.(4.13) can be combined with Eq.(4.14) to give a new set of mass balance equations expressing the non-control variables, referred to as dependent variables, in terms of the three control variables as follows:

$$\begin{cases} T_{1_j} = T_{F_j} + \beta_j \left(T_{R_j} + T_{CSD_j}\right), & (1 \leq j \leq N_s), \\ T_{2_j} = T_{R_j} + T_{CSD_j}, & (1 \leq j \leq N_s), \\ T_{3_j} = (1 - \beta_j) \left(T_{R_j} + T_{CSD_j}\right), & (1 \leq j \leq N_s), \\ T_{RC_j} = \beta_j \left(T_{R_j} + T_{CSD_j}\right), & (1 \leq j \leq N_s), \end{cases} \tag{4.15}$$

where $\beta_j$ is assumed to be measured or predicted at the $j^{th}$ sampling interval.

These dependent variables can therefore be obtained after getting the optimal control solutions (control variable values) of the problem.

#### 4.2.4.3 Limits on dependent variables

The limitations on the total mass flow rate into the VSI crusher hopper $T_1$ may be wanted. The flow rate of recirculating material $T_{RC}$ and the ones into and from the screen device, respectively, $T_2$ and $T_3$ to be transported, may also be restricted by the capacity of the belt conveyors. Based on Eqs.(4.15), these constraints are given as:

$$\begin{cases} T_1^{min} \leq T_{F_j} + \beta_j \left(T_{R_j} + T_{CSD_j}\right) \leq T_1^{max}, & (1 \leq j \leq N_s)\,, \\ T_2^{min} \leq \left(T_{R_j} + T_{CSD_j}\right) \leq T_2^{max}, & (1 \leq j \leq N_s)\,, \\ T_3^{min} \leq (1-\beta_j) \left(T_{R_j} + T_{CSD_j}\right) \leq T_3^{max}, & (1 \leq j \leq N_s)\,, \\ T_{RC}^{min} \leq \beta_j \left(T_{R_j} + T_{CSD_j}\right) \leq T_{RC}^{max}, & (1 \leq j \leq N_s)\,. \end{cases} \tag{4.16}$$

#### 4.2.4.4 Limits on mass storage states

During the normal operation of the VSI crushing process, the dynamics of the mass stored in the VSI crusher hopper and downstream storage system should be kept within allowable capacity limits of each storage device, to avoid the material overflowing.

**A. Limits on the mass storage state in the VSI crusher hopper**

The material dynamics in the VSI crusher hopper can be expressed by a discrete-time difference equation as follows:

$$M_{H_j} = M_{H_{j-1}} + t_s \left(T_{1_{j-1}} - T_{2_{j-1}}\right),\ (1 \leq j \leq N_s)\,. \tag{4.17}$$

By recurrence manipulation, the mass stored in the crusher hopper at the $j^{th}$ sampling interval can be expressed in terms of the initial mass available, $M_{H_{,0}}$ as:

$$M_{H_j} = M_{H_{,0}} + t_s \sum_{i=1}^{j} \left(T_{1_i} - T_{2_i}\right),\ (1 \leq j \leq N_s)\,. \tag{4.18}$$

Taking into account the mass balance, given by $T_{1_j} = T_{F_j} + \beta_j \left(T_{R_j} + T_{CSD_j}\right)$ and $T_{2_j} = T_{R_j} + T_{CSD_j}$ in Eqs.(4.15), the limitations on mass storage state in the VSI crusher hopper can be finally written as:

$$M_H^{min} \leq M_{H,0} + t_s \sum_{i=1}^{j} T_{F_i} + (\beta_i - 1)\left(T_{R_i} + T_{CSD_i}\right) \leq M_H^{max}, (1 \leq j \leq N_s)\,. \tag{4.19}$$

**B. Limits on the mass storage state in the storage system**

Following the same procedure as above, the limitations on mass storage state in the downstream storage system are given as:

$$M_S^{min} \leq M_{S,0} + t_s \sum_{i=1}^{j} \left[(1 - \beta_i)\left(T_{R_i} + T_{CSD_i}\right) - T_{C_i}\right] \leq M_S^{max}, (1 \leq j \leq N_s)\,, \tag{4.20}$$

where $M_{S,0}$ is the initial mass available in the storage system.

#### 4.2.4.5 Production requirement

For reliability purposes, the total amount of crushed material fed to the consumption point (plant) should be greater than or equal to the total consumption of the plant. This is expressed as:

$$\sum_{j=1}^{N_s} T_{3_j} t_s \geq \sum_{j=1}^{N_s} T_{C_j} t_s, \tag{4.21}$$

which can be rewritten as:

$$\sum_{j=1}^{N_s} (1 - \beta_j)\left(T_{R_j} + T_{CSD_j}\right) t_s \geq \sum_{j=1}^{N_s} T_{C_j} t_s, \tag{4.22}$$

with $T_{3_j} = (1 - \beta_j)\left(T_{R_j} + T_{CSD_j}\right)$ as given in Eqs.(4.15). Note that the material consumption rate $T_C$ is assumed to be predicted for a given control horizon.

#### 4.2.4.6 Product quality requirement

In both mining and aggregate crushing plants, one of the requirements is that the mean size of the product material, $d_P$, has to be lower than a specified value, $d_P^{max}$, regardless of the variation of the feed mean size, $d_F$. For a given $d_F$, the relationship between $d_P$ from a VSI crusher and the VSI crusher speed, $V_t$, is given as follows [74]:

$$d_P = \left(\frac{4.472 K l_c d_{F_j}}{2\rho V_p V_{t_j}}\right)^{2/3} \leq d_P^{max}, \quad (1 \leq j \leq N_s)\,, \tag{4.23}$$

where $d_F$ is considered as a predictable parameter at each $j^{th}$ sampling interval. In Eq.(4.23), other notations not yet defined, such as $Klc$, denote the fracture toughness (mode 1) of the rock ($Pa\ m^{0.5}$) and $V_p$ the propagation velocity ($m/s$) of the elastic waves in the rock. Eq.(4.23) shows that the VSI crusher speed can be continuously adjusted to meet the product quality requirement.

#### 4.2.4.7 Limits on bi-flow or cascade ratio

Usually, the cascade or bi-flow ratio is maintained at a constant value, depending on the nature of the rock material to be crushed [75]. The bi-flow material increases the rock-to-rock impact action by improving the efficiency and throughput capacity of the VSI crusher. However, increasing cascading material is similar to slowing the rotor speed, leading to a negative effect on the product size distribution (coarse particle size in the product). Hence, for efficiency purposes, crusher manufacturers recommend operating the VSI crusher with a bi-flow ratio of 10-15 % [5]. Up to 10-15 % cascade material can be used without a significant change in product gradation or quality; meantime 10-15 % extra product (throughput capacity) is gained for no extra power use or wear part consumption.[5]

The bi-flow or cascade ratio, noted $\alpha_{CSD}$, is defined as the ratio between the cascade feed rate $T_{CSD}$ and the material feed rate into the crusher rotor $T_R$.

At each $j^{th}$ sampling interval, the constraint on the cascade ratio can be expressed as follows:

$$\frac{T_{CSD_j}}{T_{R_j}} = \alpha_{CSD},\ (1 \leq j \leq N_s)\,, \tag{4.24}$$

which can be rewritten in a linear form as follows:

$$T_{CSD_j} = \alpha_{CSD} T_{R_j},\ (1 \leq j \leq N_s)\,. \tag{4.25}$$

## 4.3 CURRENT CONTROL STRATEGY

In practice, the VSI crushing process operates continuously, while the flow rates are adjusted in such a way as to meet the system constraints and achieve the total plant production target/requirement. Hence, the current control strategy can be formulated as an optimal control

[5]Metso, Barmac VSI crushers, <http://www.metso.com>

problem with the objective function being the quadratic deviation between the total actual plant production and the total plant target for a given control horizon. The mathematical model of the current control strategy of the VSI crushing process as shown in Fig. 4.2 is therefore given as:

$$min\, J_{PR} = \left[\sum_{j=1}^{N_s} (1-\beta_j)\left(T_{R_j} + T_{CSD_j}\right) t_s - \sum_{j=1}^{N_s} T_{C_j} t_s\right]^2, \tag{4.26}$$

subject to constraints (4.12)-(4.25).

## 4.4 CASE STUDY: CRUSHING PROCESS IN A COAL-FIRED POWER PLANT

The work presented in [13] investigates the optimal control strategies of a coal conveying system in order to minimize the energy cost associated with belt conveyor systems. The coal crusher present in the aforesaid coal conveying system is not included in the optimal energy control problem since it is stated that the coal crusher system follows its own optimal control strategy. In this work, the coal crusher in [13] is assumed to be a VSI crushing machine and therefore the same system is used to simulate the optimal energy control strategy of a VSI crushing process developed in this research work. This assumption is reasonable since for pulverized hard coal-fired power plants such as those found in South Africa, for instance, VSI crushers are appropriate to be used in the last stage of the crushing circuit before the crushed coal is sent to the grinding mill circuit for coal pulverization. This is because VSI crushers offer the advantage of producing significantly more fine material compared to other crushers used for hard rocks. Hence, a relatively large amount of fines smaller than 75 $\mu$m (pulverized coal) can be screened and sent directly to the boiler while the coarser coal particles are sent to the grinding mill. Moreover, it is reported in [5] that the higher fine content obtained by VSI crushing is valuable for the subsequent grinding mill since this will reduce the work and hence the power needed by the mill.

### 4.4.1 Data presentation

#### 4.4.1.1 Coal consumption and coal storage system

In view of the above, data such as power plant capacity, coal bin capacity, load assignment and forecast coal consumption are obtained from [13]. In this reference, with a given load assignment profile, the coal consumption is predicted based on a quadratic function. The predicted coal consumption rate $T_C$ is shown in Fig. 4.6. Based on the given coal-fired power plant with two 600 $MW$ units, the estimated total bin capacity (TBC) is 5595.5 $t$.

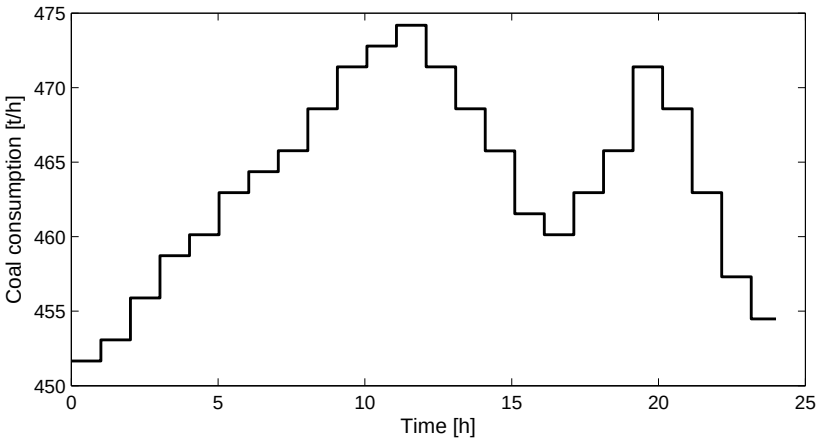


**Figure 4.6:** Forecast coal consumption rate

In this work, the upper limit $M_S^{max}$ and lower limit $M_S^{min}$ of the downstream storage system (coal bin) are set, respectively, to 90 % and 20 % of TBC. The initial mass stored $M_{S,0}$ in the storage system is assumed to be 50 % of TBC.

#### 4.4.1.2 Coal characteristics

The bulk density $\rho$ of the anthracite coal is 1506 $kg/m^3$, the propagation velocity of its longitudinal elastic waves $V_p$ is 1890 $m/s$ and its fracture toughness $Klc$ is 0.19325 $Mpa\ m^{0.5}$.

#### 4.4.1.3 VSI crusher

A 400 $kW$ (600 $hp$) Barmac VI-series VSI crusher[6] is used for simulation purpose in this work. In order to allow the cascade feed material for such a soft material to be crushed, the maximum operation tip speed $V_t$ is set 45 $m/s$. The cascade ratio $\alpha_{CSD}$ is considered to be 10 %. The rotor outer radius $R_2$ is 0.525 $m$. The maximum rotor feed rate $T_R^{max}$ is set to 700 $t/h$. With the cascade ratio of 10 %, the maximum feed rate $T_1^{max}$ is obtained to be 770 $t/h$. The power model coefficients are $k_1 = 7.1\times10^{-4}$, $k_2 = 2\times10^{-1}$ and $k_3 = 0.6256\times10^{3}$ as derived in Section 4.2.3. The overall drive efficiency $\eta$ is assumed to be 95 %.

#### 4.4.1.4 Time-of-use electricity tariff

The recent Eskom Megaflex Active Energy-TOU electricity tariff is used for simulation purposes. To be more specific, the crushing station is supposed to operate under the non-local authority rate. The control horizon in this work is assumed to be within the high-demand season (from June to August) weekday. This is given as:[7]

$$p(t) = \begin{cases} p_o = 0.3656R/kWh \; if \; t\epsilon\,[0,6] \cup [22,24]\,, \\ p_s = 0.6733R/kWh \; if \; t\epsilon\,[6,7] \cup [10,18] \cup [20,22]\,, \\ p_p = 2.2225R/kWh \; if \; t\epsilon\,[7,10] \cup [18,20]\,, \end{cases} \tag{4.27}$$

with $p_o$, $p_s$ and $p_p$, respectively, the off-peak, standard and peak TOU active energy tariffs for higher demand season (June-August); $R$ is the South African currency Rand and $t$ is the time of any weekday in hours (from 0 to 24).

### 4.4.2 Simulation results and discussion

The control horizon $[t_0,\, t_f]$ and sampling time $t_s$ of, respectively, 24 $h$ and 15 $min$ are used for both current control and optimal control strategies. For all simulations, the recirculated material is not considered, that is, $\beta = 0$. The upper limit on the flow rates of all belt conveyors is set to 770 $t/h$, which corresponds to the higher limit of the total throughput rate of the crusher (including the cascade feed rate). To account for the product quality requirement, the maximum product mean size $d_P^{max}$ is set to 3 $mm$.

[6] Metso, Nordberg Barmac VI-Series VSI Crusher, <http://www.metso-bulgaria.com>

[7] Eskom, Tariffs & Charges Booklet 2013/2014, <http://www.eskom.co.za>

The *fmincon* function of MATLAB Optimization Toolboox is used to solve all the problems in this work.

The comparative simulation results between the current control and optimal control strategies are shown in Figs. 4.7-4.10 and Tables 4.1-4.3. In these figures, the dotted lines denote the upper and lower bounds of the corresponding variable. Note that the legend of Fig. 4.7 also applies to Fig. 4.8. The feasibility of both current control and optimal control strategies are demonstrated from these figures where it can be seen that the crushing process operates under the specified constraints.

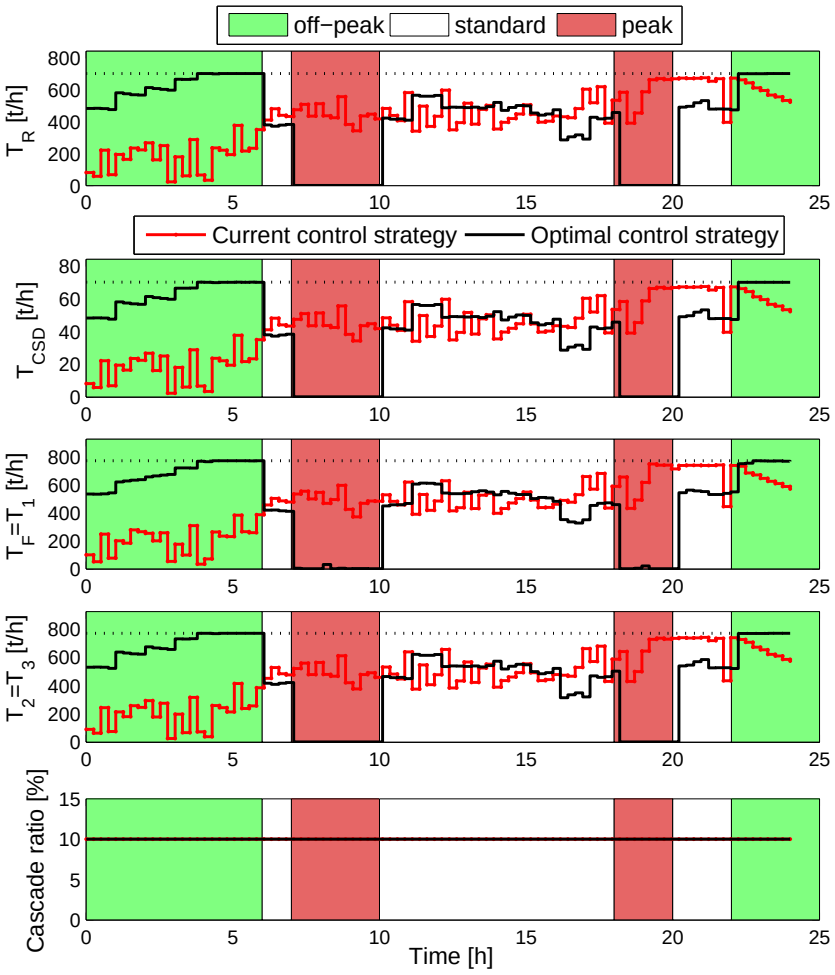


**Figure 4.7:** Coal flow rates and cascade ratio

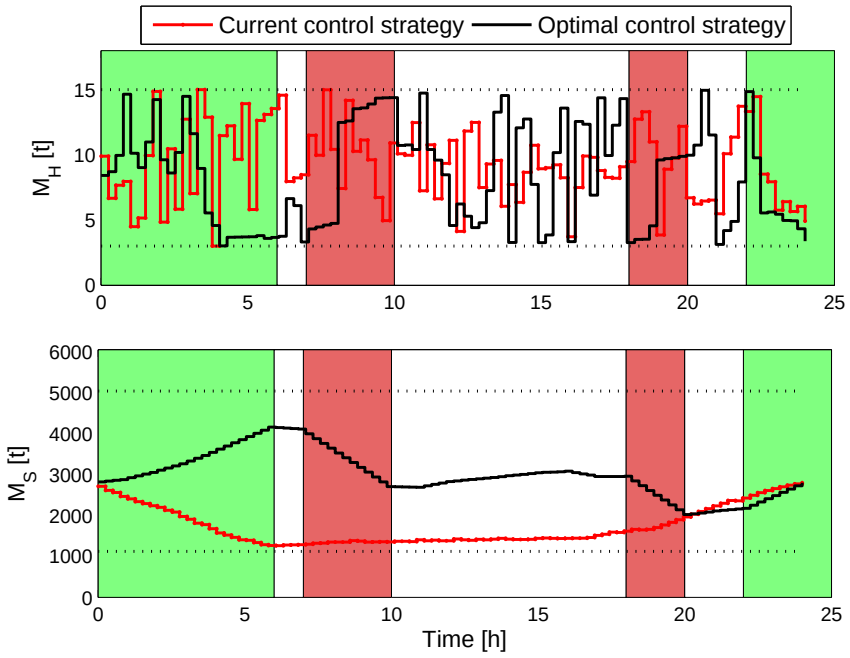


**Figure 4.8:** Coal level in the storage systems

**Table 4.1:** Total production and corresponding energy cost and consumption

| Strategy | Total production (t) | Energy cost (R) | Energy consumption (kWh) |
|---|---|---|---|
| Current control strategy | 11,130 | 4407.64 | 4527.92 |
| Optimal control strategy | 11,130 | 2213.37 | 3833.22 |

**Table 4.2:** Cost savings of the optimal control strategies

| Strategy | Unit energy cost (R/t) | Cost saving (%) |
|---|---|---|
| Current control strategy | 0.3960 | / |
| Optimal control strategy | 0.1989 | 49.77 |

#### 4.4.2.1 Cost saving discussion

Although the feasibility of both control strategies are technically proved through simulation results, it can be seen from Fig. 4.7, that the current control strategy runs the VSI crushing

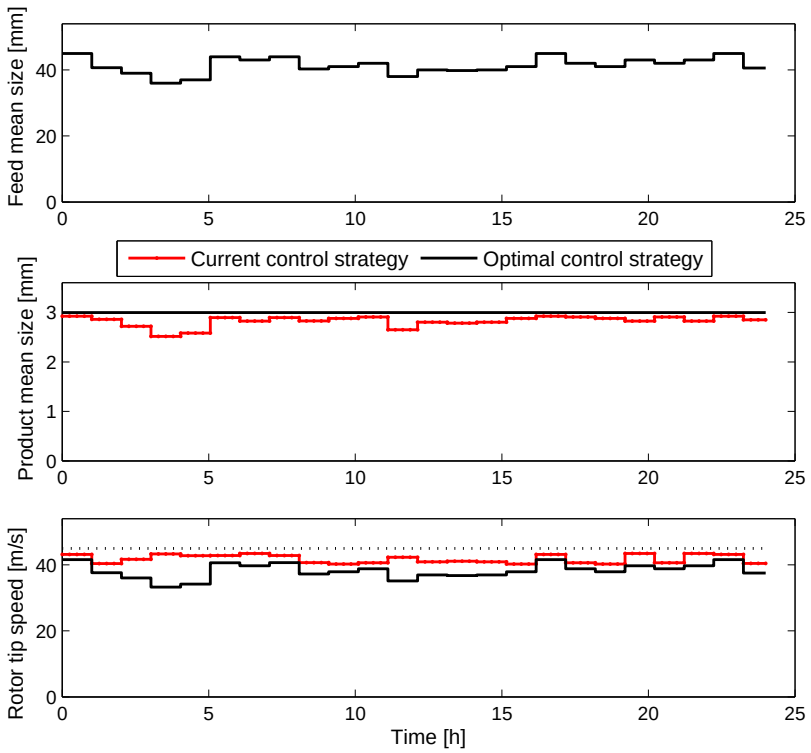


**Figure 4.9:** Coal mean sizes and VSI crusher speed

**Table 4.3:** Energy savings of the optimal control strategies

| Strategy | Unit energy consumption (kWh/t) | Energy saving (%) |
|---|---|---|
| Current control strategy | 0.4068 | / |
| Optimal control strategy | 0.3444 | 15.34 |

process without consideration of the TOU electricity tariff. With this, the load (coal flow rates) is almost evenly distributed across the 24 hours-control horizon without shifting the load out of peak time. The reason is that the current control strategy does not have any information on the TOU tariff during the process control. As result of this, a higher energy cost is incurred. Simulation results obtained by the current control strategy in this work reflect the practical operation of most crushing processes. In practice, most crushing processes run continuously with almost constant feeding (material feed rate) for a given operational period while achieving the total production requirement (total plant throughput) and meeting

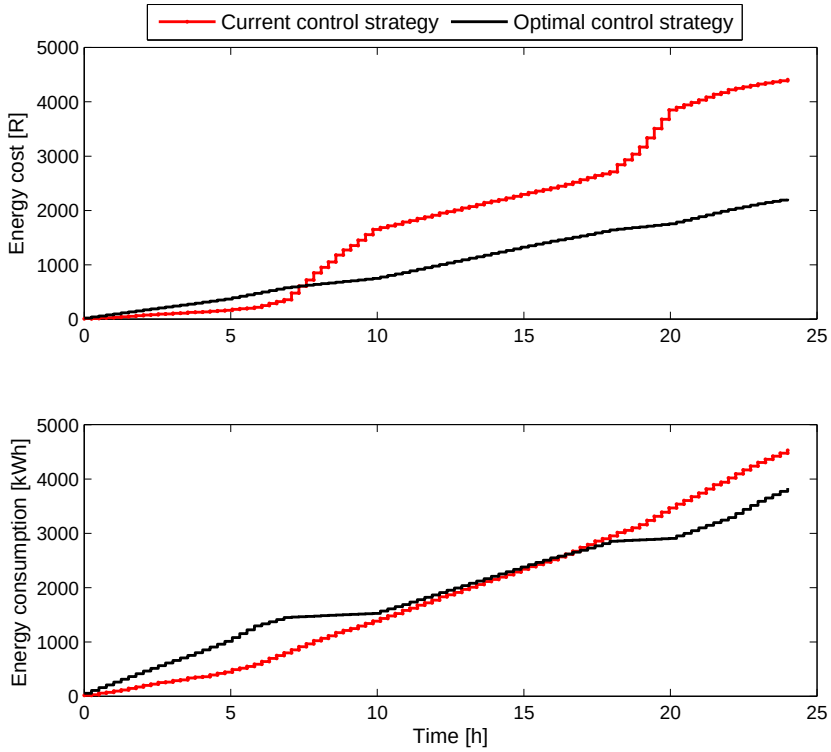


**Figure 4.10:** Cumulative energy cost and consumption

other constraints associated with the operation. The material feed rate $T_F$ is usually controlled/regulated at a certain constant value by feeding equipment such as vibrating feeders, apron feeders or belt conveyors. However, for the case of a tertiary or last crushing stage such as the VSI crushing process, the belt conveyors or vibrating feeders equipped with VSD systems are mostly employed for feeding control. Apron feeders, which are heavy-duty feeding machines, are commonly used in primary crushing processes where the feeding is usually characterized by coarse rock/ore material. However, the crushing station may be shut down in the presence of disturbances. These disturbances are, for instance, the introduction into the crusher of oversize material, which would result in imbalance of the VSI crusher but also the overload of the machine impeller.

Since the hopper of the VSI crusher is usually of negligible capacity (a maximum of 15 $t$ in this work), its dynamics $M_H$ as shown in the first graph of Fig. 4.8, does not have a considerable effect on the crusher output flow rate $T_2$, whenever the feed rate of the VSI crusher $T_1 = T_F$ changes. This justifies the fact that the crusher feed rate $T_1 = T_F$ almost equals its output flow rate $T_2$, as shown in the third and fourth graphs of Fig. 4.7.

On the other hand, from the same figure (Fig. 4.7), it is seen that the optimal control strategy runs the VSI crushing process by optimally shifting the load from peak time to off-peak and standard time in order to minimize the associated energy cost. It can be seen that during peak time, the coal feed rate into the VSI crusher rotor $T_R$ is zero in order to save energy cost, whilst during off-peak time, this is maximized in order to meet the production target at a cheaper energy cost. The second graph of Fig. 4.7 shows that the cascade flow rate $T_{CSD}$ varies proportionally with the rotor feed rate $T_R$ in order to maintain the cascade ratio constantly to its reference value of 10 % as demonstrated through the last graph of the same figure. The effectiveness of the optimal energy control strategy can also be seen with reference to the coal levels in the storage systems. Fig. 4.8 shows that unlike the current control strategy, during peak time, the amount of coal in the upstream storage system (VSI crusher hopper), $M_H$, increases while during off-peak time, this decreases. The reason is that, with optimal control, the coal material is stored instead of being fed to the crusher during peak time, while during off-peak time, the coal material is drawn from the hopper and processed by the crusher at a cheaper energy cost. In the downstream storage system, it is seen that the coal amount $M_S$ decreases during peak time while during off-peak time, this increases. This is due to the fact that the coal material, which was processed during off-peak and standard time when the cost of energy is cheap, is now fed to the coal grinding station (if available) or consumption point (boiler) during peak time, when the crusher is not allowed to process the coal material because of the higher energy cost.

The cumulative energy cost and energy consumption of the current control and optimal control strategies are shown in Fig. 4.10, while Tables 4.1-4.3 summarize the performance of the optimal control strategy. The analysis of Fig. 4.10 clearly shows that, at the end of the control horizon (24 $h$), the optimal control strategy dramatically reduces the energy cost with comparison to the current control strategy taken as baseline. The actual energy cost saving obtained is evaluated to about 49.7 %, as shown in Table 4.2.

#### 4.4.2.2 Energy saving discussion

The simulation results reflected in the second graph of Fig. 4.10 demonstrate that the energy consumption is also reduced, although the energy cost is considered as performance index. The reason for the energy consumption reduction is that the optimal control strategy runs

the VSI crusher at a slightly reduced speed when compared to the current strategy, as can be seen in the third graph of Fig. 4.9, by operating the system at the boundary of the admissible operating region limited by the product quality constraint, as shown in the second graph of Fig. 4.9. It can therefore be observed that, in order to minimize the economical performance objective such as energy consumption, the operating point of the VSI crushing process has to be obtained by pre-setting the product quality index at its worst but feasible value (limits). This is due to the conflict between the economical performance objectives (energy consumption, energy cost, etc.) and the technical performance objectives (product size reduction ratio, maximum product size, etc.), which makes the crushing process a multi-objective optimization problem in reality. For this case study where the product quality index is considered to be the product mean size, its maximum value has been set to 3 $mm$, as can be seen in the second graph of Fig. 4.9.

An energy saving of about 15.3 % is achieved. This means that not all of the 49.7 % energy cost saving is achieved through load shifting. Some energy cost saving is due to the 15.3 % energy reduction. However, most of this cost reduction comes from optimal load shifting. Note that the rotor speed cannot be further reduced for more energy reduction owing to the product quality constraint.

Practically, most VSI crushing stations are equipped with real-time monitoring and control systems, which include VSD systems. This means that no systems upgrade or extra capital cost is normally needed in order to achieve the energy consumption based on the optimal coordination of the VSI crusher speed or the energy cost reduction based on optimal load shifting.

Although simulation results in this work show great potential to reduce both energy consumption and cost of a VSI crushing process, some challenges related to the implementation of the optimal energy control strategy need to be addressed in practice. Firstly, all the input parameters to the model, such as TOU electricity tariff, recirculated mass flow ratio, material consumption rate, and particle size distribution of the feed material need to be accurately and continuously predicted. Secondly, if an open-loop optimal control strategy (optimal setting values are manually entered by the operators in the supervisory control and data acquisition system) is to be used, the success of the optimal energy control strategy will depend on the skills of the process operators. Thirdly, since the energy saving is achieved through matching

the VSI crusher speed with the change in particle size distribution of the feed material, the sensor used for the continuous measurement of the feed particle size distribution has to be highly accurate.

## 4.5 SUMMARY

A practical model to improve the operation efficiency of a VSI crushing process is firstly developed in this chapter. The energy cost with integration of the TOU tariff is minimized under several technical and operating constraints. Secondly, in order to evaluate the feasibility of the model, a case study of a crushing process in a fire-coal power plant is undertaken. The simulation results performed through MATLAB Optimization Toolbox demonstrate the feasibility of the model. Although the energy cost is taken as performance objective, it is shown that the optimal energy control strategy developed in this work can potentially achieve both energy saving and cost saving on a VSI crushing process, while meeting the specified physical and operational constraints of the system. About 15.3 % energy saving and 49.7 % energy cost saving were achieved. It is observed that most of the energy cost saving comes from the optimal shifting of the load, while the energy saving is due to the optimal coordination of the VSI crusher speed.

# CHAPTER 5

# OPTIMAL ENERGY MANAGEMENT OF A PARALLEL HPGR CRUSHING PROCESS

## 5.1 INTRODUCTION

While Chapter 4 deals with the energy management optimisation model of a VSI crushing process, in this chapter, an optimal energy control model of a parallel HPGR crushing process is studied. Although the HPGR crusher is also based on compressive action, like the jaw crusher studied in Chapter 3, the working principles of the two machines are different. The compressive action in a jaw crusher occurs between two plates, of which one is fixed and the other one is moveable (swinging action), while in the HPGR crusher, the rock is pressed between two counter-rotating rolls (rotating action). Chapter 5 also analyzes the parallel configuration of HPGR crushing machines.

In this chapter, the energy cost associated with the operation of the parallel HPGR crushing process is minimized by accounting for the TOU tariff and process constraints. The control variables are the rolls operating pressure, HPGR rotating speed and the HPGR fee rate. A case study is done in order to show the effectiveness of the proposed model with comparison to the current control strategy. The content of this chapter has been published in [76].

## 5.2 PERFORMANCE MODEL OF THE HPGR

Before applying systems optimization to any energy system, its performance model needs to be expressed in terms of the control/decision variables. Hence, in this section, different performance indices of the HPGR are derived and expressed in terms of the control vari-

ables.

### 5.2.1 Overview of the HPGR machine

The operational principle of the HPGR is explained in [7]. As can be seen in Fig. 5.1 (adapted from [7]), the ore material is force-fed into the machine from the top and crushed by compression breakage action between two counter-rotating rolls. Although the two rolls rotate at the same speed, $N$, one of them, referred to as a fixed roll, rotates on a fixed axis while the other, referred to as a moveable or floating roll, is allowed to move linearly with a pressing force applied to it. Hence, in order to achieve material size reduction, the floating roll is forced up against the ore material found in the gap formed by the two rolls using a hydraulic oil cylinder system [7].

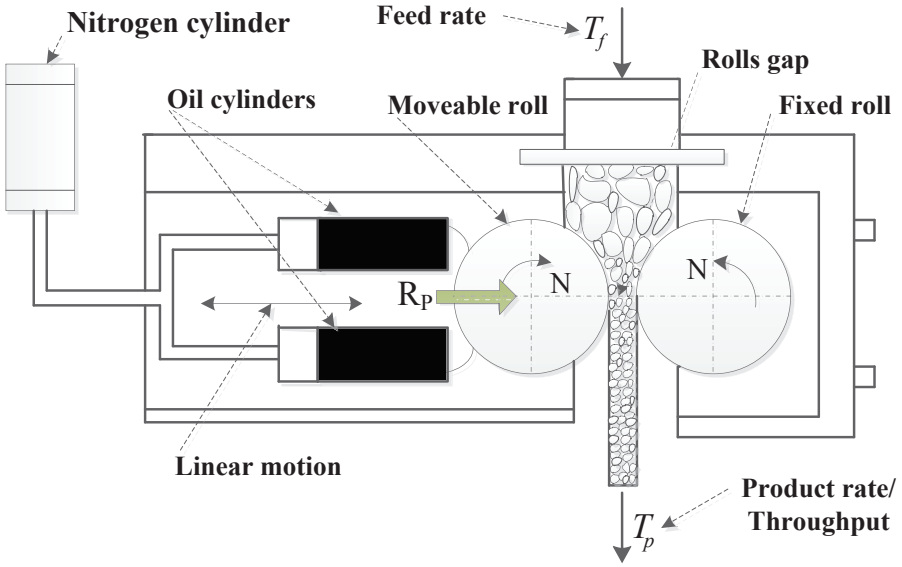


**Figure 5.1:** Cross-sectional representation of HPGR

The two main variables or flexible operating parameters that influence the HPGR performance, that is, the energy consumed, throughput rate and product quality, are the rolls rotational speed, $N$, and the rolls operating pressure, $R_P$ [77]. In practice, the HPGR rotational speed, $N$, is automatically adjusted through a VSD system, while the rolls operating pressure, $R_P$, is automatically adjusted through a hydraulic oil cylinder system, as previously mentioned. The fresh feed rate, $T_f$, is considered a third control variable in order to continuously equal the HPGR throughput rate, $T_p$. For the tertiary crushing process, the feeding

control is usually done through belt conveyors equipped with a VSD system, as opposed to primary crushing processes where the feeding control is usually based on vibrating grizzly feeders or apron feeders equipped with a VSD system because of the coarseness of the feed ore/rock material.

### 5.2.2 Formulation of performance indices

As discussed earlier, systems optimization of any crushing process is traditionally based on one of three performance indices: energy consumption, throughput rate and product quality. However, because of the continual increase in the electricity price, energy cost is becoming a major concern in mining industries. A new performance index is therefore progressively introduced in mineral processing circuits. This consists of the cost associated with the energy consumption of the processing machines, while traditional performance indices are considered as constraints. Although the performance prediction model of the HPGR has been analytically derived in [77], this is not explicitly expressed in terms of the control variables. Hence, one of the objectives in this work is to express all the performance indices of the HPGR as a function of the control variables, suitable for systems optimization.

#### 5.2.2.1 Energy model

In order to obtain the energy consumption and energy cost expressions of HPGR, its electrical power consumption first has to be formulated. In [77], the net mechanical power draw, $P_{net}$ $(kW)$, of the HPGR is expressed as a function of the compression force, $F(kN)$, the inter-particle compression angle, $\alpha_{IP}$ $(^o)$, and rolls peripheral speed, $V(m/s)$, as follows:

$$P_{net} = 2F \sin\left(\frac{\alpha_{IP}}{2}\right) V. \tag{5.1}$$

Since the angle $\frac{\alpha_{IP}}{2}$ is small [77], Eq.(5.1) can be simplified to Eq.(5.2) by using Taylor series expansion around zero (also called MacLaurin series expansions) of the term $\sin\left(\frac{\alpha_{IP}}{2}\right)$.

$$P_{net} = FV\alpha_{IP}. \tag{5.2}$$

The inter-particle angle, $\alpha_{IP}$, in Eq.(5.2) has been found to vary with the rolls gap, $s_0$, as [77, 49]:

$$\cos\alpha_{IP} = \frac{1}{2D}\left[(s_0 + D) + \sqrt{(s_0 + D)^2 - \frac{4Ds_0\delta}{\rho_a}}\right], \tag{5.3}$$

or

$$\cos\alpha_{IP} = \left[1 - \left(\frac{\delta}{\rho_a} - 1\right)\frac{s_0}{D}\right], \tag{5.4}$$

where the rolls gap $s_0$ is linked to the rolls operating pressure, $R_P$, through an exponential function of the form [78]:

$$s_0 = AR_P^{-b}. \tag{5.5}$$

In Eqs.(5.3)-(5.5), $D$ denotes the rolls diameter $(m)$; $\delta$ is the ore band density $(t/m^3)$ at the extrusion zone; $\rho_a$ is the feed bulk density $(t/m^3)$; $A$ and $b$ are constants of model fitting.

The compressive force, $F(kN)$, is expressed in terms of the rolls operating pressure, $R_P(N/mm^2)$, as follows (adapted from [77]) :

$$F = 1000R_P\frac{D}{2}L \tag{5.6}$$

where $L$ is the rolls length or width $m$. Hence, after converting the rolls peripheral speed, $V(m/s)$ to rotational speed, $N(rpm)$, using the relationship, $V = \frac{ND\pi}{60}$ and substituting Eqs.(5.3)-(5.6) in Eq.(5.2), the HPGR net mechanical power consumption, can finally be expressed as a function of the two flexible operating parameters (control variables), $N$ and $R_P$ as follows:

$$P_{net} = kNR_P f\left(R_P\right), \tag{5.7}$$

where $k = \frac{25\pi}{3}D^2L$ and

$$f\left(R_P\right) = \begin{cases} \cos^{-1}\left(\frac{1}{2D}\left[\left(AR_P^{-b} + D\right) + \sqrt{\left(AR_P^{-b} + D\right)^2 - \frac{4DAR_P^{-b}\delta}{\rho_a}}\right]\right), \\ or \\ \cos^{-1}\left[1 - \left(\frac{\delta}{\rho_a} - 1\right)\frac{AR_P^{-b}}{D}\right]. \end{cases}$$

To obtain the total mechanical power consumption of the HPGR machine, the no-load power consumption needs to be added to the net mechanical power model given by Eq.(5.7). The no-load power, which is the power consumed by the HPGR when no material is being fed in, can be expressed as a function of the speed. Since both crushing and grinding machines generally behave as constant loads, their torque characteristics (torque versus speed) is almost constant for a given loading level.[1] Knowing that the mechanical power is proportional to

[1]Bill Horvath (2013), Selecting motor controls for mining process torque demands, <http://www.wmea.net [Last accessed: 03 July 2014]

the rotational speed, the mechanical power of the HPGR can therefore be approximated to a linear function of the speed with the proportional constant being the torque demand. This is proven by Eq.(5.7) where it is seen that for a given rolls operating pressure, the HPGR mechanical power is proportional to its speed. It is therefore found reasonable to assume in this work, that the HPGR no-load power follows the trend of the full load power (shaft power). The expression of the total mechanical power consumption, $P_{mech}$, of the HPGR is therefore written as follows:

$$P_{mech} = kNR_P f\left(R_P\right) + cN, \tag{5.8}$$

where $c$ is the proportional constant of no-load power, which is in reality the HPGR no-load torque. The LSQ parameter estimation algorithm [72] can be used to estimate the coefficient $c$ based on either field test data or manufacturer's datum. At least one experimental data is needed to estimate the value of $c$ when the HPGR crusher is operated under no-load conditions. This means that $c$ can easily be determined if the no-load power consumption of the HPGR crusher is known at the nominal rotational speed, $N$.

Finally, the electrical power consumption, $P_{el}$, of the HPGR is expressed as:

$$P_{el}\left(N, R_P\right) = \frac{1}{\eta_D}\left(kNR_P f\left(R_P\right) + cN\right), \tag{5.9}$$

where $\eta_D$ is the overall drive efficiency, composed of electric motor drive efficiency, drive coupling efficiency and gearbox (speed reducer) efficiency. For $n$ HPGR crushing machines, the total electrical energy, $J_E$, consumed during the control horizon, between the initial time, $t_0$ and final time, $t_f$, is expressed as below:

$$J_E = \int_{t_0}^{t_f} \sum_{i=1}^{n} P_{el}\left(N(t), R_P(t)\right) dt. \tag{5.10}$$

With a given time-based electricity price, $p(t)$ $(currency/kWh)$, the total electrical energy cost, $J_C$, during the same time period between $t_0$ to $t_f$ can be estimated as follows:

$$J_C = \int_{t_0}^{t_f} \sum_{i=1}^{n} P_{el}\left(N(t), R_P(t)\right) p(t) dt. \tag{5.11}$$

#### 5.2.2.2 Throughput model

The HPGR throughput, $T_p(t/h)$, is expressed in [77] as a function of the linear speed, $V$, and rolls gap, $s_0$, as:

$$T_p = 3600\delta s_0 LV. \tag{5.12}$$

By converting the linear speed, $V$, to rotating speed, $N$, and substituting Eq.(5.5) in Eq.(5.12), the HPGR throughput can be expressed in terms the two variable controls as given below:

$$T_p = k_1 N R_P^{-b}, \tag{5.13}$$

where $k_1 = 60\pi ALD\delta$.

The HPGR power consumption can also be expressed as a function of the throughput and rolls operating pressure by substituting Eq. (5.12) or Eq. (5.13) into Eq. (5.1) to eliminate the rolls speed.

#### 5.2.2.3 Product quality model

The performance index of the product quality model of any crushing or grinding process is generally a parameter that affects the product particle size distribution from the comminution machine. These are for instance, the 50 % (or average) product size reduction ratio index, $S_{50\%}$, the 80 % product size reduction ratio index, $S_{80\%}$, the 50 % (or average) passing size of the product, $P_{50\%}$, the 80 % passing size of the product, $P_{80\%}$ [79] and the maximum product particle size, $P_{max}$ [78]. All these parameters are based on empirical models. For HPGR, these product quality indices have been found to be more dependent on the rolls operating pressure than the rolls speed [80]. When the rolls operating pressure is within its operating range, for a given moisture amount in the feed product, the product size reduction ratio index can be expressed as function of the rolls operating pressure through a linear relationship as [79]:

$$S_x = \frac{F_x}{P_x} = a_x R_P + b_x, \tag{5.14}$$

where $x$ is the $x$ % passing percentage (50 %) or (80 %); $S_x$ is the $x$ % product size reduction ration index $(-)$; $F_x$ and $P_x$ are the $x$ % passing size $(m)$ of the feed material and product material, respectively; $a_x$ and $b_x$ are constants of model fitting. It can be seen that for a given passing size of the feed material, $F_x$, $P_x$ can also be derived from Eq.(5.14) as:

$$P_x = \frac{F_x}{a_x R_P + b_x}. \tag{5.15}$$

The maximum product particle size, $P_{max}$ $(m)$, is expressed by a hyperbolic relationship as follows [78]:

$$P_{max} = A_1 R_P^{-b_1}, \tag{5.16}$$

where $A_1$ and $b_1$ are constants of model fitting.

### 5.2.3 Energy model analysis

Fig. 5.2 depicts the 3D analytical performance of HPGR in terms of the power consumption (left-hand side of graph) and the throughput rate (right-hand side of graph). The data of this HPGR are found in [77]. The analysis of this figure shows that both rolls speed and

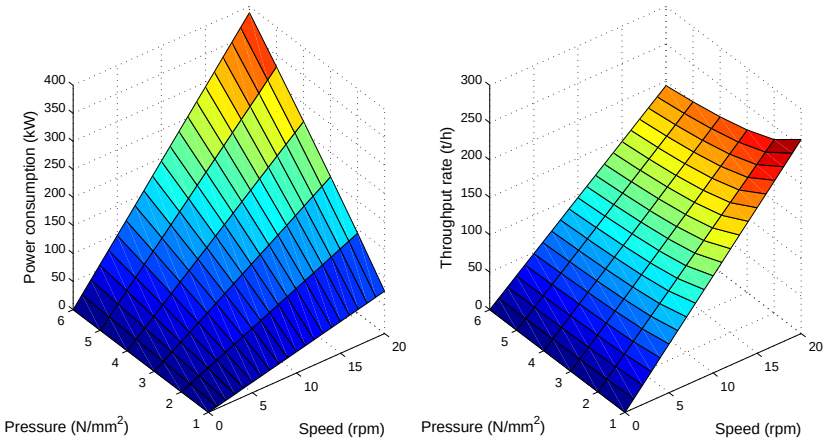


**Figure 5.2:** 3D plots of the analytical models of power consumption and throughput rate of HPGR machine

rolls operating pressure have considerable effect on the HPGR power consumption, while the throughput rate is more dependent on the rolls speed than the rolls operating pressure. It is therefore seen that the HPGR power consumption can be minimized by either reducing the rolls speed or the rolls operating pressure. However, the reduction of the rolls speed will unfortunately result in a HPGR throughput rate decrease. On the other hand, if the rolls operating pressure is decreased for power consumption minimization, the product quality performance will decay, as this will lead to smaller reduction ratio (see Eq.(5.14)) or bigger product size (see Eq.(5.15)).

The analysis above clearly shows that the optimization of an HPGR process circuit is in reality a multi-objective problem because of the trade-off between the three traditional performance indices.

In comminution processes, when the product quality index is set as a requirement or con-

straint, the two remaining performance indices (power consumption and throughput rate) are combined in a unique performance index through which the two performance indices can be simultaneously optimized. This is referred to as specific energy consumption, defined as the ratio between power consumption and throughput rate. Hence, minimizing the HPGR specific energy consumption means minimizing its power or energy consumption by maximizing its throughput rate. The specific energy consumption of HPGR is shown in Fig. 5.3. From this figure, it is seen that the variation in rolls speed has no effect on the HPGR specific energy consumption, while the increase in rolls operating pressure leads to an increase in specific energy consumption. This observation is also demonstrated through experimental results in [80].

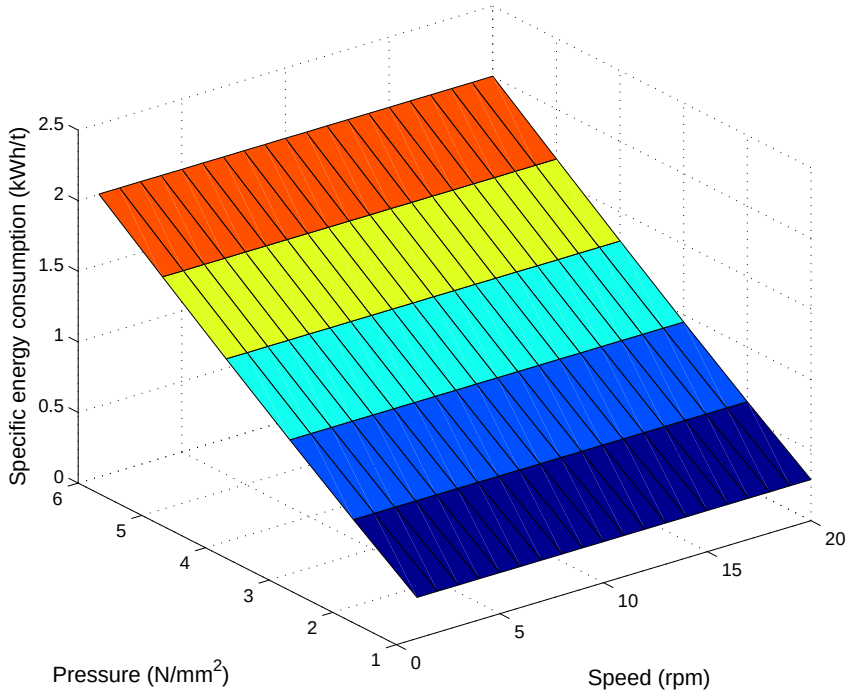


**Figure 5.3:** 3D plot of the analytical specific energy model of HPGR machine

It is therefore observed that the only control variable affecting the specific energy consumption of the HPGR process is the rolls operating pressure. However, in practice, the rolls speed still needs to be taken as additional flexible operating parameter in order to control the HPGR throughput rate in such a way as to compensate continuously for the feed rate change due to the upstream circuit schedule or load shifting scheme. It is noted that Figs. 5.2-5.3

represent the operating region of the HPGR crusher analysed above where this machine can be operated at different operating points depending on the desired product quality (fixed by the rolls operating pressure) and throughput (fixed by the rolls speed) to be achieved at various periods.

## 5.3 ENERGY OPTIMIZATION MODEL

### 5.3.1 Description of a parallel HPGR crushing circuit

As previously discussed, the HPGR machine is usually employed in comminution circuit, for replacement of primary grinding machines such as ball mills, AG mills and SAG mills or in the last stage crushing process such as tertiary and quaternary crushing. In this work, the author considers a case where the HPGR machine is used in a last stage crushing station with a parallel configuration as shown in Fig. 5.4. The Vasilkovskoye gold mine in Central Asia

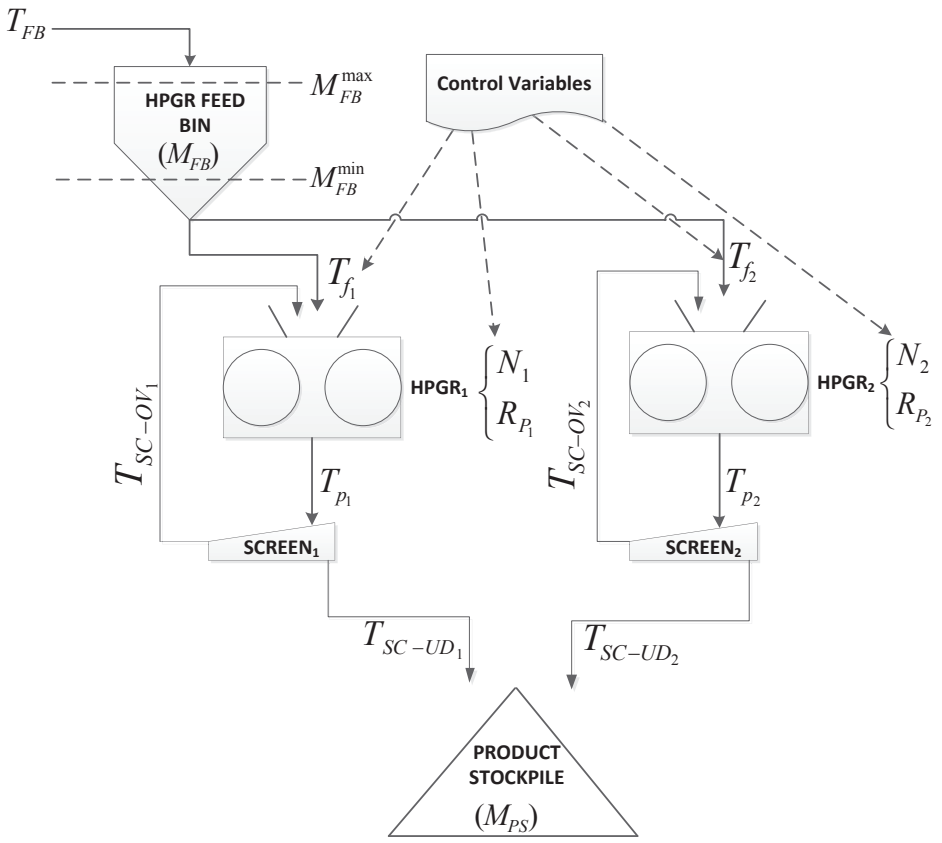


**Figure 5.4:** Schematic of a parallel HPGR crushing circuit with two machines

is an industrial example where a parallel configuration with two Humboldt Wedag HPGR crushers has been operating since 2009 [81].

In a tertiary crushing process such as shown in Fig. 5.4, the ore material from the crusher bin is processed by the two parallel HPGRs, at fresh feed flow rates of $T_{f_1}$ and $T_{f_2}$, respectively, before being discharged to the screens at flow rates of $T_{p_1}$ and $T_{p_2}$, respectively. The upstream crusher bin is supposed to receive the ore material from a secondary crushing station at a feed flow rate of $T_{FB}$. During operation, the mass of ore in the crushing bin, $M_{FB}$, is subject to certain maximum and minimum capacity limits of receptively, $M_{FB}^{max}$ and $M_{FB}^{min}$. After the ore product has been discharged to the screens for size control, the amount of ore material of a size higher than the screen aperture, called screen oversize, is fed back or recirculated to the crusher bin, at flow rates of $T_{RC-OV_1}$ and $T_{RC-OV_2}$, respectively. The ore material of a size less than the screen aperture, called screen undersize, goes to the downstream grinding stockpile, at flow rates of respectively, $T_{SC-UD_1}$ and $T_{SC-UD_2}$. The total crushed material is stored in the product stockpile of mass $M_{PS}$.

### 5.3.2 Objective function

The performance index considered in this work is the total energy cost to be minimized by taking advantage of the TOU electricity tariff. Hence, for $n$ HPGRs in parallel, the objective function in Eq.(5.11) is discretized for simplicity and expressed as:

$$min \sum_{i=1}^{n} \sum_{j=1}^{N_s} P_{el_i} \left( N_i^j, R_i^j \right) p^j t_s, \tag{5.17}$$

where $N_s$ is the total number of sampling intervals; $j$ is the $j^{th}$ sampling interval; $p^j$ is the electricity price at $j^{th}$ sampling interval; $t_s$ is the sampling time, expressed as $t_s = \frac{t_f - t_0}{N_s}$.

### 5.3.3 Constraints

During operation, the parallel HPGR circuit is subject to physical and operational or technical constraints. Physical constraints are the physical limitations of crushing circuit equipment according to their design specifications. According to Fig. 5.4, these are, for instance, the bin upper level, $M_{FB}^{max}$, to prevent ore material from overflowing and bin lower level, $M_{FB}^{min}$, to avoid the bin running empty. Each HPGR also has limitations on rolls speed, $N$, rolls operating pressure, $R_P$, rolls gap, $S_0$, and throughput rate, $T_p$, which need to be maintained

within a certain range based on design specifications.

On the other hand, operational or technical constraints are those that are directly linked to the HPGR crushing process for production maximization as well as product quality improvement. These are, for instance, the mass balances in the HPGR and screens.

#### 5.3.3.1 HPGR feed bin level limits

At any time, for $n$ parallel HPGRs, the quantity of the ore stored or available in the HPGR feed bin can be calculated based on the first difference equation as follows:

$$M_{FB}^{j} = M_{FB}^{j-1} + t_s \left( T_{FB}^{j-1} - \sum_{i=1}^{n} T_{fi}^{j-1} \right). \tag{5.18}$$

Based on induction reasoning, the dynamics of the bin level can be expressed in terms of the initial level, $M_{FB}^{0}$, as follows:

$$M_{FB}^{j} = M_{FB}^{0} + t_s \sum_{k=1}^{j} \left( T_{FB}^{k} - \sum_{i=1}^{n} T_{fi}^{k} \right). \tag{5.19}$$

The bin level constraints can therefore be written as:

$$M_{FB}^{min} \leq M_{FB}^{0} + t_s \sum_{k=1}^{j} \left( T_{FB}^{k} - \sum_{i=1}^{n} T_{fi}^{k} \right) \leq M_{FB}^{max}, \ (1 \leq i \leq n; 1 \leq j \leq N_s). \tag{5.20}$$

#### 5.3.3.2 HPGR variable limits

These are upper and lower bounds on each HPGR operational parameters. These constraints are given as follows:

$$\begin{cases} N_i^{min} \leq N_i^{j} \leq N_i^{max}, \ (1 \leq i \leq n; 1 \leq j \leq N_s), \\ R_{P_i}^{min} \leq R_{P_i}^{j} \leq R_{P_i}^{max}, \ (1 \leq i \leq n; 1 \leq j \leq N_s), \\ S_{0_i}^{min} \leq S_{0_i}^{j} \leq S_{0_i}^{max}, \quad (1 \leq i \leq n; 1 \leq j \leq N_s), \\ T_{P_i}^{min} \leq k_{1_i} N_i^{j} R_{P_i}^{-bj} \leq T_{P_i}^{max}, \quad (1 \leq i \leq n; 1 \leq j \leq N_s), \\ T_{f_i}^{min} \leq T_{f_i}^{j} \leq T_{f_i}^{max}, \quad (1 \leq i \leq n; 1 \leq j \leq N_s). \end{cases} \tag{5.21}$$

#### 5.3.3.3 HPGR circuit operational requirement

These constraints are given as follows:

• Mass balance in HPGRs

For efficient operation of HPGR, the fresh feed rate should always equal the throughput rate in order to avoid the HPGR crushing zone from being obstructed. This constraint is given as:

$$T_{f_i}^j + T_{SC-OV_i}^j = T_{p_i}^j = k_{1_i} N_i^j R_{P_i}^{-bj}, \ \ (1 \leq i \leq n; 1 \leq j \leq N_s)\,. \tag{5.22}$$

By relating the throughput rate $T_p$ to the screen oversize flow rate $T_{SC-OV}$ through a ratio, referred to as recirculated mass ratio $\alpha$, as $T_{SC-OV} = \alpha T_p$, Eq.(5.22) can be rewritten and expressed in terms of the control variables as follows:

$$T_{f_i}^j = \left(1 - \alpha_i^j\right) T_{p_i}^j = \left(1 - \alpha_i^j\right) k_{1_i} N_i^j R_{P_i}^{-bj}, \ \ (1 \leq i \leq n; 1 \leq j \leq N_s)\,. \tag{5.23}$$

• Throughput capacity requirement

Each mining operator has a daily, weekly, monthly or annual production target to be achieved on the crushing circuit. To ensure this, the total amount of ore crushed should be greater than or equal to the throughput capacity target (requirement), $M_{SP}^{target}$, stored in the product stockpile for a given period. This can be expressed as:

$$\sum_{i=1}^{n} \sum_{j=1}^{N_s} T_{SC-UD_i}^j t_s \geq M_{PS}^{target}. \tag{5.24}$$

The screen undersize flow rate $T_{SC-UD}$ can be written as $T_{SC-UD} = (1 - \alpha)\, T_p$ knowing that $T_p = T_{SC-OV} + T_{SC-UD}$. With this, Eq.(5.24) can be rewritten and expressed as follows:

$$\sum_{i=1}^{n} \sum_{j=1}^{N_s} \left(1 - \alpha_i^j\right) k_{1_i} N_i^j R_{P_i}^{-bj} t_s \geq M_{PS}^{target}. \tag{5.25}$$

• Product quality requirement

The more practical product quality index can be considered to be the maximum particle size in the product, $P_{max}$. During HPGR operation, this should be kept smaller than a specified

value, $P_{max}^{spec}$. According to reference [78], this constraint can be written as follows:

$$A_1 R_{P_i}^{-jb_1} \leq P_{max}^{spec}, \ (1 \leq i \leq n; 1 \leq j \leq N_s)\,. \tag{5.26}$$

## 5.4 CASE STUDY AND SIMULATION RESULTS

In order to demonstrate the feasibility of the proposed technique, an anonymous parallel $HRC^{TM}800$ HPGR crushing process as shown in Fig. 5.4 is used for simulations under three different scenarios. The rock processed is copper ore. The effectiveness of the proposed optimal energy control model is analyzed by comparing its simulation results to those of the current control technique considered as baseline. The current control technique is formulated as in Chapters 3 and 4, where the objective is to meet the total plant production target under given system constraints. For simplicity, an open circuit HPGR application is considered in all simulations, hence the recirculated material is zero ($\alpha = 0$). As previously discussed, in practice, the rolls operating pressure $R_P$ is varied in such a way as to yield a constant product quality requirement index for any change in material feed size. $R_P$ is pre-set to a constant value for a given constant feed size distribution, and hence the rolls rotational speed $N$ and fresh feed rate $T_f$ remain as the only control variables. Since the rolls operating pressure is fixed, the optimal energy control model becomes a linear programming problem and hence, the *linprog* function of Matlab Optimization Toolbox is used. The optimal results from the *linprog* function of Matlab Optimization Toolbox are also compared to those obtained with the *opti* function of Opti Toolbox.

### 5.4.1 Data presentation

#### 5.4.1.1 Time-of-use electricity tariff

The same Eskom Megaflex electricity tariff for larger industrial consumers, used in Chapter 4, is considered for simulations.

#### 5.4.1.2 HPGR crusher and ore characteristics

The technical data for the two identical HPGRs are given as follows:[2] the installed electric power is 220 $kW$ (300 $hp$) each; the rolls diameter $D$ and width $L$ are 800 $mm$ and 500 $mm$, respectively; the maximum value of the rolls rotational speed $N$ is 32 $rpm$; the synchronous speed is 1800 $rpm$ (A four-pole squirrel cage induction motors at 60 $Hz$); the maximum value of the rolls operating pressure $R_P$ is 4.5 $N/mm^2$; the maximum feed size is 32 $mm$; the maximum value of the throughput rate $T_p$ is about 120 $t/h$ (however, in this work, 110 $t/h$ is used as maximum throughput rate). Although the motor synchronous speed of the $HRC^{TM}$800-series HPGR crusher is 1800 $rpm$ at 60 $Hz$, in this work, the synchronous frequency is taken as 50 $Hz$ as this is standard in South Africa; hence a synchronous speed of 1500 $rpm$ for a four-pole squirrel induction motor. With this, the gearbox reduction ratio is therefore about 46.4 : 1 (with the rotor speed of the squirrel cage induction motor being about 1485 $rpm$ for a slip of 1 %). The motor considered is assumed to be a premium efficiency motor-IE3 whose efficiency is 95.4 % for each 110 $kW$ motor rating.[3] With a gearbox efficiency of 85 % for medium-ratio helical-worm speed reducers (20:1 to 60:1) [82], and a drive coupling efficiency of 99 % [83], the overall drive efficiency is calculated as $0.954 \times 0.85 \times 0.99 = 80.28$ %. The no-load power is assumed to be 6 % of the full power, compared to 3.75 % for bigger HPGR crushers in [84]. Hence, the proportional constant of no-load power $c$ is calculated as $\frac{220\ kW \times 0.8028 \times 0.06}{32\ rpm} = 0.33\ kW/rpm$. The characteristics of the copper ore used are as follows: the specific gravity (density) $\rho$ is 2.7 $t/m^3$; the bulk density $\rho_a$ of 1.6 $t/m^3$ and the maximum feed size is 30 $mm$

#### 5.4.1.3 HPGR feed bin

The fresh feed rate to the HPGR feed bin, $T_{FB}$ is given in Tables 5.1-5.3. This is assumed to be predicted with an average value of 138 $t/h$ to which a randomly distributed inaccuracy/uncertainty or error $\mathcal{W}$ within $[-\varepsilon, \varepsilon]$ $t/h$ as given by the following equation:

$$T_{FB}^{j} = 138 + \mathcal{W}^{j} \tag{5.27}$$

[2] Metso, $HRC^{TM}$800, <http://www.metso.com> [Last accessed: 08 October 2014]

[3] ABB, Technical note-IEC 60034-30-1 Standard on efficiency classes for low voltage AC motors, <http://www.abb.com> [Last accessed: 09 March 2015]

with $\mathcal{W}^j = -\varepsilon + 2\varepsilon r(j)$, where $r(j)$ are uniformly distributed random numbers on $[0, 1]$ and $\varepsilon$ is a given error bound [85]. In all simulations, $\varepsilon$ is assumed to be 4 $t/h$; the capacity of the feed bin is 1875 $t$; the upper limit and lower limit of the feed bin are set, respectively, to 80 % and 24 % of the bin capacity; and the initial ore level $M_{FB}^0$ is set to 64 % of the bin capacity.

**Table 5.1:** Fresh feed rate for 24 h

| Time [h] | 1 | 2 | 3 | 4 | 5 | 6 | 7 | 8 |
|---|---|---|---|---|---|---|---|---|
| Feed rate [t/h] | 135.5 | 135.9 | 136.8 | 137.6 | 138.0 | 138.9 | 139.3 | 139.7 |

**Table 5.2:** Fresh feed rate for 24 h (continued)

| Time [h] | 9 | 10 | 11 | 12 | 13 | 14 | 15 | 16 |
|---|---|---|---|---|---|---|---|---|
| Feed rate [t/h] | 140.6 | 141.4 | 141.8 | 139.3 | 141.4 | 140.6 | 139.7 | 138.5 |

**Table 5.3:** Fresh feed rate for 24 h (continued)

| Time [h] | 17 | 18 | 19 | 20 | 21 | 22 | 23 | 24 |
|---|---|---|---|---|---|---|---|---|
| Feed rate [t/h] | 134.6 | 138.9 | 139.7 | 141.4 | 140.6 | 138.9 | 137.2 | 136.3 |

### 5.4.2 Simulation results

The sampling period $t_s$ of 10 $min$ within a control horizon $[t_0, t_f]$ of 24 $h$ and total production target $M_{PS}^{target}$ of 3500 $t$ are considered for all simulations.

***Case I: Optimal energy control with equal overall drive efficiency***

In this scenario, the two HPGRs are assumed to have equal overall drive efficiency of $\eta_{D_1} = \eta_{D_2} = 80.28$ %. The rolls operating pressure is pre-set to 4.5 $N/mm^2$. The feasibility of the current control technique is shown in Fig. 5.5, while that of optimal energy control techniques based on *linprog* of Matlab Optimization Toolbox and *opti* of Opti Toolbox are, respectively, shown in Figs. 5.6 and 5.7.

The performance of the two optimal energy control techniques is compared in Fig. 5.8 and

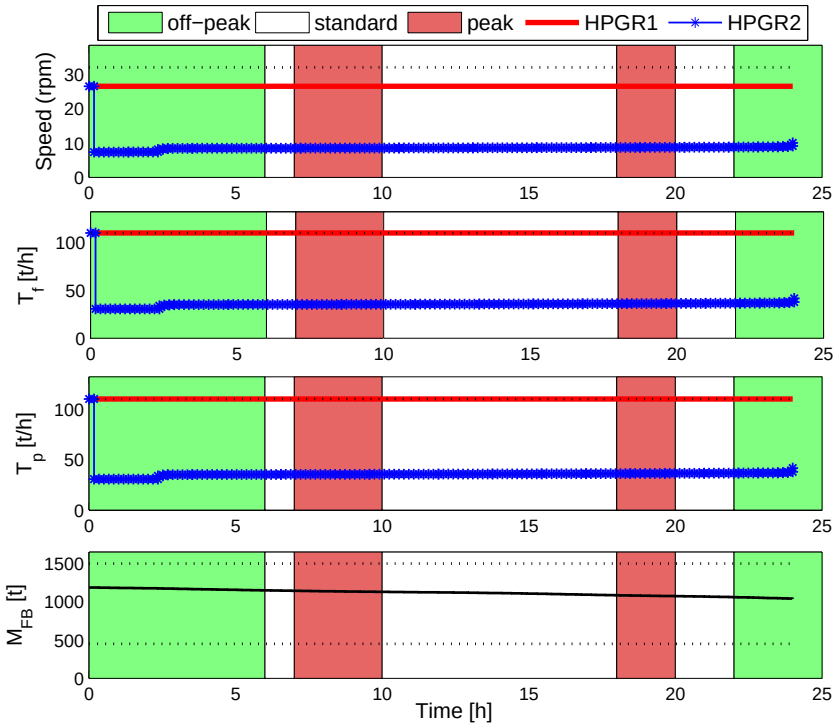


**Figure 5.5:** Current control technique

Tables 5.4-5.6. The dotted lines in Figs. 5.5-5.7 denote the maximum and minimum of the corresponding variable. It is shown that both current control and optimal energy control techniques operate the parallel HPGR under the given constraints.

However, on the one hand, Fig. 5.5 shows that the current control scheme runs the two HPGR crushers under almost constant speed, leading therefore to an even distribution of both fresh feed rate $T_f$ and product rate (throughput rate) $T_p$ along the 24 $h$ control horizon. Also, it can be seen that current control chooses to run the first HPGR at a high speed of around 26.5 $rpm$, which corresponds to its maximum loading level of 110 $t/h$. The second HPGR is therefore used as a buck-up crushing machine with a lower loading level of about 36 $t/h$ in order to meet the daily production target assigned to 3500 $t$. Since the crushing load is evenly distributed along the control horizon because of the lack of TOU tariff consideration, the energy cost reduction through load shifting cannot be achieved using the current control technique. Consequently, a high energy cost is incurred.

On the other hand, Figs. 5.6-5.7 show that both optimal energy control techniques run the two parallel HPGRs with equal loading level by shifting the load from peak time to off-peak

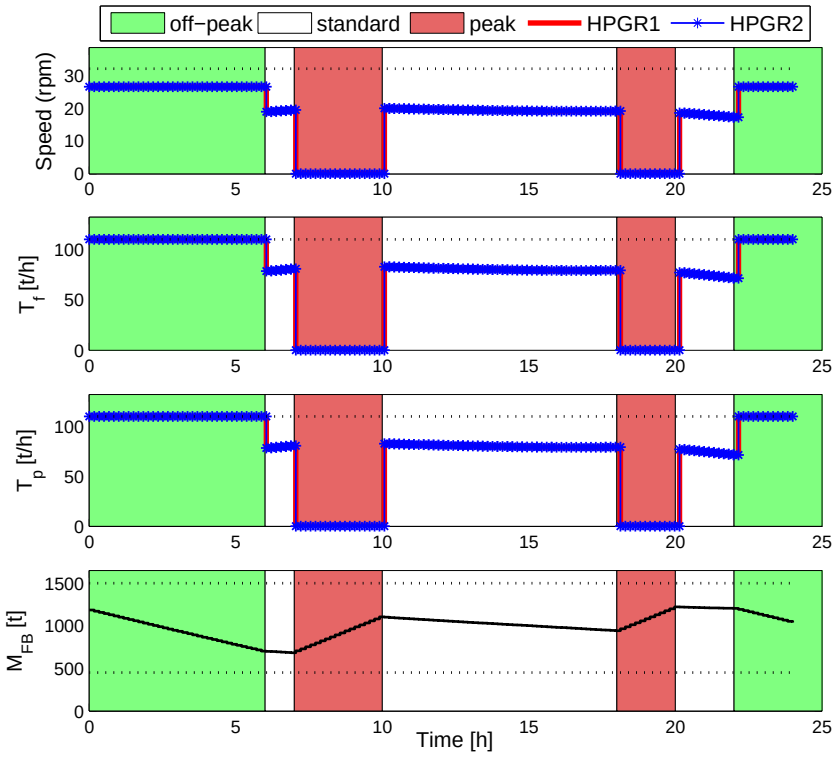


**Figure 5.6:** Optimal energy control technique with equal overall drive efficiency, $\eta_{D_1} = \eta_{D_2} = 80.28$ % using the *linprog* function of Matlab Optimization Toolbox

and standard time in order to reduce the energy cost. The reason for the optimal energy controllers running the two HPGRs with equal load is that the two machines are assumed to have equal overall efficiency. In the current control, although the two HPGRs have equal overall efficiency, their loading levels are not necessarily the same because the energy model is not taken into account in the cost function.

The performance indices in terms of cumulative energy cost and energy consumption of both current control and optimal energy control techniques are presented in Fig. 5.8 and Tables 5.4-5.6. It is seen that at the end of the control horizon (24 $h$), the energy cost is sensibly reduced when optimal energy control techniques are used. About 41.93 % energy cost saving is achieved with both optimal energy control techniques. However, simulation results do not show any energy consumption reduction or energy saving. The reason is that the rolls operating pressure which is the main variable controlling the specific energy consumption of the HPGR, is constant in order to yield a constant required product size distribution.

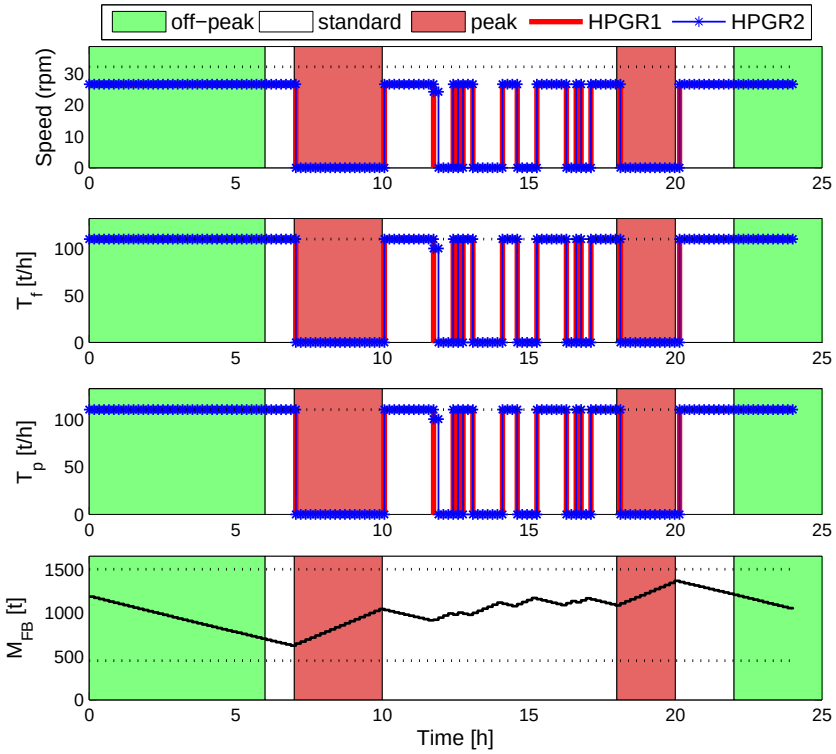


**Figure 5.7:** Optimal energy control technique with equal overall drive efficiency, $\eta_{D_1} = \eta_{D_2} = 80.28$ % using the *opti* function of Opti Toolbox

**Table 5.4:** Production and corresponding energy cost and consumption with equal overall drive efficiency, $\eta_{D_1} = \eta_{D_2} = 80.28$ %

| Technique | Production (t) | Energy cost (R) | Energy consumption (kWh) | Simulation time (s) |
|---|---|---|---|---|
| Current control | 3500.2 | 6038.7 | 6761.8 | / |
| Optimal energy control using the *linprog* function | 3500.0 | 3506.3 | 6761.4 | 0.302 |
| Optimal energy control using the *opti* function | 3500.0 | 3506.3 | 6761.4 | 0.271 |

Although both optimal energy control techniques give the same performance as shown in Fig. 5.8 and Tables 5.4-5.6, comparison of Fig. 5.6 and Fig. 5.7 reveals that the load profiles from the two techniques are different, especially during standard periods. It is shown that during standard periods, the optimal energy control technique based on the *linprog* function

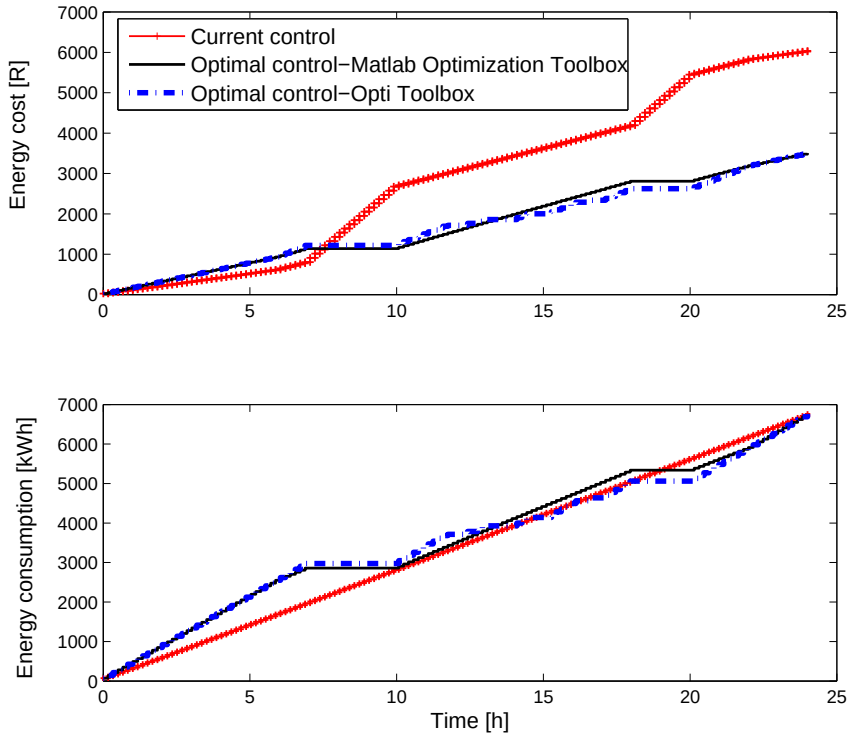


**Figure 5.8:** Cumulative energy cost and consumption with equal overall drive efficiency, $\eta_{D1} = \eta_{D_2} = 80.28\ \%$

**Table 5.5:** Cost saving of optimal energy control technique with equal overall drive efficiency, $\eta_{D_1} = \eta_{D_2} = 80.28\ \%$

| Technique | Specific energy cost (R/t) | Cost saving (%) |
|---|---|---|
| Current control | 1.7252 | / |
| Optimal energy control using the *linprog* function | 1.0018 | 41.93 |
| Optimal energy control using the *opti* function | 1.0018 | 41.93 |

of Matlab Optimization Toolbox smoothly operates each HPGR crusher at a reduced speed of about 19 $rpm$, corresponding to a loading level of about 80 $t/h$. With the *opti* function of Opti Toolbox, however, each HPGR crusher is frequently switched on and off from its

**Table 5.6:** Energy saving of optimal energy control technique with equal overall, $\eta_{D_1} = \eta_{D_2} = 80.28$ %

| Technique | Specific energy consumption (kWh/t) | Energy saving (%) |
|---|---|---|
| Current control | 1.9318 | / |
| Optimal energy control using the *linprog* function | 1.9318 | 0.00 |
| Optimal energy control using the *opti* function | 1.9318 | 0.00 |

maximum loading level of 110 $t/h$ to its minimum loading level of 0 $t/h$, which in practice, may lead to extra energy consumption during the starting period of the machine. The high current required during starting periods will not only lead to extra energy consumption, but also to electrical stress on the electric motors, cables, transformers, breakers, transmission lines, etc. Moreover, the resulting high starting torque pulsations will generally lead to mechanical stress on transmission shafts, bearings, mechanical drive coupling and vibrations of the concrete foundation supporting the HPGR crusher. However, as shown in Table 5.4, the optimal solutions when using the *opti* function are obtained with less computational time.

***Case II: Optimal energy control with different overall drive efficiency***

This scenario investigates the influence of the discrepancy between the overall efficiency of two parallel crushing machines, HPGR1 and HPGR2, during operation due to the unequal feeding characteristics of the two crushers. During the control horizon of 24 $h$, the first crusher, HPGR1, is assumed to run with a decreased overall efficiency of $\eta_{D_1} = 76$ % while the overall efficiency of the second crusher, HPGR2, is kept at its initial value of $\eta_{D_2} = 80.28$ %. The rolls operating pressure of the two machines is also pre-set to 4.5 $N/mm^2$.

Simulation results for this scenario are given in Figs. 5.9-5.11 and Tables 5.7-5.9. It can be seen from Figs. 5.9-5.10 that both optimal energy control techniques shift the loads of the two HPGRs from peak time to off-peak and standard time for energy cost minimization. However, unlike case I, the same figures (Figs. 5.9-5.10) show that the optimal energy control

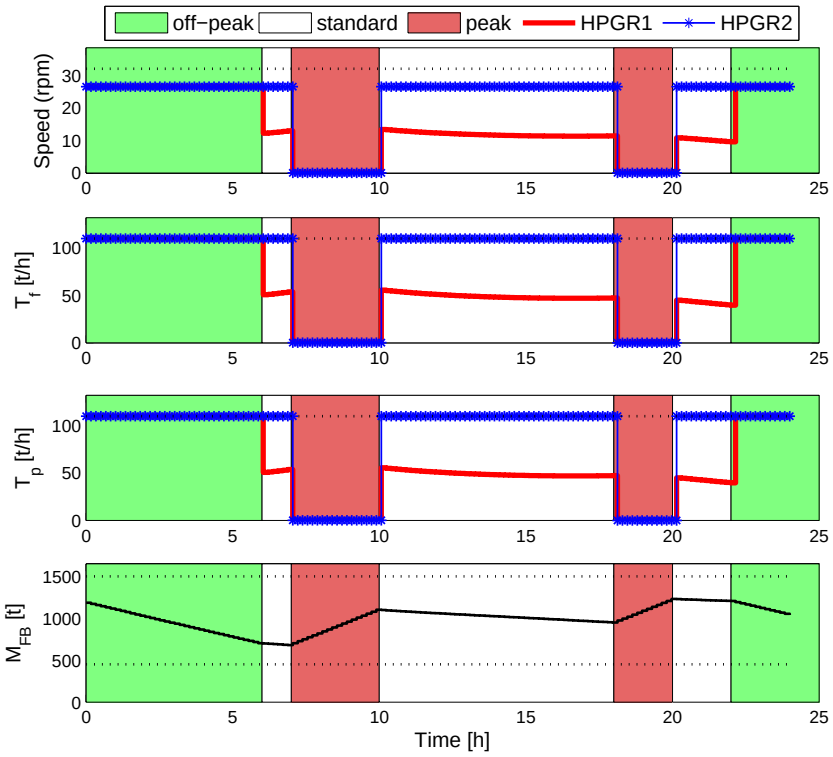


**Figure 5.9:** Optimal energy control technique with different overall drive efficiency, $\eta_{D_1} = 76\%, \eta_{D_2} = 80.28$ % using the *linprog* function of Matlab Optimization Toolbox

**Table 5.7:** Production and corresponding energy cost and consumption with different overall drive efficiency, $\eta_{D_1} = 76\%, \eta_{D_2} = 80.28$ %

| Technique | Production (t) | Energy cost (R) | Energy consumption (kWh) | Simulation time (s) |
|---|---|---|---|---|
| Current control | 3500.2 | 6292.3 | 7045.7 | / |
| Optimal energy control using the *linprog* function | 3500.0 | 3579.2 | 6913.0 | 0.308 |
| Optimal energy control using the *opti* function | 3500.0 | 3579.2 | 6913.0 | 0.277 |

techniques detect the discrepancy between the two machines' overall efficiencies and therefore run HPGR2, which has higher overall efficiency at a higher loading level, while HPGR1 is operated at a lower loading level for most of the time because of lower overall efficiency. The

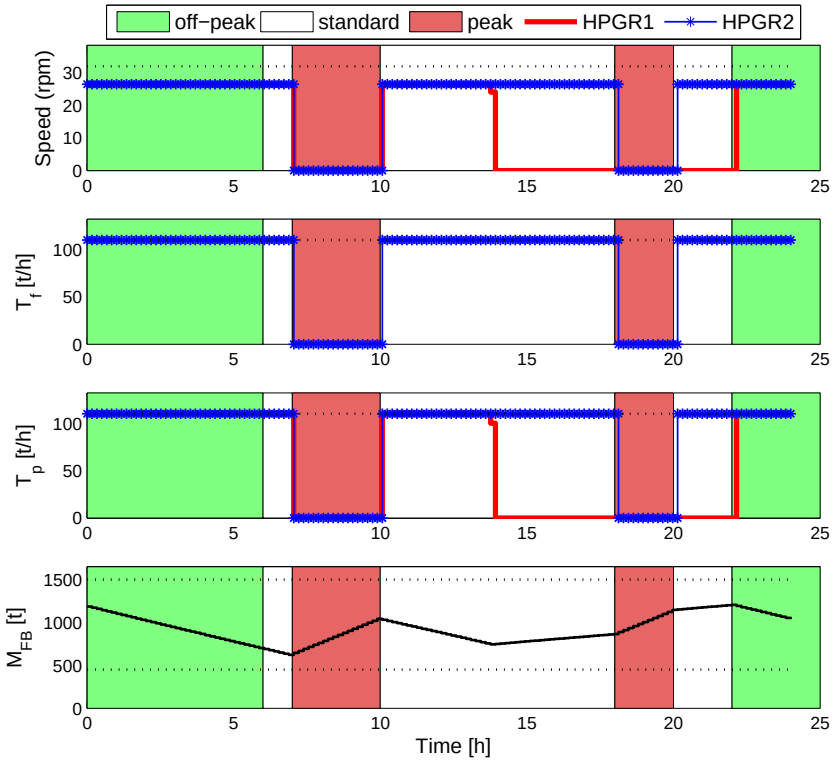


**Figure 5.10:** Optimal energy control technique with different overall drive efficiency, $\eta_{D_1} = 76\%, \eta_{D_2} = 80.28$ % using the *opti* function of Opti Toolbox

**Table 5.8:** Cost saving of systems optimization control technique with different overall drive efficiency, $\eta_{D_1} = 76\%, \eta_{D_2} = 80.28$ %

| Technique | Specific energy cost (R/t) | Cost saving (%) |
|---|---|---|
| Current control | 1.7977 | / |
| Optimal energy control using the *linprog* function | 1.0226 | 43.17 |
| Optimal energy control using the *opti* function | 1.0226 | 43.17 |

reason for this is to reduce system energy consumption. From a multi-objective optimization point of view, smaller overall efficiency means higher weight and bigger overall efficiency means lower weight. This is due to the fact that the overall efficiency is inversely proportional to the electric power consumption as shown in Eq.(5.9). Fig. 5.11 shows a reduction in both

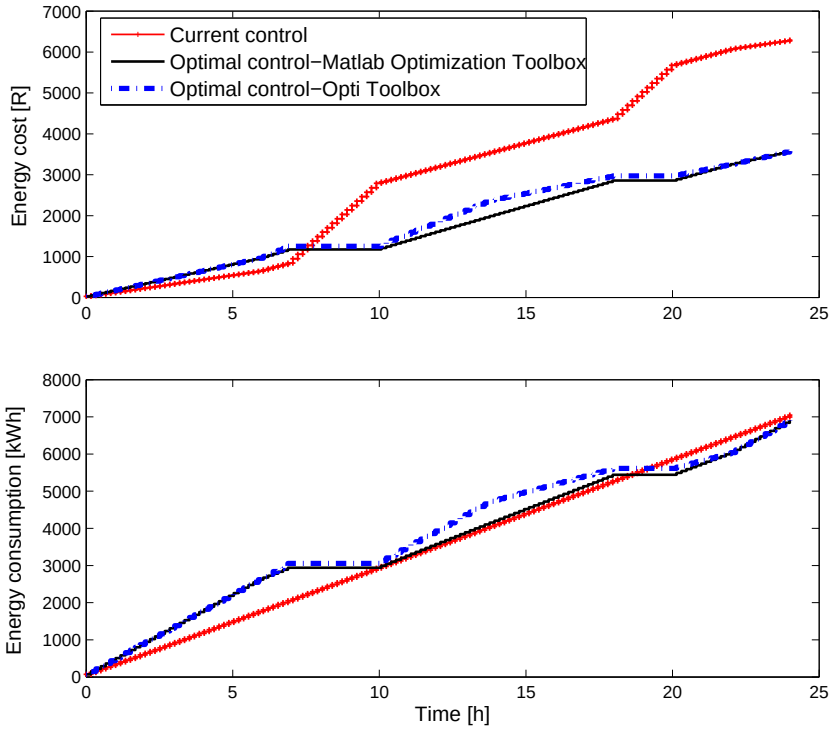


**Figure 5.11:** Cumulative energy cost and consumption with different overall drive efficiency, $\eta_{D_1} = 76\%, \eta_{D_2} = 80.28$ %

**Table 5.9:** Energy saving of systems optimization technique with different overall, $\eta_{D_1} = 76\%, \eta_{D_2} = 80.28$ %

| Technique | Specific energy consumption (kWh/t) | Energy saving (%) |
|---|---|---|
| Current control | 2.0129 | / |
| Optimal energy control using the *linprog* function | 1.9752 | 1.87 |
| Optimal energy control using the *opti* function | 1.9752 | 1.87 |

energy cost and energy consumption. As shown in Tables 5.8-5.9, the corresponding energy cost saving is 43.17 % and energy saving is 1.87 % for both optimization techniques. The small increase in energy cost saving of about 1.24 % compared to case I (41.93%) comes from the 1.87 % energy saving and the rest comes from load shifting.

Similar to case I, with the *lingrop* function, the crusher with lower efficiency (HPGR1) is smoothly operated at a reduced loading level of about 50 $t/h$ during standard periods while with the *opti* function, the machine is switched on and off between its maximum and minimum loading levels.

In practice, however, the feasibility of the proposed model in saving the energy under this scenario depends on the predictability of the overall drive efficiency of each HPGR crusher with respect to the feed characteristics and feeding condition.

***Case III: Sensitivity of rolls operating pressure on energy and cost savings***

As discussed in Section 5.2.3, the rolls operating pressure is the unique control variable affecting the specific energy consumption of the HPGR crusher.

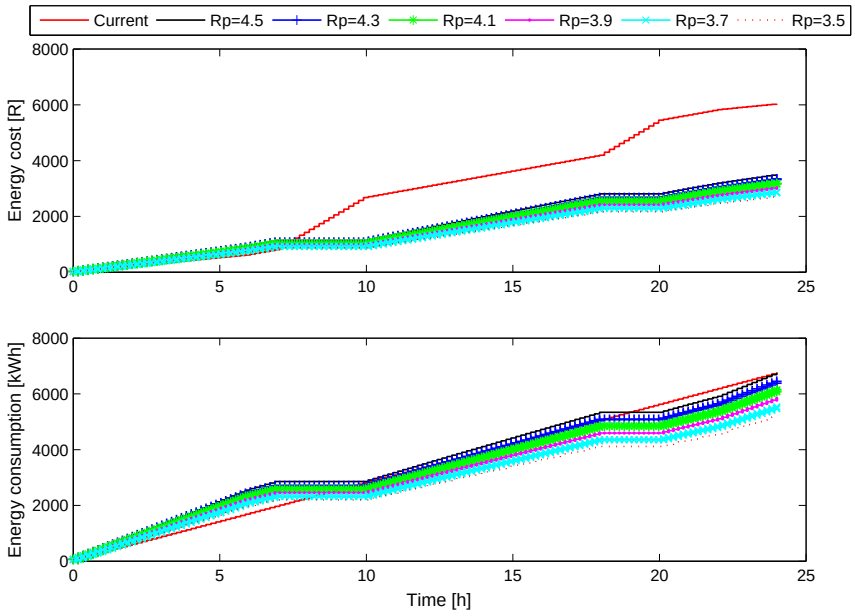


**Figure 5.12:** Sensitivity of rolls operating pressure on cumulative energy cost and energy consumption

However, owing to the trade-off between energy consumption and product quality (product particle size distribution), any attempt at decreasing the HPGR energy consumption by decreasing the rolls operating pressure will lead to coarser particles in the product. In this scenario, small variations in the rolls operating pressure on HPGR energy saving and product

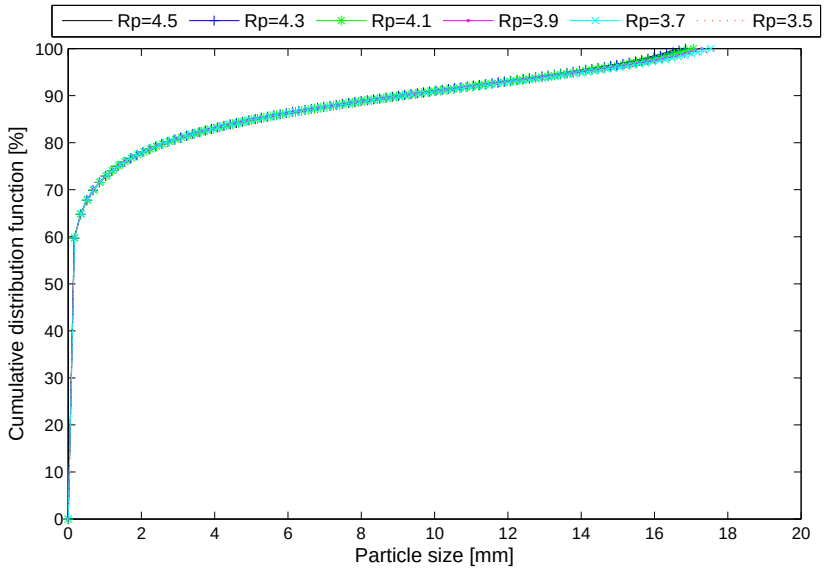


**Figure 5.13:** Sensitivity of rolls operating pressure on product size distribution

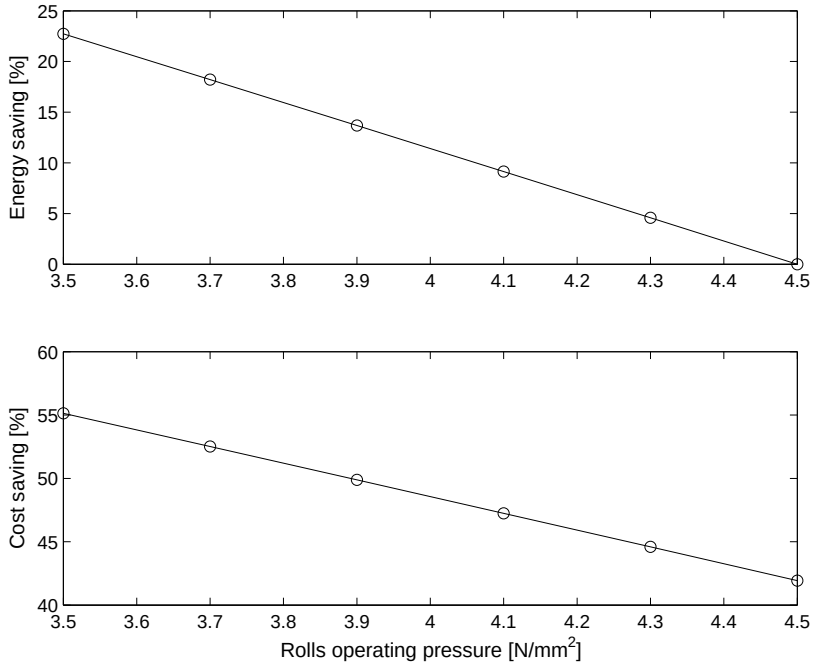


**Figure 5.14:** Sensitivity of rolls operating pressure on Energy and cost savings

particle size distribution are investigated. The product particle size distribution is based on the modified Rosin-Ramler Bennets' distribution, expressed as a function of the rolls operating pressure as given in [78]. The rolls operating pressure is decreased from 4.5 $N/mm^2$

to 3.5 $N/mm^2$ with a step of 0.2 $N/mm^2$. The overall efficiency of the two HPGR machines is the same as in case I ($\eta_{D_1} = \eta_{D_2} = 80.28$ %). Simulation results are shown in Figs. 5.12-5.14. It can be seen from Fig. 5.12 that a small decrease in the rolls operating pressure leads to considerable energy consumption and cost reduction without significant change in product particle size distribution as shown in Fig. 5.13. The actual savings obtained are shown in Fig. 5.14. This figure shows that for every 0.2 $N/mm^2$ decrement in the rolls operating pressure, the energy saving and energy cost saving linearly increase by approximately 4.5 % and 2.6 %, respectively, while the product quality remains almost unaltered. For a total decrement in rolls operating pressure of 1 $N/mm^2$, an energy saving of 22.72 % and energy cost saving of 55.13 % are achieved.

However, in practice, in order to achieve the energy saving of the HPGR process through a small change in the rolls operating pressure by maintaining the product quality performance, a highly accurate regulatory controller is required to track and maintain the desired small changes in the rolls operating pressure.

## 5.5 CONCLUSION

An optimal energy control model is proposed for the energy management of a parallel HPGR crushing process. A case study of a tertiary copper crushing process is formulated and solved under three different scenarios.

In the first scenario, where two HPGRs are assumed to have equal overall drive efficiency with a fixed rolls operating pressure, simulation results reveal the potential of reducing the specific energy cost of about 41.93 % without any energy consumption reduction.

In the second scenario, where the overall drive efficiency of two parallel HPGR are different with a fixed rolls operating pressure, it is shown that the energy saving is achieved by minimizing the loading level of the less efficient HPGR machine and maximizing the loading level of the more efficiency HPGR machine. A potential of energy saving of 1.87 % and energy cost saving of 43.17 % is shown.

In the last scenario where the sensitivity of rolls operating pressure is investigated on the trade-off between energy saving and product quality, it is shown that the specific energy

consumption of the HPGR is more sensitive to the change in the rolls operating pressure than the product quality is. For any small decrement of 0.2 $N/mm^2$ in the rolls operating pressure, a potential 4.5 % increase in energy saving is shown without a significant change in product quality.

# CHAPTER 6

# LABORATORY EXPERIMENTS FOR PERFORMANCE ANALYSIS OF A JAW CRUSHER

## 6.1 INTRODUCTION

A considerable number of research work has been undertaken with regard to the performance modeling of the jaw crusher. The crusher throughput rate has been studied in [86, 87, 61]. The specific energy consumed during the comminution process has traditionally been expressed by the Bond work index theory [88, 49]. As for the product quality index, the 80 % passing sieve size of the product, $P_{80}$ has been studied in Refs. [87, 61]. However, a more practical product quality index, which is the maximum particle size of the product, has not been discussed in the literature. Moreover, in these previous works, the prediction models of the throughput rate and specific energy consumption of the jaw crusher are discussed in terms of process design and not operation. The objective of this chapter is firstly to express all three performance prediction models of the jaw crusher in terms of the main operational control variable, the CSS. Secondly, through a laboratory jaw crusher setup with anthracite coal as feed material, the CSS variation effect is discussed.

## 6.2 PERFORMANCE MODEL OF JAW CRUSHER

The jaw crusher is one of the simpler crushing machines where the ore/rock is fragmented between two plates, referred to as jaws. One of the jaws, which is movable, called the moving jaw, applies the force on the particles pressed against the fixed jaw. The crushing action

stops when the size of the crushed particles is less than the bottom gap, referred to as CSS. More details about the working principle of the jaw crusher are found in [49], to which the reader may refer for more in-depth information.

The performance prediction model of a jaw crusher traditionally consists of the throughput rate, specific energy consumption and product quality index. As discussed previously, for operation efficiency optimization, this model needs to be expressed in terms of the control variable, considered to be the CSS.

### 6.2.1 Throughput rate

The first analytical prediction model of the jaw crusher throughput rate was studied by Hersam [86] in 1923 and later improved by Rose and English [87] in 1967. However, the analysis of these models revealed some deficiencies, as discussed in [61]. Most of these deficiencies come from the effect of the feed size, effect of throw and effect of the nature of the rock material, which were not quantified in [86, 87]. As already discussed in Chapter 3, an improved model to predict the jaw crusher throughput rate was studied by Sastri [61] in 1994 and expressed by Eq.(3.22) as $Q_p = 60Nw\left(CSS + 0.5\mathcal{T}\right)\left(\frac{D_V\mathcal{T}}{G-(CSS+\mathcal{T})}\right)K_1K_2K_3\rho$. However, the use of this equation assumes that the jaw crusher operates below its critical speed (maximum speed) condition, which is the case in practice.

### 6.2.2 Specific crushing energy

As discussed in Chapter 3, an empirical model that has been universally accepted for comminution energy prediction is based on the Bond work index theory [88, 49] and expressed by Eq.(3.2) as $E_{c_p} = 10W_i\left(\frac{10^{-3}}{\sqrt{P_{80}}} - \frac{10^{-3}}{\sqrt{F_{80}}}\right)$, where $E_{c_p}$ and $W_i$ are expressed in $kWh/metric{-}ton$, $P_{80}$ and $F_{80}$ in $m$ instead of $\mu m$.

For unscalped (unscreened) feed ($S_C = 0$), the specific crushing energy can be expressed as a function of the control variable, CSS, by substitution of Eq.(3.4) in Eq.(3.2). The new specific crushing energy is therefore expressed as:

$$E_{c_p} = 0.01W_i\left(\frac{1.0846}{\sqrt{(CSS+\mathcal{T})}} - \frac{1.1180}{\sqrt{(0.8S_FF_{max})}}\right). \tag{6.1}$$

### 6.2.3 Product quality index

Several performance indices can be considered to represent the ore product quality from a jaw crusher. However, the most practical one that can be related to CSS are the 80 % passing sieve size of the product, $P_{80}$ and the maximum particle size of the product, $P_{max}$. The empirical model of $P_{80}$ is given by the first expression of Eq.(3.4) as $P_{80} = 0.85\,(CSS + \mathcal{T})$.

Based on various data from manufacturers of jaw crushers [1], the maximum particle size $P_{max}$ has been shown to be directly proportional to CSS and is given as:

$$P_{max} = aCSS, \tag{6.2}$$

where the proportional constant $a$ depends on the hardness of the feed material. The softer the feed material, the bigger the value of $a$ is. For hard feed material such as gold or copper ore for instance, $a$ is about 1.5.[2, 3] while for soft feed material such as coal, $a$ can be expected to go up to about 2.8.

## 6.3 EXPERIMENTAL TEST WORK

In order to analyze the performance model of the jaw crusher that can be used for process optimization, a laboratory jaw crusher setup available at the Geology laboratory is used in this work. This is a single-toggle, overhead eccentric, Blake-type jaw crusher. The advantage of this crusher is that it allows the adjustment of the CSS compared to the jaw crusher available in minerals processing laboratory. Anthracite coal is used as feed material to the jaw crusher.

### 6.3.1 Feed rock material

As can be seen in Figs. 6.1-6.2, five samples of anthracite coal of about 1 $kg$ each, were prepared and used during experiments. The particle size distribution analysis of these samples was not possible owing to the lack of big sieves. Hence, the mean size of particles in each sample was measured by a digital vernier caliper and this is given in Table 6.1.

[1] Metso, C Series jaw crushers, <http://www.metso.com>

[2] Metso, C Series jaw crushers, <http://www.metso.com>

[3] Institute of Quarrying Australia (IQA), Technical briefing paper no 6, Jaw crushers , <https://www.quarry.com.au>

**Figure 6.1:** A sample of anthracite coal

**Figure 6.2:** Five samples of about 1 $kg$ each

### 6.3.2 Laboratory jaw crusher setup

The jaw crusher was operated five times for the given five samples, at different values of CSS obtained through the adjustment of levers, as can be seen in Fig. 6.3. The complete setup is shown in Fig. 6.4. The main purpose of this setup was to obtain the measured throughput rate and specific crushing energy of the jaw crusher at different CSS values.

During the coal crushing, the electrical power consumption of the jaw crusher were monitored

**Table 6.1:** Feed particle mean size

| Particle mean size (mm) | Sample 1 | Sample 2 | Sample 3 | Sample 4 | Sample 5 |
|---|---|---|---|---|---|
| $d_{1_{mean}}$ | 72.04 | 70.26 | 71.45 | 68.87 | 70.72 |
| $d_{2_{mean}}$ | 72.06 | 69.48 | 62.46 | 71.05 | 64.67 |
| $d_{3_{mean}}$ | 68.48 | 73.56 | 63.40 | 58.90 | 78.63 |
| $d_{4_{mean}}$ | 59.29 | 61.82 | 53.91 | 64.69 | 59.80 |
| $d_{5_{mean}}$ | 57.67 | 56.42 | 78.47 | 67.71 | 64.87 |
| $d_{6_{mean}}$ | 55.50 | 49.56 | 50.20 | 52.62 | 47.04 |
| Average feed size ($F_{av}$) | 64.17 | 63.52 | 63.32 | 63.97 | 64.29 |
| Weight | 1.000 $kg$ | 0.960 $kg$ | 1.000 $kg$ | 0.965 $kg$ | 1.005 $kg$ |

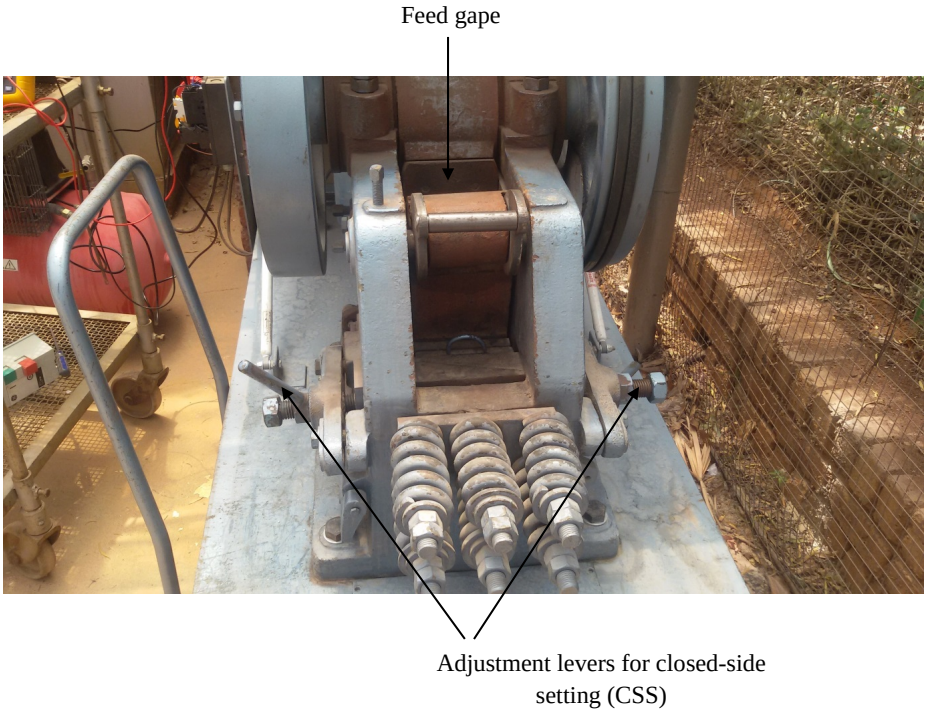


**Figure 6.3:** Adjustment of closed-side setting of jaw crusher

and the corresponding data was thereafter saved. This was possible by using a power quality analyzer, Fluke 43B, as shown in Fig. 6.4, where a single-phase current and voltage were directly measured at the switch of the jaw crusher electric motor. Although Fluke 43B has a data logger system, its capacity and flexibility are limited. A personal computer (PC) connected to the Fluke 43B through an optically isolated USB cable was therefore used as data

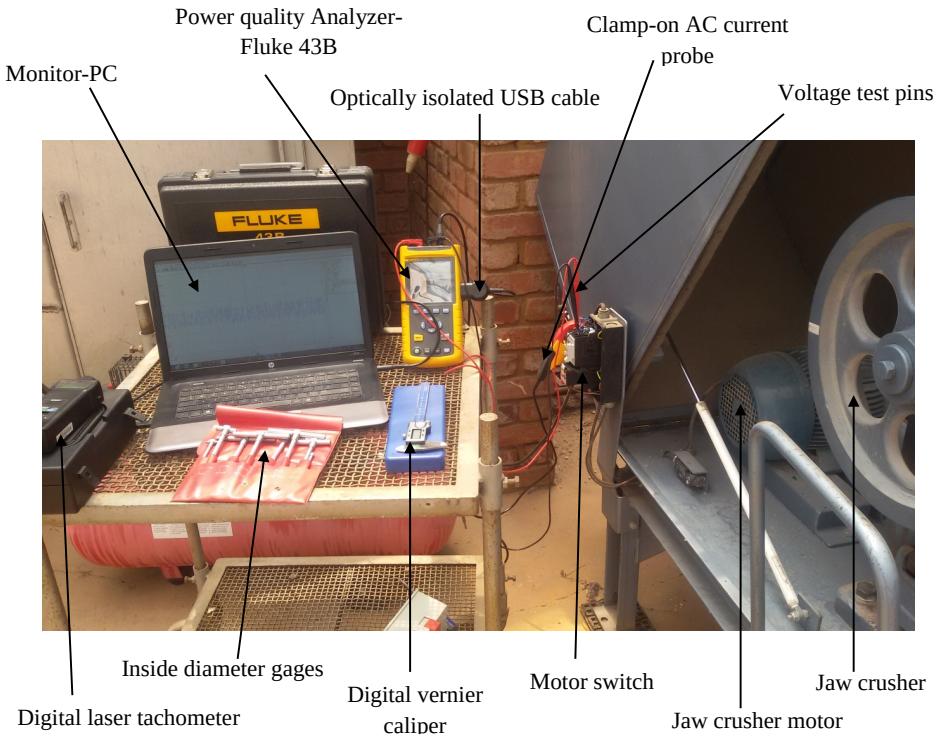


**Figure 6.4:** Laboratory jaw crusher setup

logger. Because of the limited accessibility of the CSS, a combination of the inside diameter gages and vernier caliper was used for the CSS measurement. A digital laser tachometer and stopwatch were used to measure the crusher rotational speed and the crushing time, respectively.

#### 6.3.2.1 Experimental throughput rate

The measured or experimental throughput rate was obtained based on the ratio between the sample mass $(kg)$ and the crushing time $(s)$, which is multiplied by a coefficient of 3.6 in order to be expressed in tonnes per hour $(t/h)$ (since 1 $kg = 3.6$ $t/h$) as follows:

$$Q_m = 3.6 \frac{Sample\ mass\ (kg)}{Crushing\ time\ (s)}. \tag{6.3}$$

#### 6.3.2.2 Experimental specific crushing energy

Since the net crushing power is the shaft (mechanical) power, this was obtained from the difference between the measured electrical power under load condition $P_{load_m}$ and the measured electrical power under no load condition $P_{no-load_m}$, multiplied by the overall drive efficiency $\eta_D$ as follows:

$$P_{c_m} = (P_{load_m} - P_{no-load_m})\,\eta_D. \tag{6.4}$$

The measured specific crushing energy $E_{cs}$ at different CSS was therefore obtained from the following expression:

$$E_{cs_m} = \frac{P_{c_m}}{Q_m}. \tag{6.5}$$

### 6.3.3 Coal product screening setup

After the five coal samples had been crushed, a Retsch-AS200 sieve shaker shown in Fig. 6.5, available in minerals processing laboratory, was used for product quality index or product size distribution analysis. Fourteen universal test sieves related by a factor of $\frac{1}{\sqrt{2}}$, called Tyler's

**Figure 6.5:** Laboratory sieve shaker

series, were employed for each sample screening. With this, for an initial sieve opening of

26.5 $mm$ used, the coal material was sieved down to 0.3 $mm$ (fourteenth sieve opening). However, since the maximum number of sieves on this sieve shaker is ten, two series of screening were conducted for each sample. A stack of nine sieves was first used and after screening, the product in the pan was collected and screened in another stack of five sieves. The choice of the number of sieves used was based on the fact that, after screening, the product available in the pan should be less than 10 % of the initial mass sample. Also, the higher the number of sieves, the higher the accuracy of the product size distribution. Since anthracite coal is normally characterized as soft rock, optimal settings of the vibrating frequency and screening time were chosen to be 40 $Hz$ and 20 $min$, respectively.

After screening, for each sample, the mean size of the biggest particle on the top sieve was measured using a vernier caliper. Moreover, the particle amount retained on each sieve was weighed for product size distribution analysis.

## 6.4 RESULTS AND DISCUSSION

The predicted versus experimental (measured) performance indices of the jaw crusher, namely the throughput rate, specific energy consumption and product size distribution index (maximum product size), are presented in this section. Both experiments and simulations have been performed with different values of the CSS of 7.8; 8.52; 9.83; 10.43 and 11.03 mm, considered as variable. The material and jaw crusher material parameters are given in Table 6.2. The fitting accuracy between the predicting model and the experimental results is evaluated through two indicators. The first indicator is the root mean square (RMS) error, expressed as follows [7]:

$$RMS\ error = \sqrt{\frac{\sum_{i=1}^{n}\left(\frac{y_{m_i}-y_{p_i}}{y_{m_i}}\right)}{n}}, \tag{6.6}$$

where $y_{m_i}$, $y_{p_i}$ and $n$ are, respectively, the $i^{th}$ measurement value, $i^{th}$ predicted value and number of data sets. The second indicator is the coefficient of determination, $R^2$, or $R$-squared, expressed as follows:

$$R^2 = \left(\frac{\sum_{i=1}^{n}\left[\left(y_{m_i}-\bar{y}_m\right)\left(y_{p_i}-\bar{y}_p\right)\right]}{\sqrt{\sum_{i=1}^{n}\left(y_{m_i}-\bar{y_m}\right)^2\sum_{i=1}^{n}\left(y_{p_i}-\bar{y_p}\right)^2}}\right)^2, \tag{6.7}$$

where $\bar{y_m}$ and $\bar{y_p}$ are, respectively, the mean values of the measurement set and predicted set.

**Table 6.2:** Material and jaw crusher parameters

| Parameters | Value |
|---|---|
| Coal density, $\rho$ | 1.9 $t/m^3$ |
| Bond work index of coal, $W_i$ | 12.51 $kWh/t$ |
| Material shape factor, $S_F$ | 1.7 |
| Speed of the jaw crusher, $N$ | 312 $rpm$ |
| Width of the jaw crusher, $w$ | 128.5 $mm$ |
| Gape of the jaw crusher, $G$ | 96.13 $mm$ |
| Vertical depth between jaws, $D_V$ | 220 $mm$ |
| Throw of the jaw crusher, $\mathcal{T}$ | 4.87 $mm$ |
| Drive efficiency, $\eta_D$ | 80 % |

### 6.4.1 Throughput rate

Fig. 6.6 gives the comparison results between the predicted (simulated) and experimental (measured) jaw crusher throughput rate under variation of the CSS. As can be seen from Fig.

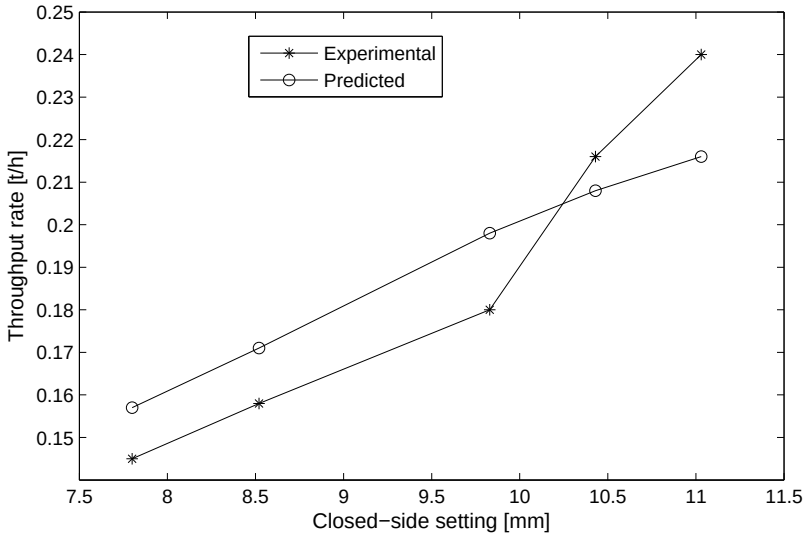


**Figure 6.6:** Throughput rate vs. closed-side setting

6.6, the trend of the predicted throughput rate is in agreement with that of the experimental one. Both results show strong proportionality between the jaw crusher throughput rate and the CSS. As predicted, the experimental result shows that the increase in CSS will result in higher throughput rate of the crusher.

This is due to the fact that more coal material will be discharged as the discharge gap, CSS, increases. From a comminution point of view, increasing the CSS of the jaw crusher reduces the number of crushing zones or actions, therefore reducing the residence time of the particle in the crushing chamber and thus leading to a throughput rate increase. The strong dependence of the jaw crusher throughput rate on the CSS makes the latter the main control variable for the control of the jaw crusher throughput rate. Fig. 6.7 shows that the RMS error of the predicted throughput rate when compared to the experimental result is only about 8.36 %. The same figure shows a coefficient of determination of 0.9025 (90.25 %),

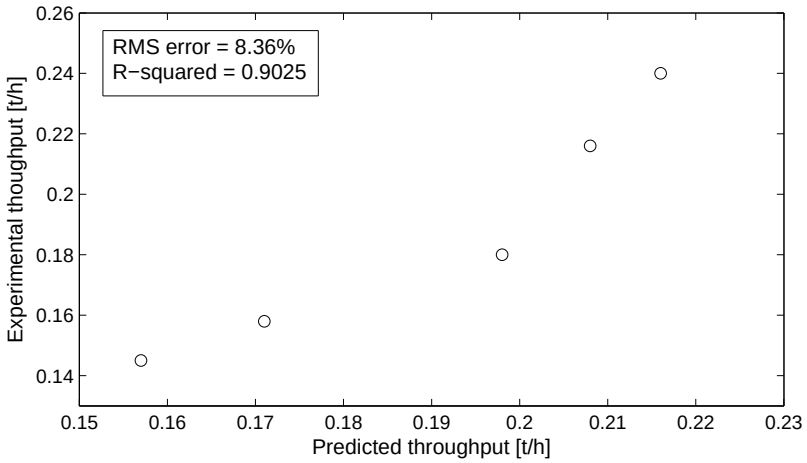


**Figure 6.7:** Correlation of throughput rate

which means the existence of a strong linear correlation between the predicted and measured throughput rate of the jaw crusher.

### 6.4.2 Specific energy consumption

Comparison results between the predicted specific energy consumption and experimental data are presented in Fig. 6.8.

Both results show that the specific energy consumption of the jaw crusher decreases with the

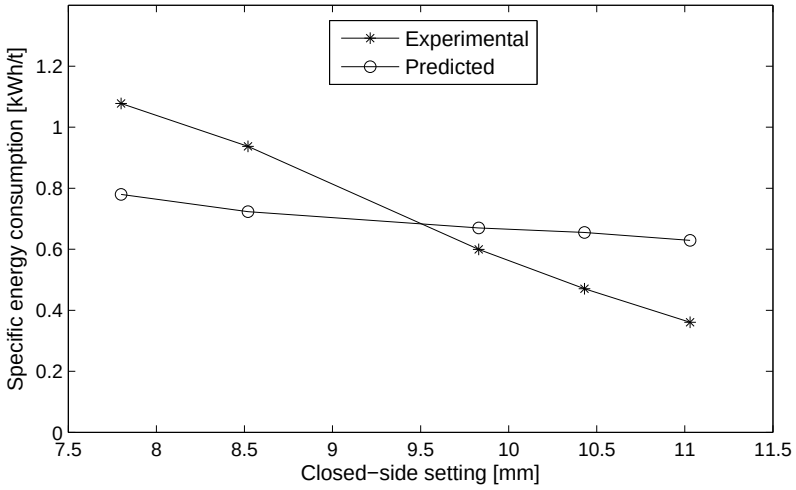


**Figure 6.8:** Specific energy consumption vs. closed-side setting

increase of the CSS. This is mainly due to two reasons. Firstly, increasing the CSS of the jaw crusher leads to an increase in the throughput rate, as previously mentioned, and therefore a decrease of the specific energy consumption. Secondly, the increase in the CSS will generally lead to a decrease in crushing force between the particle bed and the crusher liners, which will result in lower power consumption at the cost of a decrease in product quality.

In contrast to the throughput rate, the predicted specific energy (based on the Bond work index equation) shows a large RMS error of 41.25 % compared with experimental results, as can be seen in Fig. 6.9. One of the reasons for this large error is the fact that the

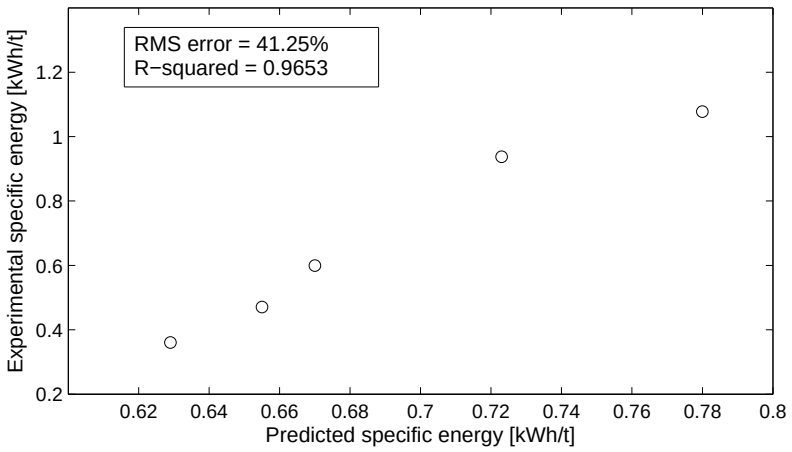


**Figure 6.9:** Correlation of specific energy consumption

Bond work index theory only represents an average value, but fair approximation of the specific energy required for particle size reduction [89]. However, since the results obtained show a strong linear correlation (with R-squared=96.53 %), this indicates a strong linear relationship between the Bond predicted specific energy and experimental specific energy. Therefore, although a large RMS error is shown with the Bond work index theory, this can still be used as a performance index or objective function for jaw crusher energy optimization. This is due to the fact that minimizing the energy consumption based on the Bond work index theory will lead to minimization of the actual specific energy of the jaw crusher, since there is a strong linear relationship with the experimental data.

### 6.4.3 Product quality

The jaw crusher product quality index has been expressed as the maximum particle size of the product. For coal material, the proportional constant of the predicted maximum particle size in Eq.(6.2) has been assumed to be 2.2.

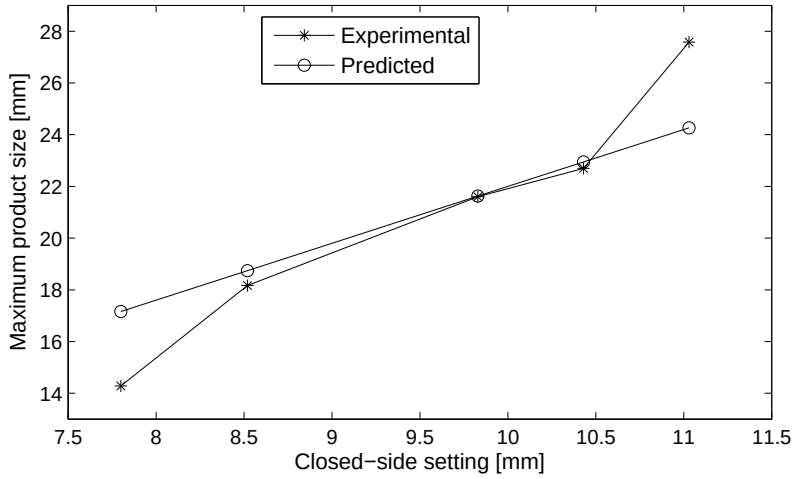


**Figure 6.10:** Maximum product size vs. closed-side setting

Comparative results between the predicted maximum product size and experimental maximum product size are shown in Fig. 6.10. An analysis of the results shows good agreement between the prediction model and experimental data. As expected, the maximum product size increases with an increase in the CSS and vice versa. As can be seen from Fig. 6.11, the predicted maximum product size shows a relatively small RMS error of 10.60 %, while a

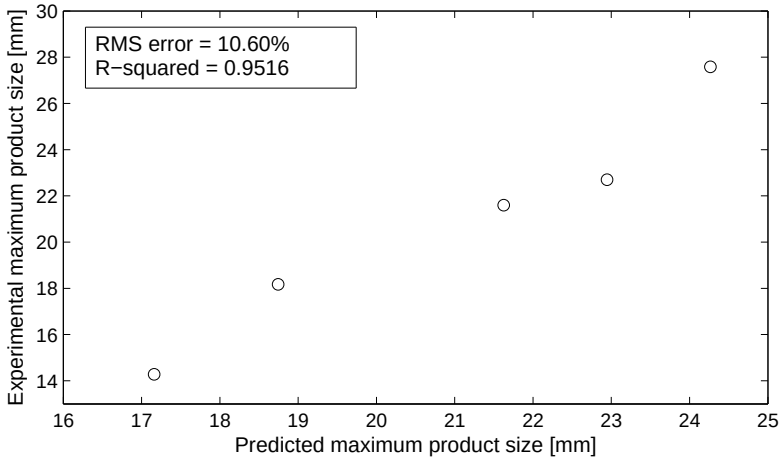


**Figure 6.11:** Correlation of maximum product size

strong linear correlation with R-squared of 95.16 % is shown. It follows that the maximum size of coal particles in the product is linearly dependent on the CSS of the jaw crusher.

Furthermore, the experimental product size distributions for different CSS values are shown in Fig. 6.12.

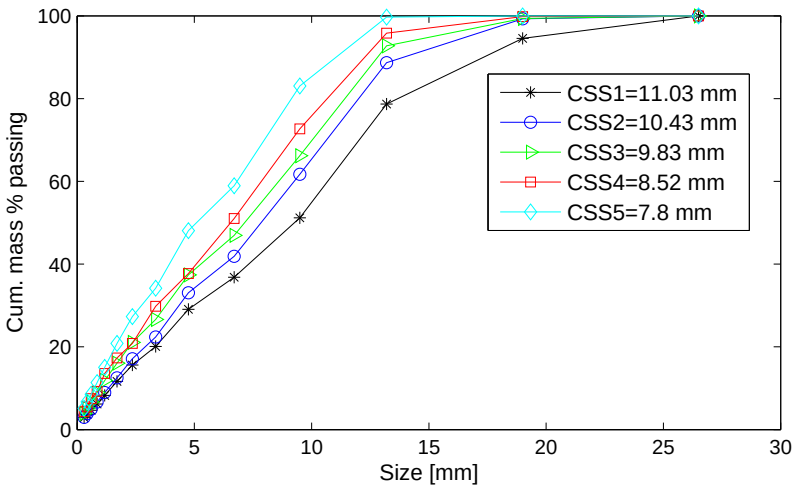


**Figure 6.12:** Experimental product size distribution

This figure shows that increasing the CSS will result in shifting the product size distribution curve upwards, therefore yielding coarser product material. If one classifies coal size into commercial value ($+6$ $mm$), then the unwanted coal size or small-sized coal in duff

coal (size fractions between $-6\ mm$ and $+0\ mm$), fine coal (size fractions between $-1\ mm$ and $+0.15\ mm$) and super-fine coal (size fractions between $-0.15\ mm$ and $+0\ mm$),[4] Fig. 6.13 shows that the unwanted coal size increases with the decrease in the CSS, while the commercial value coal size decreases and vice versa. This means that when using the jaw

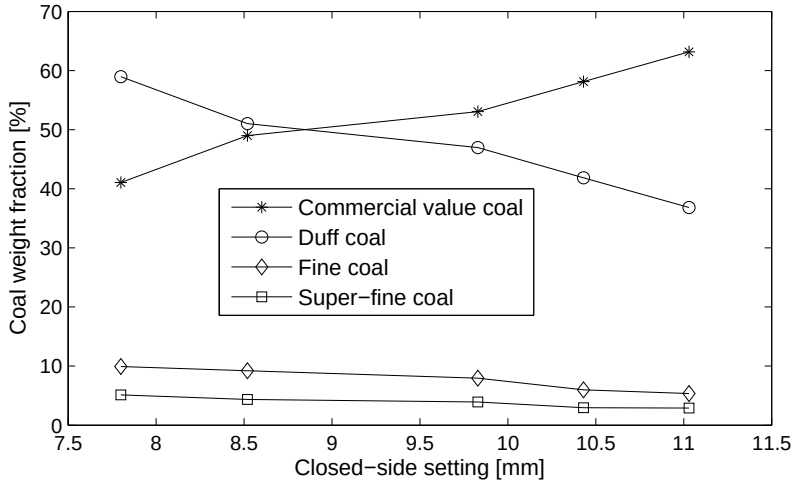


**Figure 6.13:** Experimental generated coal weight fractions

crusher in primary ROM coal crushing station, any attempt to minimize small-sized coal at this stage will result in reducing the amount of commercial value coal. This is good news for coal processing industries, since setting the jaw crusher CSS to a relatively high value in order to maximize the commercial value coal will also reduce the specific energy consumption of the jaw crusher. The results therefore reveal a conflict between minimizing the maximum product size and maximizing the amount of commercial value coal. However, coal processing engineers have to decide whether to consider the maximum product size or the amount of commercial coal value as product quality performance indicator.

## 6.5 CONCLUSION

In this chapter, the performance prediction models of a jaw crusher in terms of throughput rate, specific energy consumption and product quality index (maximum product size) are analyzed when compared to experimental results. The influence of varying the CSS of the jaw crusher is analyzed on each prediction model, with the feed material being anthracite coal.

[4]DR Hardman and G Lind, Generation of fine coal, In -section <http://www.coaltech.co.za>

The analysis of the prediction models for the throughput rate and maximum product size reveals smaller errors compared to the predicted specific energy consumption based on the Bond work index theory. However, it is seen that since a strong linear correlation is obtained between the Bond specific energy and experimental specific energy, the former can still be used as energy performance indicator for a jaw crushing energy optimisation problem.

The analysis of the product size distribution reveals a trade-off between maximizing the commercial value coal, minimizing the unwanted coal size and minimizing the maximum coal size in the product. It is shown that decreasing the CSS in order to reduce the maximum coal product size results in an increase in unwanted coal size (small-sized amount of coal) and decrease in commercial value coal.

# CHAPTER 7

# GENERAL CONCLUSION

## 7.1 SUMMARY

This work aims at developing optimal control models for the energy management of crushing processes in mines. Three types of crushing processes are studied. These are the jaw crushing process, VSI crushing process and HPGR crushing process. The control variables considered in the jaw crushing process are the CSS and apron feeder speed; the belt conveyor feed rate, rotor speed, rotor feed rate and cascade feed rate are control variables in the VSI crushing process, while for the HPGR crushing process, the control variables are the rolls operating pressure, HPGR rotating speed and HPGR feed rate. Firstly, the energy model of each machine is proposed and expressed as a function of the control variables. Secondly, an optimal control model is written for each process, with the objective to minimize the associated energy cost by accounting for the TOU electricity tariff. Both optimal energy control techniques with continuous and binary variables are modeled for the jaw crushing process, while for the VSI and HPGR crushing processes, only optimal energy control with continuous variables is modeled. Model with binary variables (switching states) is considered for the jaw crushing process to save more energy by altering the no-load energy consumption of the jaw crusher, considered to be relatively higher than that of other types of crushers. Thirdly, a case study is done for each process in order to evaluate the effectiveness of the methods developed. Lastly, results from laboratory experiments on jaw crusher performance are presented.

Through simulation results, it is shown that there is potential for reducing the energy cost and energy consumption associated with the operation of crushing processes. For all processes,

most of the energy cost reduction comes from optimal shifting of the process based on the TOU electricity tariff.

With regard to energy consumption reduction, for underground jaw primary crushing processes where a soft starter or variable speed drive is integrated, the optimal switching control technique is shown to be a good strategy to achieve considerable energy saving. This is due to the high no-load power consumption of the jaw crusher which cannot be altered by the main control variable, the CSS. It is also shown that having a big ore pass storage system is shown to be of great importance in achieving more energy cost saving in the primary jaw crushing process while improving the switching frequency profile associated with the switching controller.

In VSI crushing processes with varying feed size, it is shown that the energy consumption reduction is due to the crusher speed reduction by optimally operating the system at the boundary of the admissible operating region limited by the product quality constraint. This shows that in order to minimize economical performance such as energy consumption, the operating point of the VSI crushing process has to be obtained by pre-setting the product quality indicator at its worst but feasible value (limits). The reason for this is the conflict between economical performance objectives (energy consumption, energy cost, etc.) and technical performance objectives (product size reduction ratio, maximum product size, etc.), which makes the crushing process a multi-objective optimization problem in reality.

In HPGR crushing processes with a parallel configuration, some energy saving can be achieved through optimal control of the loading levels of HPGRs when these machines are not operating with equal efficiency. This is the case where it happens that two or more HPGR crushers of different ratings and efficiencies are to operate in parallel for reliability, planning or productivity purposes. Another reason is that during operation, the efficiency of HPGRs in parallel may differ owing to unequal feeding conditions. It is also revealed that more energy consumption reduction can be achieved through a slight decrease in the rolls operating pressure of the HPGR crusher without altering the product quality requirement.

For the three crushing processes, it is important to note that most energy cost saving is due to the optimal load shifting based on TOU electricity tariff, while the rest comes from the energy saving.

Furthermore, the analysis of the performance model of the jaw crusher reveals that the throughput rate and product quality index can be predicted with smaller prediction errors compared to the energy consumption. However, it can be noted that since a strong linear correlation is shown between the predicted specific energy and experimental specific energy, Bond specific energy can still be used as energy performance indicator for a jaw crushing energy optimization problem. With anthracite coal as crushing material, the trade-off between the maximization of commercial value coal, minimization of unwanted coal size and minimization of maximum coal size in the product is shown.

## 7.2 FUTURE WORK

The work presented in this thesis can be extended as follows:

1) Optimal energy management of other types of crushing processes. Although this work stressed crushing processes based on the jaw crusher, VSI crusher and HPGR crusher, energy management of crushing circuits based on other types of crushers such as gyratory and cone crushers can also be studied.

2) Optimal energy management of a crushing plant. In this work, each crushing circuit is individually considered, while the energy management of the whole crushing plant, from primary crushing circuit to last stage crushing circuit, can be studied as one energy system.

3) Optimal energy management of a comminution plant. A more global optimum operation may be obtained by considering both crushing plant and grinding plant as one energy process.

4) Closed-loop optimal energy control. The current work focuses on open loop optimal energy control techniques, while for real-time implementation, close-loop control techniques such as MPC might be more feasible to make it possible to compensate for the effects of unmeasured disturbances and/or model inaccuracy.

5) Model verification and scale-up of different types of crushers. In this work, a laboratory-scale jaw crusher is used to assess the accuracy level of the prediction model used. However, pilot scale tests need to be conducted in order to assess the scalability of each performance indicator (product size distribution, throughput rate and power/energy consumption).

6) Real-time implementation of optimal energy management of a crushing process. This work is limited to simulation results of optimal energy management of different types of crushing processes. However, laboratory experiments should be carried out in order to validate these simulation results.

# REFERENCES

[1] C. Gellings, "The concept of demand-side management for electric utilities," *Proceedings of the IEEE*, vol. 73, no. 10, pp. 1468–1470, 1985.

[2] P. Warren, "A review of demand-side management policy in the UK," *Renewable and Sustainable Energy Reviews*, vol. 29, pp. 941 – 951, 2014.

[3] D. Ramsbottom, "Case study into the application of time of use tariffs in the Eskom western region of South Africa in reducing peak load," in *Cigré 2009 6th South African Regional Conference. Somerset West, Western Cape, South Africa*, 17-21 August, 2009, pp. 29–33.

[4] D. Fuerstenau and A.-Z. Abouzeid, "Role of feed moisture in high-pressure roll mill comminution," *International Journal of Mineral Processing*, vol. 82, pp. 203–210, 2007.

[5] M. Lindqvist, "Energy considerations in compressive and impact crushing of rock," *Minerals Engineering*, vol. 21, no. 9, pp. 631 – 641, 2008.

[6] D. Fuerstenau and A.-Z. Abouzeid, "The energy efficiency of ball milling in comminution," *International Journal of Mineral Processing*, vol. 67, no. 1-4, pp. 161 – 185, 2002.

[7] M. Daniel and S. Morrell, "HPGR model verification and scale-up," *Minerals Engineering*, vol. 17, no. 11-12, pp. 1149 – 1161, 2004.

[8] A.-Z. Abouzeid and D. Fuerstenau, "Grinding of mineral mixtures in high-pressure grinding rolls," *International Journal of Mineral Processing*, vol. 93, no. 1, pp. 59 – 65, 2009.

[9] V. Hasanzadeh and A. Farzanegan, "Robust HPGR model calibration using genetic algorithms," *Minerals Engineering*, vol. 24, no. 5, pp. 424 – 432, 2011.

[10] H. Dundar, H. Hakan Benzer, and N. Aydogan, "Application of population balance model to HPGR crushing," *Minerals Engineering*, vol. 50-51, pp. 114 – 120, 2013.

[11] X. Xia, J. Zhang, and W. Cass, "Energy management of commercial buildings - a case study from a POET perspective of energy efficiency," *Journal of Energy in Southern Africa*, vol. 23, pp. 23–31, 2012.

[12] W. Badenhorst, J. Zhang, and X. Xia, "Optimal hoist scheduling of a deep level mine twin rock winder system for demand side management," *Electric Power Systems Research*, vol. 81, no. 5, pp. 1088 – 1095, 2011.

[13] S. Zhang and X. Xia, "Optimal control of operation efficiency of belt conveyor systems," *Applied Energy*, vol. 87, no. 6, pp. 1929 – 1937, 2010.

[14] S. Zhang and X. Xia, "Modeling and energy efficiency optimization of belt conveyors," *Applied Energy*, vol. 88, no. 9, pp. 3061 – 3071, 2011.

[15] A. Middelberg, J. Zhang, and X. Xia, "An optimal control model for load shifting - With application in the energy management of a colliery," *Applied Energy*, vol. 86, pp. 1266 – 1273, 2009.

[16] B. Matthews and I. Craig, "Demand side management of a run-of-mine ore milling circuit," *Control Engineering Practice*, vol. 21, no. 6, pp. 759 – 768, 2013.

[17] H. Zhang, X. Xia, and J. Zhang, "Optimal sizing and operation of pumping systems to achieve energy efficiency and load shifting," *Electric Power Systems Research*, vol. 86, pp. 41 – 50, 2012.

[18] X. Zhuan and X. Xia, "Optimal operation scheduling of a pumping station with multiple pumps," *Applied Energy*, vol. 104, pp. 250 – 257, 2013.

[19] A. van Staden, J. Zhang, and X. Xia, "A model predictive control strategy for load shifting in a water pumping scheme with maximum demand charges," *Applied Energy*, vol. 88, no. 12, pp. 4785 – 4794, 2011.

[20] X. Zhuan and X. Xia, "Development of efficient model predictive control strategy for

cost-optimal operation of a water pumping station," *IEEE Transactions on Control Systems tehnology*, vol. 21, no. 4, pp. 1449–1454, 2013.

[21] R. Pelzer, E. Mathews, D. le Roux, and M. Kleingeld, "A new approach to ensure successful implementation of sustainable demand side management (DSM) in South African mines," *Energy*, vol. 33, no. 8, pp. 1254 – 1263, 2008.

[22] S. Ashok and R. Banerjee, "Optimal cool storage capacity for load management," *Energy*, vol. 28, no. 2, pp. 115 – 126, 2003.

[23] Y. Wang and L. Li, "Time-of-use based electricity demand response for sustainable manufacturing systems," *Energy*, vol. 63, pp. 233 – 244, 2013.

[24] S. Mitra, L. Sun, and I. Grossmann, "Optimal scheduling of industrial combined heat and power plants under time-sensitive electricity prices," *Energy*, vol. 54, pp. 194 – 211, 2013.

[25] P. Faria and Z. Vale, "Demand response in electrical energy supply: An optimal real time pricing approach," *Energy*, vol. 36, no. 8, pp. 5374 – 5384, 2011.

[26] M. Macedo, J. Galo, L. de Almeida, and A. de C. Lima, "Demand side management using artificial neural networks in a smart grid environment," *Renewable and Sustainable Energy Reviews*, vol. 41, pp. 128 – 133, 2015.

[27] L. Merkert, I. Iiro Harjunkoski, A. Isaksson, S. Saynevirta, A. Saarela, and G. Sand, "Scheduling and energy - Industrial challenges and opportunities," *Computers and Chemical Engineering*, vol. 72, pp. 183 – 198, 2015.

[28] A. Sheikhi, M. Rayati, S. Bahrami, A. Ranjbar, and S. Sattari, "A cloud computing framework on demand side management game in smart energy hubs," *International Journal of Electrical Power and Energy Systems*, vol. 64, pp. 1007 – 1016, 2015.

[29] X. Xia and J. Zhang, "Energy efficiency and control systems - from a POET perspective," in *IFAC Conference on Control Methodology and Technology for Energy Efficiency, Vilamoura, Portugal*, 29-31 March, 2010.

[30] X. Xia and J. Zhang, "Modeling and control of heavy-haul trains," *IEEE Control Systems Magazine*, vol. 31, pp. 18–31, 2011.

[31] M. Hager and A. Hintz, "The energy-saving design of belts for long conveyor systems," *Bulk Solids Handling*, vol. 13, no. 4, pp. 749–758, 1993.

[32] A. de Almeida, P. Fonseca, and P. Bertoldi, "Energy-efficient motor systems in the industrial and in the services sectors in the European Union: Characterisation, potentials, barriers and policies," *Energy*, vol. 28, pp. 673–690, 2003.

[33] B. Mecrow and A. Jack, "Efficiency trends in electric machines and drives," *Energy Policy*, vol. 36, pp. 4336–4341, 2008.

[34] A. Tapp, "Energy saving troughing idler technology," *Bulk Solids Handling*, vol. 20, no. 4, pp. 437–449, 2000.

[35] IEC, "Rotating electrical machines - Part 30-1: Efficiency classes of line operated AC motors (IE code)-IEC 60034-30-1," International Electrotechnical Commission, Tech. Rep., 2014.

[36] G. Lodewijks, "The next generation low loss conveyor belts," *Bulk Solids Handling*, vol. 32, no. 1, pp. 52–56, 2012.

[37] M. Eissa, "Demand side management program evaluation based on industrial and commercial field data," *Energy Policy*, vol. 39, no. 10, pp. 5961–5969, 2011.

[38] P. Palensky and D. Dietrich, "Demand side management: Demand response, intelligent energy systems, and smart loads," *IEEE Transactions on Industrial Informatics*, vol. 7, no. 3, pp. 381–388, Aug 2011.

[39] M. Borell, P.-O. Backstrom, and L. Lars Soderberg, "Supervisory control of autogenous grinding circuits," *International Journal of Mineral Processing*, vol. 44-45, pp. 337 – 348, 1996.

[40] R. Lestage, A. Pomerleau, and D. Hodouin, "Constrained real-time optimization of a grinding circuit using steady-state linear programming supervisory control," *Powder*

*Technology*, vol. 124, no. 3, pp. 254 – 263, 2002.

[41] X.-s. Chen, Q. Li, and S.-m. Fei, "Supervisory expert control for ball mill grinding circuits," *Expert Systems with Applications*, vol. 34, no. 3, pp. 1877 – 1885, 2008.

[42] V. Radhakrishnan, "Model based supervisory control of a ball mill grinding circuit," *Journal of Process Control*, vol. 9, no. 3, pp. 195 – 211, 1999.

[43] E. Aske, S. Trand, and S. Skogestad, "Coordinator MPC for maximizing plant throughput," *Computers and Chemical Engineering*, vol. 32, no. 1-2, pp. 195 – 204, 2008.

[44] F. Serralunga, M. Mussati, and P. Aguirre, "Model adaptation for real-time optimization in energy systems," *Industrial and Engineering Chemistry Research*, vol. 52, no. 47, pp. 16 795–16 810, 2013.

[45] P. Antunes, P. Carreira, and M. Mira da Silva, "Towards an energy management maturity model," *Energy Policy*, vol. 73, pp. 803 – 814, 2014.

[46] E. Ngai, D. Chau, J. Poon, and C. To, "Energy and utility management maturity model for sustainable manufacturing process," *International Journal of Production Economics*, vol. 146, no. 2, pp. 453 – 464, 2013.

[47] B. Gopalakrishnan, K. Ramamoorthy, E. Crowe, S. Chaudhari, and H. Latif, "A structured approach for facilitating the implementation of ISO 50001 standard in the manufacturing sector," *Sustainable Energy Technologies and Assessments*, vol. 7, pp. 154 – 165, 2014.

[48] J. Martin, U. Bidarte, C. Cuadrado, and P. Ibañez, "DSP-based board for control of jaw crushers used in mining and quarrying industry," in *26th Annual Conference of the IEEE. Industrial Electronics Society, Nagoya, Aichi, Japan*, 22-28 October, 2000.

[49] A. Gupta and D. Yan, *Mineral Processing Design and Operations: An Introduction*. Elsevier, Amsterdam; Boston, 2006.

[50] J. Convey, "The milling of Canadian ores," in *Canada: 6th Commonwealth Mining and Metallurgical Congress*, 1957.

[51] S. Moray, N. Throop, J. Seryak, and C. Schmidt, "Energy efficiency opportunuties in the stone and asphalt industry," in *Proceedings of the Twenty-Eighth Industrial Energy Technology Conference. New Orleans*, 9-17 May, 2006.

[52] J. De la Vergne, *Hard Rock Miner's Handbook*, S. L. Andersen, Ed. McIntosh Engineering Inc, Arizona, USA, 2003.

[53] B. Numbi, J. Zhang, and X. Xia, "Optimal energy management for a jaw crushing process in deep mines," *Energy*, vol. 68, pp. 337–348, 2014.

[54] W. Hustrulid and R. Bullock, Eds., *Underground Mining Methods: Engineering Fundamentals and International Case Studies*. United States: Society for Mining, Metallurgy, and Exploration, Inc, 2001.

[55] J. Hadjigeorgiou and J. Lessard, "Numerical investigations of ore pass hang-up phenomena," *International Journal of Rock Mechanics and Mining Sciences*, vol. 44, no. 6, pp. 820–834, 2007.

[56] J. Hadjigeorgiou, J. Lessard, and F. Mercier-Langevin, "Ore pass practice in Canadian mines," *Journal of The South African Institute of Mining and Metallurgy*, vol. 105, no. 11, pp. 809–816, 2005.

[57] K. Esmaieli, "Stability Analysis of Ore Pass Systems at BRUNSWICK Mine," Ph.D., Ph.D. thesis. Québec, Canada: Facultés des Sciences et de Génie, Université Laval, 2010.

[58] B. Kennedy, Ed., *Surface Mining*, 2nd ed. Baltimore, Maryland, United States: Society for Mining, Metallurgy, and Exploration, Inc, 1990, pp.706-708.

[59] L. Pontryagin, V. Boltyanskii, R. Gamkrelidze, and E. Mishchenko, *The Mathematical Theory of Optimal Processes*, L. Neustadt, Ed. New York, United States: John Wiley and Sons, Inc., 1962.

[60] A. Refahi, B. Rezai, and J. Mohandesi, "Use of rock mechanical properties to predict the Bond crushing index," *Minerals Engineering*, vol. 20, no. 7, pp. 662 – 669, 2007.

[61] S. Sastri, "Capacities and performance characteristics of jaw crushers," *Minerals and*

*Metallurgical Processing*, vol. 11, no. 2, pp. 80–86, 1994.

[62] A. Roberts, "Recent developments in feeder design and performance," *Handbook of Powder Technology*, vol. 10, pp. 211–223, 2001.

[63] R. DeDiemar, "New concepts in jaw crusher technology," *Minerals Engineering*, vol. 3, pp. 67–74, 1990.

[64] M. Dunn and I. Menzies, "Rockpass overview and risk assessment within the AngloGold Ashanti SA region," *Journal of the South African Institute of Mining and Metallurgy*, vol. 105, no. 11, pp. 753–758, 2005.

[65] A. Gastli and M. Ahmed, "ANN-based soft starting of voltage-controlled-fed IM drive system," *IEEE Transactions on Energy Conversion*, vol. 20, no. 3, pp. 497–503, 2005.

[66] Elsevier, "Interactive soft-starters provides smooth start-up for delicate pump systems," *World Pumps*, vol. 2004, no. 448, p. 10, 2004.

[67] B. Numbi and X. Xia, "Optimal energy control of a crushing process based on vertical shaft impactor," *Applied Energy (Article in Press)*, 2014.

[68] M. Bengtsson and C. Evertsson, "Modelling of output and power consumption in vertical shaft impact crushers," *International Journal of Mineral Processing*, vol. 88, pp. 18 – 23, 2008.

[69] D. Duan, S. Wang, F. Zhao, and D. Su, "Analysis of particle motion in vertical shaft impact rotor," *Advanced Materials Research*, vol. 199-200, pp. 54–57, 2011.

[70] S. Nikolov, "A performance model for impact crushers," *Minerals Engineering*, vol. 15, no. 10, pp. 715 – 721, 2002.

[71] S. Nikolov, "Modelling and simulation of particle breakage in impact crushers," *International Journal of Mineral Processing*, vol. 74, pp. 219–225, 2004.

[72] V. Strejc, "Least squares parameter estimation," *Automatica*, vol. 16, pp. 535–550, 1980.

[73] F. Abrahamsen, F. Blaabjerg, J. Pedersen, and P. Thoegersen, "Efficiency-optimized

control of medium-size induction motor drives," *IEEE Transactions on Industry Applications*, vol. 37, no. 6, pp. 1761–1767, Nov 2001.

[74] N. Djordjevic, F. Shi, and R. Morrison, "Applying discrete element modelling to vertical and horizontal shaft impact crushers," *Minerals Engineering*, vol. 16, no. 10, pp. 983 – 991, 2003.

[75] United States Patent US 0 022 074, 2006.

[76] B. Numbi and X. Xia, "Systems optimization model for energy management of a parallel HPGR crushing process," *Applied Energy*, vol. 149, pp. 133 – 147, 2015.

[77] M. Torres and A. Casali, "A novel approach for the modelling of high-pressure grinding rolls," *Minerals Engineering*, vol. 22, no. 13, pp. 1137 – 1146, 2009.

[78] D. Saramak, "Mathematical models of particle size distribution in simulation analysis of high-pressure grinding roll operations," *Physicochemical Problems of Mineral Processing*, vol. 49, pp. 121–131, 2013.

[79] D. Saramak and R. Kleiv, "The effect of feed moisture on the comminution efficiency of HPGR circuits," *Minerals Engineering*, vol. 43-44, pp. 105 – 111, 2013.

[80] J. Drozdiak, "A pilot-scale examination of a novel high pressure grinding roll/stirred mill comminution circuit for hard-rock mining applications," Master's thesis, Vancouver, Canada: Faculty of Graduate Studies, University of British Columbia, 2011.

[81] F. van der Meer and W. Maphosa, "High pressure grinding moving ahead in copper, iron, and gold processing," *The Journal of the Southern African Institute of Mining and Metallurgy*, vol. 112, pp. 637–647, 2012.

[82] CEMA, Ed., *Belt Conveyors for Bulk Materials*. 5th ed. United States: Conveyor Equipment Manufacturers Association, 2002.

[83] A. de Almeida, F. Ferreira, and D. Both, "Technical and economical considerations in the application of variable-speed drives with electric motor systems," *IEEE Transactions on Industry Applications*, vol. 41, pp. 188–199, 2005.

[84] C. Rule and S. G. Minnar, DM, "HPGR-revolution in platinum," *The Journal of The Southern African Institute of Mining and Metallurgy*, vol. 108, pp. 23–30, 2009.

[85] X. Xia, J. Zhang, and A. Elaiw, "An application of model predictive control to the dynamic economic dispatch of power generation," *Control Engineering Practice*, vol. 19, pp. 638–648, 2011.

[86] E. Hersam, "Factors controlling the capacity of rock crushers," *Transactions of AIME*, vol. 68, pp. 463–476, 1923.

[87] H. Rose and J. English, "Theoretical analysis of the performance of jaw crushers," *Transactions of IMM*, vol. 76, no. 724, pp. C32–C43, 1967.

[88] F. Bond, "Crushing and grinding calculations," in *Bulletin No. 07R235B*. Millwauke, WI, United States: Allis Charmers, 1961.

[89] D. Legendre and R. Zevenhoven, "Assessing the energy efficiency of a jaw crusher," *Energy*, vol. 74, pp. 119–130, 2014.